UNIVERSITY OF NAPLES FEDERICO II
Department of Structural Engineering

PH.D. PROGRAMME IN SEISMIC RISK
COORDINATOR PROF. ALDO ZOLLO
XXIV CYCLE

SIMONA ESPOSITO

PH.D. THESIS

Systemic Seismic Risk Analysis of Gas Distribution Networks

TUTOR PROF. IUNIO IERVOLINO

2011

To my special persons in the past, the present.. and the future.

"Each of the professions means a prejudice.
The necessity for a career forces every one to take sides.
We live in the age of the overworked, and the under-educated;
the age in which people are so industrious that they become absolutely stupid"

Oscar Wilde, 1891

ABSTRACT

Lifeline is an earthquake engineering term denoting those systems that are necessary for human life and urban contest. Those systems are commonly used to transport water, oil, natural gas and other material. Their disruption due to earthquakes can have a devastating impact on urban context both for human losses both economic stability. Therefore, due to their vulnerabilities, it is important to assess and mitigate seismic risk of lifelines since they are intricately linked with industries, communities and security they serve. The earthquake safety of lifeline systems has attracted great attention in recent years since significant amount of damage was observed during several past earthquakes.

This thesis focuses on the seismic performance evaluation of gas distribution networks. The basic function of a gas system is to deliver gas from sources to costumers. A gas distribution system is essentially composed by pipelines, reduction stations, valves and demand nodes. Those systems are essentially located underground. As consequences gas networks are subjected to both transient ground deformation due to seismic waves, which is felt over a wide geographical area, and ground failure due to geotechnical hazards such as liquefaction and landslide, which determine localized ground failure. Moreover since buried pipelines systems generally cover large areas, a sophisticated hazard analysis is required. In particular the quantification of regional hazard is based on a large vector of spatially correlated ground motion intensities and requires the modeling of the joint distribution of intensity measures at all sites of interest. Dependencies among ground motion parameters at different sites imply the estimation of spatial correlation models to be used for the hazard assessment but since each component that characterizes the system may be sensitive to different ground motion parameters, the possibility of the existence of a cross-correlation between these parameters has also to be taken into account. Fragility analysis of gas systems is generally based on empirical data collected throughout past earthquakes. In the case of pipeline components, the usual practice is to evaluate the repair rate as a unit length of pipe, with respect to a parameter representative of ground shaking or ground failure. For processing facilities, that include many subcomponents, a quantitative vulnerability assessment is quite difficult. A possible approach is to consider these facilities as systems and to aggregate the fragility of each component into a global systemic vulnerability through the use of fault tree analysis. Further in order to evaluate the interaction between component response to earthquake and lifeline performance,

system performance indicators provide a measure of the impact of the earthquake on the system functionality.

Building on the results from past international research projects, existing tools for the vulnerability assessment, and seismic risk analysis of lifelines systems, the SYNER-G project ("Systemic Seismic Vulnerability and Risk Analysis for Buildings, Lifeline Networks and Infrastructures Safety Gain"), has been funded by the European Commission (2009-2012) with the aim to address criticalities. In relation of the objectives of this project, this thesis had the aim to determine methodologies for the probabilistic seismic risk analysis of gas distribution networks and to apply these methods to a real gas system. In literature, there are very few studies on seismic risk analysis of networks that take into account all the aspects of the component of risk (hazard, vulnerability and loss). Moreover there are fewer studies that try to calibrate the analysis on a real system, making the study interesting for network operators. The thesis, in fact, has achieved this goal with special emphasis to the medium and low pressure network of a real system, namely the L'Aquila gas distribution system managed by ENEL Rete Gas s.p.a., for which not only detailed information on the network were retrieved, but also data related to damages occurred on the network followed the 2009 L'Aquila earthquake. A geographic information system (GIS) database was developed containing data on system physical and operational characteristics provided by the network operator to chracterize the seismic behavior of all components. L'Aquila region has been characterized both in terms of transient ground deformation hazard and permanent ground deformation hazard. In particular European and Italian spatial correlation models have been estimated and used for the simulation of probabilistic scenarios earthquakes and the ground failure hazard has been characterized in terms of landslide potential. Probabilistic simulations have been performed to evaluate the system response in terms of performance indicators for different combinations.

KEYWORDS: *lifelines, spatial correlation, permanent ground deformation, connectivity*

ACKNOWLEDGEMENTS

My PhD has been a challenge. A challenge that has led me to face many difficulties but at the same time gave me the opportunity to grow up both as a person and as researcher. I think to be changed a lot.

First of all I would like to thank my advisor Professor Iunio Iervolino for his valuable technical support during the course of my PhD . Thanks to his guidance, during these three years, I had important opportunities and the possibility to deal with different interesting issues.

A special thanks goes to Dr. Sonia Giovinazzi for several research discussions, collaboration and friendship. Thanks to Enel experts for sharing the L'Aquila network data used in this dissertation and for the opportunity to process technical reports describing the repairs activities following the 6th April L'Aquila earthquake. Thanks to researchers of "Federico II" and "La Sapienza" for collaboration and for providing helpful feedback regarding this work.

A big thank you goes to all my colleagues, especially to all my roommates for the support and their friendship.

Thanks to my friends Valentina, Federica, Chiara and not only , they followed me closely during this experience and supported me.

Thanks to my family. I want to express my gratitude to them for their understanding and for the moral support.

…and thanks to all my special person in the past, the present.. and the future.

TABLE OF CONTENTS

LIST OF TABLES

LIST OF FIGURES

LIST OF ABBREVIATIONS

ATC	Applied Technology Council
CL	connectivity loss
DCI	damage consequence index
DSHA	deterministic seismic hazard analysis
DS	damage state
EPN	electric power network
ESD	European strong-motion database
GIS	geographic information system
GMPE	ground-motion-prediction-equation
GRF	Gaussian random field
GRU	smaller reduction group
HDPE	High-density polyethylene
IM	intensity measure
IS	important sampling
ITACA	Italian accelerometric archive
LNG	liquified natural gas
LP	low pressure
LSM	least square method
MCS	Monte Carlo simulation
MOP	maximum service pressure
MP	medium pressure
MRS	minimum required strength
OOP	OBJECT-ORIENTED Paradigm
PDF	probability density function
PGA	peak ground acceleration
PGD	permanent ground deformation
PGD_i	peak ground displacement
PGV	peak ground velocity
PI	performance indicator
PVC	polyvinyl chloride
PSHA	probabilistic seismic hazard analysis
RG	reduction group
SCADA	Supervisory Control and Data Acquisition

SDOF	single-degree-of-freedom
SDR	standard dimension ratio
SR	serviceability ratio
SSI	system serviceability index
TGD	transient ground deformation
WSS	water supply system

Chapter 1 – INTRODUCTION

1.1. Background

Lifeline is an earthquake engineering term denoting those systems that are necessary for human life and urban contest. Those systems basically convey food, water, fuel, energy, information, and other materials necessary for human existence. Disruption of lifelines caused by earthquakes can therefore have a considerable impact both in the short term for life security and in the long term for the effects on the economy and social stability of a region. Therefore, due to their vulnerabilities, it is important to assess and mitigate seismic risk of lifelines since they are intricately linked with industries, communities and security they serve.

The critical importance and earthquake vulnerability of lifelines were first strongly emphasized in the in San Francisco earthquake and ensuing fires in 1906 (ATC-25, 1991). The earthquake disaster, which continues today to be the worst one in U.S. history, was in large part attributable to the failure of several lifelines, including: breakage of gas distribution and service lines, damage to fire stations, hundreds of breaks to the water distribution system resulting in total loss of water for fire-fighting purposes. Following 1906, several earthquakes continued to illustrate the importance of lifelines in earthquakes. The 1971 San Fernando Earthquake, for example, illustrated more than any other event the effects that earthquake can be have on lifelines; there were damage to electrical substations, hundreds of breaks in the water distribution system, loss of telephone service due to this damage, near-collapse of a major dam, numerous breaks in the gas distribution system, collapse of major freeway overcrossings, damage to emergency facilities, including collapse and major loss of life at a hospital, and major damage or partial collapse at several other hospitals.

Lifeline earthquake engineering is a relatively new field one. Its formal recognition came in the 1970's with the establishment in the United States of ASCE's Technical Council on Lifeline Earthquake Engineering (Duke and Matthiesen, 1973). In September 1988 Applied Technology Council (ATC) was awarded a contract by the Federal Emergency Management Agency to assess the seismic vulnerability and impact of disruption of lifeline systems nationwide with the purpose to better understand the impact of disruption of lifelines from earthquakes and to assist in the identification and prioritization of hazard mitigation measures. A concerted research

effort since then has made up but many challenges remain. Recent disastrous seismic events have widely documented the crucial role of the lifelines networks in supporting the emergency management and in facilitating the response and recovery phases following an earthquake, thus raising the interest of both the scientific community and the stakeholders in identifying proper risk mitigation and risk management strategies for lifelines systems. Management of lifeline seismic risk is useful for several decision makers (e.g. emergency management, insurance modelers, industrial company) for the prediction (pre earthquake) and the estimation (post earthquake) of economical (e.g. monetary losses) and social impacts (e.g. casualties) observing in future events or in the aftermath of an earthquake.

Figure 1.1 Damages on roads (left) and rails (right) due to surface faulting following the 4 September 2010 M_w 7.1 Canterbury, New Zealand Earthquake (Eidinger, 2011)

In general, each lifeline is a network within there are sources, transmission lines, storages and distribution systems and share four common characteristics (Wang and O'Rourke, 2008): geographical distribution, interconnectivity, diversity and interdependencies. In fact they are spatially distributed, i.e. they are usually constructed over a wide geographical area where communities they serve are dispersed, and because of this characteristic it is not practical to characterize all sites that lifeline systems cover with the same degree of detail. Moreover they are interconnected since customers and networks are interconnected through components as pipelines, roads, bridges etc. In fact damage to lifelines not only results in the physical impact and cost of repair at specific location, but also in the losses of connectivity and functionality throughout the network. All interconnected systems are characterized by critical links and their performance is influenced by the degree of physical and operational redundancy: systems with more redundant connectivity will perform better than less redundant systems. Another important aspect is represented by the degree of diversity of components that characterize each system.

Consider, for example a gas system. Many gas systems are composed by pipelines manufactured by steel, polyethylene, which have significantly different mechanical properties and perform differently under seismic load. Therefore properties as material, joint type, design procedures, degree of deterioration may influence performance of lifeline systems. Lifeline systems have also interdependencies, both by physical proximity and operational interactions. Damage to one lifeline system may affect other systems. For example loss of electricity can affect the flow pressure in the gas system or water system, a break in a water trunk line along a main street can block the traffic.

This thesis focuses on the seismic performance evaluation of gas distribution networks. The basic function of a gas system is to deliver gas from sources to costumers. A gas distribution system is essentially composed by pipelines, reduction stations, valves and demand nodes. Those systems are essentially located underground. As consequences, ground movements triggered by earthquakes in the form of transient ground deformation (TGD), caused by the passage of seismic waves (ground shaking) which is felt over a wide geographical area, and permanent ground deformation (PGD), caused by surface faulting, liquefaction, landslides which determine localized ground failure, have direct effects on the integrity of systems components and system performance. The earthquake safety of buried pipeline systems has attracted great attention in recent years since significant amount of damage was observed in pipelines after severe past earthquakes. In Table (1.1) information about four of the most severe earthquakes which have occurred in southern California are summarized; it provides data on earthquake characteristics (magnitude, intensity, epicentral location), portion of pipeline systems subjected to strongest shaking and general observations about gas transmission and distribution line response.

Building on the results from past international research projects, existing tools for the vulnerability assessment, and seismic risk analysis of lifelines systems, the SYNER-G project ("Systemic Seismic Vulnerability and Risk Analysis for Buildings, Lifeline Networks and Infrastructures Safety Gain"), has been funded by the European Commission (2009-2012) with the aim to address criticalities. In relation of the objectives of this project, this thesis had the aim to determine methodologies for the probabilistic seismic risk analysis of gas distribution networks and to apply these methods to a real gas network. In literature, there are very few studies on seismic risk analysis of networks that take into account all the aspects of the component of risk (hazard, vulnerability and loss). Moreover there are fewer studies that try to calibrate the analysis on a real system, making the study interesting for network operators.

Therefore to understand gas network performance during earthquakes, this thesis has been conducted in collaboration with Enel Rete Gas S.p.A. (http://www.enel.it/it-

IT/reti/enel_rete_gas/), which manages about 31.000 kilometers of local gas distribution networks in 1.200 Italian municipalities. In particular the gas distribution network operating in L'Aquila (central Italy) has been chosen as case study.

Table 1.1 Summary of major earthquakes in the area of the Southern California gas system (O'Rourke and Palmer, 1996)

Earthquake	Magnitude[1] / Intensity[2]	Location of Epicenter	Area Most Severely Affected	Gas Pipeline Performance
1933 Long Beach	M_L = 6.3 MM VIII - IX	5.6 km (3.5 mi) southwest of Newport Beach	Long Beach, Compton, and shore areas from Manhattan to Laguna Beach	Extensive damage to pipelines of Long Beach Municipal Gas Department, particularly areas of liquefaction
1952, 1954 Kern County	M_S = 7.7 MM VIII - X	40 km (25 mi) south of Bakersfield near Wheeler Ridge	Area of approximately 10,000 km (4000 mi^2) south of Bakersfield	Damage to several transmission lines within 10 to 25 km (6 to 16 mi) of Wheeler Ridge
1971 San Fernando	M_L = 6.4 MM VIII - X	13 km (8 mi) northeast of San Fernando	Area of approximately 520 km^2 (204 mi^2) around San Fernando	Serious damage to transmission and supply lines and disruption of service in San Fernando and Sylmar
1979 Imperial Valley	M_S = 6.6 MM VI - VII	3 km (1.9 mi) south of U.S.-Mexico border and 10 km (6.2 mi) from Mexicali	Imperial Valley from Brawley to Calexico and Holtville	No damage to transmission lines, although three transmission lines were crossed by surface ruptures along the Imperial fault. The lines were excavated for inspection and stress relief
1994 Northridge	M_S = 6.8 MM VIII - IX	North central portion of San Fernando Valley	San Fernando Valley, Sylmar, Santa Monica, and Fillmore	Damage to transmission pipelines and widespread disruption of distribution system

1.2. Objectives of this study

This thesis focuses on the seismic performance assessment of gas distribution systems. The overall objective is to develop a methodology for evaluating the seismic performance of gas distribution systems, investigating the different aspects that are involved. The process make use of probabilistic seismic hazard analysis, empirical relations to estimate pipeline response, fragility curves for the evaluation of reduction cabins vulnerability, performance indicators to characterize the functionality of the gas network. The thesis, in fact, has achieved this goal with special emphasis to the medium and low pressure network of a real system, namely the L'Aquila gas distribution system managed by ENEL Rete Gas s.p.a., for which not only detailed information on the network were retrieved , but also data related to damages occurred on the network followed the 2009 L'Aquila earthquake. A geographic information

system (GIS) database was developed containing most of relevant data on system component provided by the network operator, pipeline damage and strong motion data after 2009 L'Aquila earthquake. Moreover, the thesis rigorously includes the analysis of seismic hazard for gas systems (including geotechnical hazards), the analysis of vulnerability of system components, the analysis of systemic vulnerability in terms of performance measures, and probabilistic simulations for risk assessment.

1.2.1. Framework for seismic risk assessment of lifelines

A general framework for evaluating lifelines performance under seismic events is presented and described below with a particular focus on peculiarities characterizing gas distribution systems. For the quantification of seismic risk of spatially-distributed systems, there are several aspects that differ from the risk analysis of single structures. As shown in Fig. (1.1), where the most important differences (in green) respect to single structure seismic analysis are also reported, the evaluation of seismic risk for lifelines is not straightforward.

The first complication is in the hazard evaluation: it is based on large vector of ground motion-intensities (for all sites that describe the region where the system is located). Moreover earthquake characteristics at separate sites are neither perfectly dependent nor perfectly independent. Given an expected characteristic at each site (ground motion values conditional upon the earthquake), derivations from the expected values are correlated from site to site because of common source parameters and depending on the sites, perhaps a common propagation path and site conditions (Mc Guire, 2004). Dependencies among ground motion parameters at different sites imply the estimation of correlation models to use for the hazard assessment but since each component that characterizes the system may be sensitive to different ground motion parameters, the possibility of the existence of a cross-correlation between these parameters has also to take into account. Further, most of lifeline systems are located underground (e.g. water, gas and oil systems) and, as consequences, they are subjected to earthquake-induced effects such as liquefaction and landslides which potential for damage is very high due to the large deformations they impose on unburied systems.

Then, starting from the evaluation of seismic demand for each component, fragility analysis has to be computed. The most used and straightforward approach is based on empirical data collected throughout past earthquakes. In the case of pipeline components, the usual practice is to evaluate the repair rate as a unit length of pipe, with respect to a parameter representative of ground shaking or ground failure. For processing facilities, that include many subcomponents, a quantitative vulnerability assessment is quite difficult. A possible approach is to consider these facilities as

systems and to aggregate the fragility of each component into a global systemic vulnerability through the use of fault tree analysis.

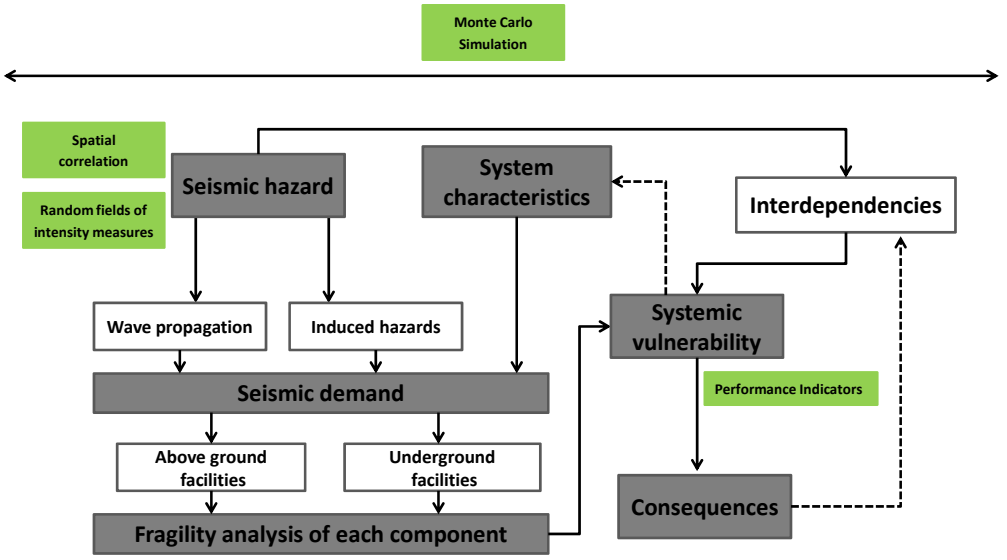

Figure 1.2 Framework for lifeline seismic risk assessment

Further system performance measures are used in order to evaluate the interaction between component response to earthquake and lifeline performance. Performance indicators provide a measure of the impact of the earthquake on the system functionality.

For the specific case of the gas network, the performance may be related to the capacity of the system to deliver gas with sufficient pressure to costumers; in this case hydraulic analysis is used to assess the overall system performance given the estimation of earthquake-induced damage at the component level. Since the link between the system component damage measures and the systemic vulnerability is usually not available in closed form, optimization procedures based on Monte Carlo simulations (MCS) based approaches, instead of analytical approaches are used: repeated simulations of network performance, each of which is based on randomly samples of hazard intensities and corresponding component status are performed in order to estimate in a probabilistic framework the systemic response of the lifeline system. Moreover an extra vulnerability could be considered when the failure of one element is dependent on the failure of elements in other networks: the damage disruption to the system may affect other networks (interdependencies) and vice versa because of physical proximity or operational interaction. For example gas network

depends on electricity because of compressor station backup system. At the same time power network depends on gas system for fuel production.

Finally, since lifeline systems are interwoven with the communities they serve, the engineering output of system response evaluation may be utilized in the social and economical impact evaluation by economist and social scientists in order to quantify earthquake effects in terms of business interruption and social consequences.

1.2.2. Seismic hazard characterization of L'Aquila gas network

An important objective of this work is to describe the characterization of seismic hazards of the L'Aquila region in order to evaluate the effects of earthquakes on the L'Aquila gas distribution network. To this aim probabilistic scenarios earthquakes have been generated in a regular grid covering the gas network using as source the Paganica fault on which L'Aquila (central Italy) 2009 earthquake was originated, computed for a characteristic earthquake of moment magnitude M_w 6.3 and occurrence rate of $\nu = 1/750$ (Pace *et al*., 2006). Strong ground motions, in terms of peak acceleration and velocity, are evaluated though a European ground motion prediction equation, and in order to model the spatial variability of these parameters, *ad hoc* spatial correlation models have been estimated and used for the simulation of probabilistic scenarios earthquakes. Site condition effects are followed according to the ground motion prediction equation based amplification factors. Moreover the PGD hazard has been integrated, in particular focusing on the effects induced by landslide, in order to estimate the seismic demand due to geotechnical hazard. In fact a process jointly developed by Department of Hydraulic Engineering, Geotechnical and Environmental and Department of Structural Engineering of University of Naples, "Federico II", the landslide potential of the region of interest, in terms of critical acceleration map, has been performed according to the HAZUS (FEMA, 2004) procedure.

1.2.3. System characterization of L'Aquila gas network

L'Aquila gas distribution network, operated by ENEL Rete Gas s.p.a., has been utilized as a test bed in this work. A process jointly developed with the network operator has allowed the characterization of the system, necessary for the evaluation of gas system seismic performance. A geographic information system (GIS) database was developed containing data on system physical and operational characteristics provided by the network operator. The system is connected to the high-pressure transmission lines (operated at a national level by SNAM, http://www.snamretegas.it) via three Metering/Pressure Reduction Stations, M/R Stations (Re.Mi. "Regolazione e Misura"

stations, in Italian) providing gas to about 42300 customers in five municipalities (L'Aquila, Lucoli, Tornimparte, Ocre, Rocca di Cambio e Rocca di Mezzo). The distribution system is made of 621 km of pipes: 234 km of pipes operating at medium pressure (2.5 – 3 bar), and the remaining 387 km with gas flowing at low pressure (0.025 – 0.035 bar) and it also consists of Metering/Pressure reduction stations (M/R stations), Reduction Groups and demand nodes. The knowledge of physical and operational characteristics of the system has allowed the evaluation of the seismic behavior of all components that has been also compare with data resulting from the analysis of the damages occurred on the gas network following the 6th April L'Aquila earthquake.

1.2.4. System performance evaluation of L'Aquila gas network

The methodology presented has been tested via the implementation of the case study in the OOFIM software developed in a Matlab environmental (Mathwork, 2010) by the University of Rome "La Sapienza". The software, created in relation of the objectives of the Syner-G project, adheres to the OBJECT-ORIENTED Paradigm (OOP) where the problem is described as a set of objects, "software containers" grouping together related procedures and data. Data elements are called attributes of an object. Procedures which operate on data specific for an object are called methods. Objects are instances (concrete realizations) of classes (abstract models) that are used to model the system. In the context of modeling the gas distribution network, the system is represented as a graph with nodes and links as elementary components. For the purpose of the thesis the programme has been equipped with the *GAS* class including attributes and methods, in order to evaluate seismic performance of the L'Aquila network.

1.3. Outline of the thesis

This thesis is divided in five chapters, the first of which presents introductory comments on lifeline seismic risk assessment.

Chapter 2 describes the general process to characterize seismic hazard of gas networks and how to determine seismic demand for each system component. In particular, detailed information on characterization of wave propagation and PGD hazards are presented. Wave propagation hazard is characterized by random fields of intensity measures that can be estimated though ground motion prediction equations (GMPEs) that provide the mean value conditional on a set of explanatory variables describing the earthquake source, wave propagation path and local geological conditions, and spatial correlation models that characterize the spatial variability of

these parameters. Since correlation models available in literature have been estimated starting from dense observations of different earthquakes outside Europe, in order to characterize spatial correlation fields for the case study, spatial models have been estimated for different intensity measures (peak ground acceleration, peak ground velocity, spectral acceleration) using the European Strong-Motion Database (ESD) and the Italian Accelerometric Archive (ITACA) through the use of geostatistical tools. Moreover since the performance of spatially distribute systems may be conditional upon the failure of many components within the system, each of which is sensitive to different intensity measures (IMs), the possibility of the existence of a cross-correlation between IMs has been taken into account through the use of the conditional hazard. This technique starts from the assumption that two IMs considered are jointly distributed according to a bivariate Gaussian distribution, and it has the advantage to avoid making assumptions about the structure of the cross correlation between the two IMs.

Geotechnical hazards induced from earthquakes have been the subject of a considerable amount of researches in the last decades. Their potential for damage is very high since they impose large deformation on pipeline systems. The principal forms of permanent ground deformation are surface faulting, landsliding, seismic settlement and lateral spreading due to soil liquefaction. There are many models available in literature that have the intent to relate the degree of deformation (PGD) and the probability of occurrence of each geotechnical hazard to the strength of ground motion but the main limiting factor of many models is the requirement of very detailed geotechnical data that could make difficult the implementation of these models for many lifeline systems. Therefore the use of simpler models that may be implemented in the widest variety of applications has been taken into account to characterize the geotechnical hazard potential of L'Aquila region.

Chapter 3 focus on the system characterization and fragility analysis of gas distribution system components. In particular, fragility curves provide the probability of failure of a component as a function of an intensity measure. Unfortunately, for gas systems, there are no exhaustive studies in the literature on seismic behavior of all components. Therefore to this aim, seismic vulnerability of some components characterizing the L'Aquila gas network has been investigated through the use of fault tree analysis. Moreover fragility curves available in literature have been validated through an analysis of the damages occurred on the gas network following the 6th April L'Aquila earthquake by processing technical reports from Enel Rete Gas describing the repairs and replacements activities following the seismic event.

After evaluating the interaction between seismic demand and the component response, system performance assessment proceeds to system integration, in which performance is evaluated according the functionality and the serviceability of the entire network. More specifically, in **Chapter 4** different performance indicators (PIs) are introduced in order to provide a measure of the impact of the earthquake on the system functionality.

Chapter 5 summarizes the process for seismic performance evaluation of L'Aquila gas system and presents the probabilistic results. For the case study, a GIS database was developed; it containing most of relevant data on system component provided by the network operator, pipeline damages and strong motion data during 2009 L'Aquila earthquake developed during this research. L'Aquila region has been characterized both in terms of TGD hazard and PGD hazard and system response simulations have been performed utilizing a specific software developed in a Matlab environmental (Mathwork, 2010).

Chapter 2 – GAS NETWORKS HAZARD CHARACTERIZATION

2.1. Introduction

Seismic performance evaluation of gas networks requires as first step the seismic hazard characterization affecting the system. The traditional approaches for seismic hazard evaluation at a particular site are essentially two: the probabilistic approach and the deterministic approach. In deterministic seismic hazard analysis, DSHA, (Reiter, 1991), a particular earthquake scenario is assumed and the hazard is computed respect to the single selected earthquake. Probabilistic seismic hazard analysis, PSHA, (Cornell, 1968) instead, considers explicitly the uncertainties (e.g. in earthquake size, location, time of occurrence) evaluating the effects of all possible earthquakes that can affect the site of interest.

The hazard analysis, regardless of deterministic or probabilistic, starts with identification and evaluation of earthquake sources. Then a recurrence relationship, which specifies the average rate at which an earthquake of some size will be exceeded during a specified period of time, is used to characterize seismicity of each source zone. Earthquake effects are then estimated computing the level reached by one or more parameters used to characterize the ground motion. Generally, this goal is pursued using ground motion prediction equations (GMPEs) that express the selected ground motion parameter as function of all the effects that can modify its value (e.g. the seismic source, the magnitude and site effects). Finally, PSHA combines the uncertainties evaluating the effects of all selected earthquakes of different size, occurring at different locations inside the sources with different probabilities of occurrence to obtain the "hazard curve" (Fig. 2.1) that shows the probability that the ground motion level will be exceeded during a particular time period at the site of interest. Therefore for each earthquake source, the hazard integral λ represents the mean frequency of exceedance of a specific value of a ground motion intensity measure denoted IM (e.g. peak ground acceleration, PGA) in a specific site calculated as in Eq. (2.1):

$$\lambda = \nu \cdot \int_M \int_R P\left[IM > im^* \mid M, R \right] \cdot f_{M,R}\left(m, r\right) \cdot dm \cdot dr \tag{2.1}$$

where $f_{M,R}(m,r)$ is the joint distribution of magnitude and distances referred to a particular seismic source , ν is the rate of occurrence of earthquakes on it and $P\left[IM > im^* \mid M, R \right]$ is a conditional probability that, for a given magnitude-distance couple, gives the probability of exceeding the level of the selected intensity measure and it is generally calculated via a GMPE. Under the basic assumption of a Poissonian model for the characterization of the temporal occurrence of the earthquakes, the exceeding probability *P* of the selected range of values of an IM for a time period *t* can be expressed by Eq. (2.2):

$$P = 1 - \exp\left(-\lambda \cdot t\right) \tag{2.2}$$

On the other side, for a given time period, the hazard map shows the values of the selected IMs that have the same exceeding frequency evaluated though PSHA for all points in the map.

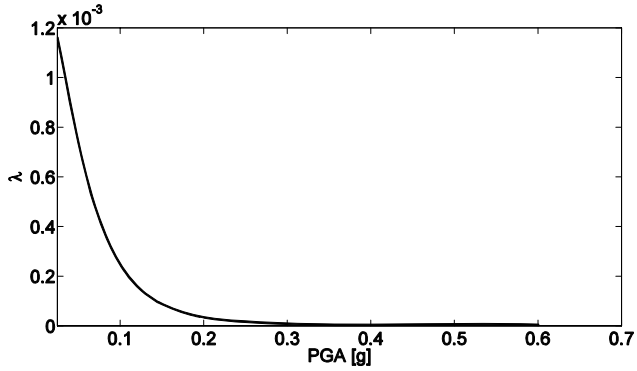

Figure 2.1 Hazard curve: frequency of exceeding the level of the selected intensity measure (i.e. PGA expressed in g) in a specific site

For a single structure, numerical integration is sufficient to evaluate λ. For a group of sites or for a facility that extends over a large area (such as a gas network) a more sophisticated hazard analysis is required since it is based on a large vector of ground motion intensities. The scalar value IM in Eq. (2.1) is replaced by a vector of IMs which adds complexity to the integral. Moreover ground motion intensities also shown spatial statistical correlation (i.e. dependencies between IMs as function on inter-separation distance), which needs to be modeled and incorporated into the hazard integral (Crowley and Bommer, 2006; Park *et al*., 2007). Considering for example a region discretized in *n* sites in which there is a seismic source (characterized by the rate of occurrence ν); the hazard integral of Eq. (2.3) provides such annual rate of joint

exceedance in a region, if the same assumptions of site-specific hazard analysis are retained (McGuire, 2004).

$$\lambda = \nu \cdot \int_{M} \int_{\bar{R}} P\left[IM_1 > im^*, ..., IM_n > im^* \mid M, \bar{R} \right] \cdot f_{M,\bar{R}}\left(m, \bar{r}\right) \cdot dm \cdot d\bar{r} \tag{2.3}$$

where $f_{M,\bar{R}}(m,\bar{r})$ is the joint distribution of magnitude and distances referred to the seismic source, and $P\left[IM_1 > im^*, ..., IM_n > im^* \mid M, \bar{R} \right]$, the term affected by spatial correlation, is the conditional probability that the same[1] *im** threshold is exceeded at the *n* sites in which the region is discretized and whose distances from the source are represented by the vector $\bar{R} = \{R_1, ..., R_n\}$ (the integral is conventionally written as if it was a scalar). The complexity of the integral, growing with the number of sites of interest, makes difficult to evaluate seismic hazard though numerical integration. Hence, many past research works use Monte Carlo simulation (MCS)-based approaches instead of analytical approaches (Bazzurro and Luco, 2005; Crowley and Bommer, 2006) where possible future earthquakes are probabilistically simulated in the region of interest, considering all possible scenarios that could occur, and use them for the loss assessment. This approach has the advantages of including in a simple way spatial correlation among sites to evaluate lifeline loss exceedance curves (Jayaram and Baker, 2009b).

In the case of gas networks, another important aspect to consider in seismic hazard analysis is that the presence of buried components (i.e. pipelines) implies the consideration of two types of hazard: wave propagation hazard and permanent ground deformation hazard (O'Rourke and Liu, 1999) as shown in Fig. (2.2). The earthquake-induced ground motion deforms the ground and affects the system by transient and permanent ground deformation. Wave propagation hazard is characterized by the transient strain and curvature in the ground due to travelling wave effects. Permanent ground deformation (PGD) hazards (such as landslide, liquefaction induced lateral spread and seismic settlement) are characterized by the amount, geometry and spatial extent of the PGD zone. The fault-crossing PGD hazard is characterized by the permanent horizontal and vertical offset at the fault and the pipe-fault intersectional angle. Damage on the network may be caused by TGD or PGD or a combination of two. The relative impact of different effects on buried pipelines varies from earthquake to earthquake. Transient effects are common to all earthquakes and are felt over a wide geographical area and associate pipeline damage rate (in terms of breaks

[1] This is only a possible criterion and others are possible.

per unit length of pipe) are low but the number of pipe breaks may be relatively high. PGD damage typically occurs in isolated and localized areas with high damage rates.

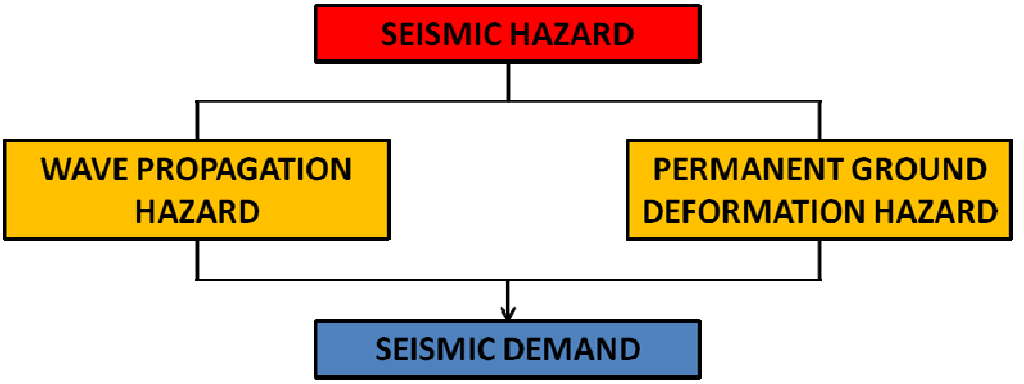

Figure 2.2 Framework for gas networks hazard characterization

This chapter describes the general process to characterize seismic hazard of gas networks and how to determine seismic demand for each system component. In particular, detailed information on characterization of wave propagation and PGD hazards are presented.

2.2. Wave propagation hazard

When an earthquake occur, seismic waves radiate away from the source to the ground surface and travel rapidly though the earth's crust. Reaching the surface, seismic waves produce shaking which strength and duration depends on the size and location of the earthquake and on the characteristics of the site. In fact although seismic waves travel through the rock for the majority of their trip from the source to the ground surface, the final part of the trip is through soil, which characteristics may influence the nature of shaking at the ground surface. The soil tends to act as a "filter" to seismic waves attenuating or amplifying the motion. Since soil conditions over short distances, levels of ground shakings may vary dramatically also within a small area.

The ground shaking felt at a given location will be made up of a combination of body waves and surface waves. Body waves propagate through earth and they are generating by seismic faulting while surface waves travel along the ground surface and in most of cases are generated by the reflection and refraction of body waves. Body waves (Fig. 2.3) include compressional waves (P-waves) where the ground moves parallel to the direction of propagation, and shear waves (S-waves) where the ground moves perpendicular to the direction of propagation; moreover depending on

the direction of particle movement, S-waves can be divided in SV (vertical plane movement) and SH (horizontal plane movement). Surface waves (Rayleigh and Love waves, Fig. 2.4), instead, are more complex: for Rayleigh waves the particle motion traces a retrograde ellipse in a vertical plane with the horizontal component of motion being parallel to the direction of propagation; for the Love waves, the particle motion is along a horizontal line perpendicular to the direction of propagation.

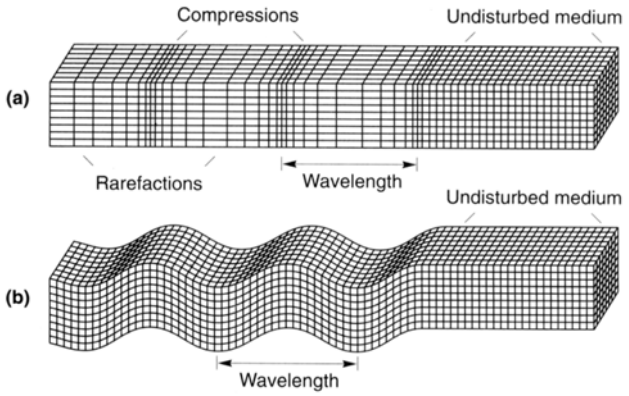

Figure 2.3 Deformations produced by body waves: a) P- waves b) S-V waves (Kramer, 1996)

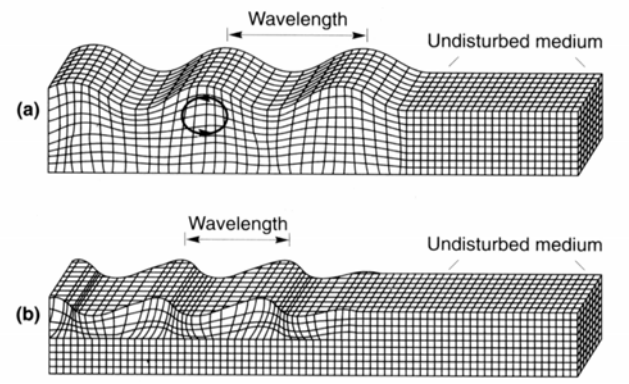

Figure 2.4 Deformations produced by surface waves: a) Rayleigh waves b) Love waves (Kramer, 1996)

The amplitude of ground motion reduces with distance from the source of seismic energy release. This is due to a combination of geometric attenuation, which accounts for the spread of the wavefront as it moves away from the source, and anelastic attenuation, which is caused by material damping. In the immediate locality of the fault rupture, body waves will dominate the motion while ground motion at large distances to the source is generally dominated by surface waves because of the

geometric attenuation is different for the two types of waves (Tromans, 2004): assuming that the earthquake rupture zone may be represented as a point source and R is the distance from the rupture zone, the amplitude of body waves decreases in proportion to $1/R$, while the amplitude of surface waves decreases in proportion to $1/\sqrt{R}$.

Both types of waves are of interest when considering the response of buried pipelines to seismic ground shaking. S-waves are normally considered more hazardous to buried pipelines as they carry more energy than P-waves while, in the case of surface waves, R-waves are the most important, inducing axial strains in buried pipelines of much more significance than the bending strains induced by L-waves (O'Rourke and Liu, 1999).

In order to describe the most important characteristics of strong motion in quantitative form different ground motion parameters may be used. The motion parameter may be acceleration, velocity or displacement. Typically, one of those quantities is measured directly and the others computed from it by integration and/or differentiation. The most commonly used amplitude parameter is the horizontal component of PGA. Horizontal accelerations have been commonly used to describe ground motion because of their relationship with inertial forces; indeed, the largest dynamical forces induced in some types of structures (i.e. stiff structures) are closely related to PGA. The horizontal component of peak ground velocity (PGV) is another useful parameter for characterization of ground motion amplitude. Since the velocity is less sensitive to the higher frequency component of ground motion (Kramer, 1996), PGV is more likely than PGA to characterize ground motion amplitude accurately at intermediate frequencies. Therefore for structures or facilities that are sensitive to loading in this intermediate frequencies ranges (e.g. bridges), PGV may provide an accurate indication of the potential of damage than the PGA. Horizontal component of peak ground displacements (PGD_i) are related more to the low-frequency content of strong ground motion. Due to the signal processing errors in the filtering and in the integration of accelerograms and by the presence of long-period noise, the reliability of displacements in characterizing aspects of the ground motion is significantly limited. For earthquake engineering applications, duration and frequency content are other important strong motion characteristics. Duration of strong ground motion often influences the level of earthquake damage. In the presence of certain ground conditions (e.g. liquefiable deposits), repeated stress or load cycles of moderate amplitude, over an extended period, can cause more damage than higher amplitude motion over a shorter period. Moreover frequency content of input motion highly influences response of structures to earthquakes. The Fourier amplitude spectrum of

strong ground-motion shows how the amplitude of the motion is distributed with frequency (or natural period) while the response spectrum describes the maximum response of a single-degree-of-freedom (SDOF) system to a given input motion as a function of the natural frequency (or natural period) and damping ratio of the SDOF system. Response and Fourier spectra can be expressed in terms of displacement, velocity and acceleration. More details on those parameters can be found in Kramer (1996).

Usually, in the area of lifeline earthquake engineering, the wave propagation hazard is characterized by the peak amplitude of ground motion parameters as well as the ground strain (O'Rourke and Liu, 1999). In particular, ground strain, which is closely related to PGV, controls the behavior of buried pipelines, while facilities are more sensitive to PGA. Different ground motion parameters are therefore appropriate for different types of structure.

As it will be explained in the following sections, those parameters can be estimated through GMPEs that describe, in a very simplified way, how the ground motion decreases from the seismic source to the surface.

2.2.1. Seismic zone characterization

The first step in performing seismic hazard analysis is the identification and the characterization of seismic sources that can affect the site of interest. There are two general types (McGuire, 2004):

- Area sources: areas within for which future seismicity is assumed to have distributions of source properties and locations of energy release that do not vary in time and space.
- Fault sources: are faults or zones for which the tectonic features causing earthquakes have been identified. These are usually individual faults, but they may be zones comprising multiple faults or regions of faulting if surface evidence is lacking but the faults are suspected from evidence (e.g. seismicity patterns).

In the probabilistic approach to the seismic hazard, each zone is considered as a configuration within it is assumed that earthquakes occur at the same rate with respect to size or magnitude regardless of the location (i.e. uniform seismicity rates).

Once the geometrical configuration is assigned, for each zone, a recurrence relationship is required. This relation indicates the chance of an earthquake of a given size occurring anywhere inside the source during a specified period of time. Most applications of seismic hazard analysis use the exponential probability distribution to

represent the relative frequency of different earthquake magnitudes since his function allows considerable analytical convenience in the hazard calculations (Mc Guire, 2004); the most used recurrence law is the one proposed by Gutenberg and Richter (1954) which expresses the cumulative number of earthquakes with a magnitude greater than a fixed one as in Eq. (2.4):

$$\log_{10} n(m) = a - b \cdot m \tag{2.4}$$

where n is the number of earthquakes of magnitude m or grater per unit of time, and a and b are constants.
For seismic hazard analysis, this is usually expressed in the equivalent form:

$$n(m) = \nu \cdot \exp(-\beta \cdot m) \tag{2.5}$$

where $\nu = 10^a$ is the number of earthquakes per unit of time with $m \geq 0$ (seismicity rate), and $\beta = b \cdot \ln(10)$. Those parameters are usually estimated though historical seismicity. The general formulation of the Gutenberg-Richter recurrence law covers an infinite range of magnitudes, but often a lower and un upper-bound, $m_{\min}$ and $m_{\max}$ respectively, are used resulting in a truncated exponential distribution for magnitude frequency. The minimum magnitude is generally linked to the fact that not all the earthquakes can produce damages to the structures and a threshold on the magnitude is thus fixed. The selection of the maximum magnitude is more complicate because it is generally estimated by using geologic evidence, geophysical data, analogies to similar tectonic regimes, or other methods (Mc Guire, 2004).

Alternative magnitude distributions other that the truncated exponential distribution are available for modeling earthquake magnitudes as Characteristic Magnitude Distribution. This distribution is used when continuous distributions encompassing all magnitudes are not appropriate. Large earthquakes may occur with a characteristic magnitude whose frequency of occurrence is higher than obtained extrapolating from the smaller magnitude earthquakes. In any case, the best distribution to adopt depends on which magnitudes are most critical for the seismic hazard analysis and which ones therefore influence the seismic risk mitigation decision.

2.2.2. Ground motion estimation

Traditionally, ground motion is modeled, for engineering purposes, via GMPEs, which provide probabilistic distribution of the chosen IM (the predicted variable characterizing the level of shaking) conditional on a set of explanatory variables

describing the earthquake source, wave propagation path and local geological conditions. GMPEs are obtained by regression of recorded data from historical events and they are the oldest estimates in seismic hazard analysis, dating from the 1960s. Explanatory variables usually include the earthquake magnitude, factors describing style of faulting, a measure of source to site distance, and parameters describing site classes; other factors that are known to influence the motion are not included in the equation because of lack of information in advance. For the factors considered in the equations, the general formulation of a GMPE generally have a simple mathematical expression compared to the complexity of the physical process involved in ground motion generation and propagation. They typically have the following type form as in Eq. (2.6):

$$\log Y = \overline{\log Y}\left(M, R, \underline{\theta}\right) + \varepsilon \tag{2.6}$$

where Y denotes the IM of interest; $\overline{\log Y}\left(M, R, \underline{\theta}\right)$ is the mean of the logs conditional on parameters such as magnitude (M), source-to-site distance (R), and others $\left(\underline{\theta}\right)$; the difference between the observed and the predicted ground motion is the ground motion residual ε that represents the unexplained part of the model. Coefficients of GMPEs are usually estimated though nonlinear least-square regression analysis but the implicit nature of earthquake data violates many assumptions of this approach (Mc Guire, 2004). In fact observations of *Y* are not independent: multiple records are used from the same earthquake and these are correlated by common source and path, while multiple records from the same site but different events are correlated by common soil conditions.

The inclusion of correlation among observations from common earthquake can be handled more efficiently using the random effects model (Brillinger and Priesler, 1985; Abrahamson and Youngs, 1992): this is an iterative procedure that requires the numerical solution of a likelihood function within the iteration, but it gives ground motion estimates that include the variance attributable to the random effect caused by earthquake-to earthquake variability. In particular the residual is expressed as the sum of two components: an interevent term, which is constant for each earthquake (common for all sites) and represents average source effects not explicitly appearing in the model covariates, and an intraevent term representing the site-to-site variability of the IM (Strasser *et al*., 2009).

Therefore for a particular site *p* and earthquake *j* the logs of ground-motion intensities and related heterogeneity may be expressed as in Eq. (2.7).

$$\log Y_{pj} = \overline{\log Y_{pj}}\left(M, R, \underline{\theta}\right) + \eta_j + \varepsilon_{pj} \tag{2.7}$$

where η_j denotes the interevent residual, which is a constant term for all sites in a given earthquake and represents a systematic deviation from the mean of the specific seismic event (i.e. average source effects not explicitly appearing in the model covariates); and ε_{pj} is the intraevent variability of ground motion. Residuals ε_{pj} and η_j are usually assumed to be independent random variables, normally distributed with zero mean and standard deviation σ^2_{intra} and σ^2_{inter}, respectively. Then, $\log Y_{pj}$ is modeled as a normal random variable with mean $\overline{\log Y_{pj}}\left(M, R, \underline{\theta}\right)$ and standard deviation, σ_T, where $\sigma^2_T = \sigma^2_{intra} + \sigma^2_{inter}$. Appropriately plugging this distribution into the probabilistic seismic hazard analysis leads to the distribution of the IM at the site of interest (McGuire, 2004).

2.2.3. Spatial correlation models for peak ground motion parameters

In recent research, it was demonstrated that another form of correlation may exists among residuals beyond the correlation due to the source effects not explicitly appearing in GMPEs. Boore *et al*. (2003) demonstrated that intraevent residuals, for example those referring to peak ground acceleration (PGA), are spatially correlated[2]. In fact the ground-motion intensities at two sites generated from the same earthquake are expected to be correlated for a variety of reasons, such as a common source earthquake, similar locations to fault asperities, similar seismic travel path from the source; moreover similar site conditions and very simple schemes used in GMPE for example to characterize site classes may cause a correlation among intraevent residuals. Therefore, IMs at different sites result correlated both because of inter- and intraevent residuals, and it is important to account for these dependencies in seismic risk assessment when a region is of concern (Crowley and Bommer, 2006; Park *et al*., 2007; Goda and Hong, 2008b, Crowley *et al.,* 2008).

Several correlation models are available in the literature, which depend uniquely on inter-site separation distance. Most of the studies are based on dense observations of single events (e.g., Boore *et al*., 2003; Wang and Takada, 2005; Jayaram and Baker,

[2] This kind of spatial correlation of ground motion consists of similarity between IMs (e.g., peak values of time-history) observed at different sites within the same event. It is also worth to mention here *coherency* of ground motion signals, which represents the similarity of ground motion in frequency domain, and describes the degree of positive or negative correlation between amplitudes and phases angles of two time histories at each of their component frequencies (e.g., Zerva and Zervas, 2002).

2009a) from different major earthquakes outside Europe, such as Northridge (1994) or Chi-Chi (1999). A few works have, instead, combined data from multiple events to obtain a unique estimate of correlation (e.g., Goda and Hong; 2008a, Goda and Atkinson, 2009; Goda and Atkinson, 2010; Sokolov *et al*., 2010).Different authors, for a given IM, provide different distance limits for correlation to disappear (i.e., distance beyond which IMs may be considered uncorrelated), and this is supposed to depend on the dataset considered, the GMPE chosen to compute residuals, and the working assumptions of the estimation. For example, Goda and Atkinson (2009) investigated the effects of earthquake types (i.e., shallow and deep events) on correlation using datasets from K-NET and KiK-net Japanese strong motion networks without finding any significant dependency. On the other hand, Sokolov *et al*. (2010), starting from the strong-motion database of Taiwan Strong Motion Instrumentation Program (TSMIP) network in Taiwan, estimated correlation for various areas, site classes and geological structures, asserting that a single generalized spatial model may not be adequate for all of Taiwan territory. In some cases (e.g., Wang and Takada, 2005; Jayaram and Baker, 2009a) existing GMPEs are used, while, in others (e.g., Goda and Hong, 2008a; Goda and Atkinson, 2009; Sokolov *et al*., 2010), *ad hoc* fit on the chosen dataset is adopted. Generally, regressions analysis used to develop prediction equations does not incorporate the correlation structure of residuals as an hypothesis. Hong *et al*. (2009) and Jayaram and Baker (2010a), evaluated the influence of considering the correlation in fitting a GMPE, finding a minor influence on regression coefficients and a more significant effect on the variance components. Goda and Atkinson (2010) investigated the influence of the estimation approach, emphasizing its importance when residuals are strongly correlated.

In Fig. (2.5), several models for PGA and PGV, as mentioned above, are shown; the correlation coefficient is expressed by Eq. (2.8), where *a*, *b* and *c* are the model parameters (to follow) and *h* is the inter-site separation distance (in km).

$$\rho(h) = \max\left\{(1\text{-}c) + c \cdot \mathrm{e}^{-a \cdot \mathrm{h}^{b}}, 0\right\} \tag{2.8}$$

If the hazard assessment at two or more sites is of concern, the joint probability density function (PDF) for the IMs at all locations is required. A simple way to model for the joint PDF of the IM, conditional on the GMPE covariates, is the multivariate normal (e.g., Jayaram and Baker, 2008). It is assumed that the logs of IM form a Gaussian random field (GRF), defined as a set of random variables $\log\left[IM(\mathbf{u})\right]$, one for each site $\mathbf{u}$ in the study area $S \in R^2$, $\left\{\log\left[IM(\mathbf{u})\right], \forall \mathbf{u} \in S\right\}$. To any set of *n* sites

$\mathbf{u}_p$, $p=1,\ldots,n$, corresponds to a vector of n random variables that is characterized by the covariance matrix, $\boldsymbol{\Sigma}$, as in Eq. (2.9) where the first term produces perfectly correlated inter-event residuals (Malhotra, 2008), while the second term (symmetrical) produces partially correlated intraevent residuals.

$$\boldsymbol{\Sigma} = \sigma^2_{inter} \cdot \begin{bmatrix} 1 & 1 & \cdots & 1 \\ 1 & 1 & \cdots & 1 \\ \vdots & \vdots & \ddots & \vdots \\ 1 & 1 & \cdots & 1 \end{bmatrix} + \sigma^2_{intra} \cdot \begin{bmatrix} 1 & \rho_{12} & \cdots & \rho_{1n} \\ \rho_{21} & 1 & \cdots & \vdots \\ \vdots & \vdots & \ddots & \vdots \\ \rho_{n1} & \rho_{n2} & \cdots & 1 \end{bmatrix} \tag{2.9}$$

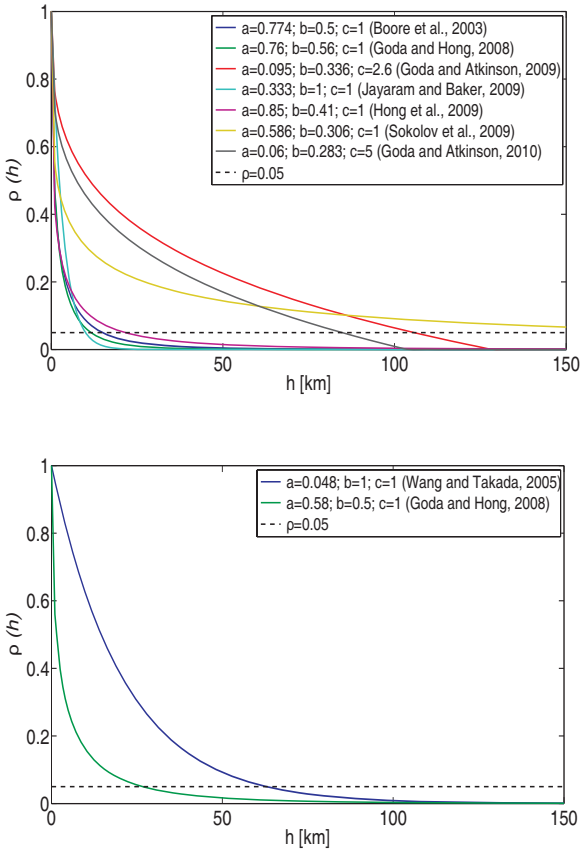

Figure 2.5 Some correlation models available in literature for PGA (up) and PGV (down) the black dotted line intersects the curves at the distance at which the correlation is conventionally considered as almost, lost being the correlation coefficient equal to 0.05

In Eq. (2.9), the correlation is heterogeneous as it depends on the pairs of sites considered, and the intra-event variance is homoscedastic as it is constant for all sites

(this assumed in most of GMPEs, although some studies have found dependence of intraevent variability on distance, magnitude and non-linear site effects; Strasser *et al*., 2009). If the spatial correlation for intraevent residuals is a function of the relative location of sites, it becomes as in Eq. (2.10), where *p* and *q* are two locations at the ends of $\mathbf{h_{pq}}$ (the separation vector between the two sites).

$$\rho_{pq} = \rho\left(\mathbf{h_{pq}}\right) \tag{2.10}$$

To briefly review the features of a GRF, let $\mathbf{u_p} \in R^2$ be the generic site in a two-dimensional Euclidian space and suppose that the intra-event residuals in a specific earthquake, $\varepsilon_j\left(\mathbf{u}_p\right) = \varepsilon_{pj}$, is a GRF in a domain $S \in R^2$ (the region of interest). The GRF is fully described by the mean $E\left[\varepsilon_j(\mathbf{u})\right]$ and the covariance, *Cj,* between two generic locations $\mathbf{u_p}$ and $\mathbf{u_q}$ defined in Eq. (2.11).

$$C_j(\mathbf{u}_p, \mathbf{u}_q) = E\left[\varepsilon_j(\mathbf{u}_p)\cdot\varepsilon_j(\mathbf{u}_q)\right] - E\left[\varepsilon_j(\mathbf{u}_p)\right]\cdot E\left[\varepsilon_j(\mathbf{u}_q)\right] \tag{2.11}$$

Under the hypothesis of second-order stationarity of the GRF (Cressie, 1993), the mean is constant and the covariance is location-independent as defined in Eq. (2.12).

$$C_j(\mathbf{h}) = E\left[\varepsilon_j(\mathbf{u})\cdot\varepsilon_j(\mathbf{u}+\mathbf{h})\right] - E\left[\varepsilon_j(\mathbf{u})\right]\cdot E\left[\varepsilon_j(\mathbf{u}+\mathbf{h})\right] \tag{2.12}$$

In this case, the two points' statistics depend only on the separation vector **h** and the reference to a particular location **u** can be dropped. Herein it is assumed intra-event residuals may be modeled as a stationary GRF, and all data available from different earthquakes and regions, therefore deemed homogeneous, are used to fit a unique model. If the GRF is isotropic correlation depends only on the separation distance h = ||**h**||. An anisotropic random field implies, instead, the possibility of having a spatial variability that depends on the direction considered. Past research has shown that the hypothesis of isotropic random field, which is also retained herein, is reasonable (Wang and Takada, 2005; Jayaram and Baker, 2009a).

2.2.3.1. Geostatistical analysis

A common tool to quantify spatial variability of random fields is the semivariogram, $\gamma_j(h)$. It measures the average dissimilarity between georeferenced data, and it is used to model the covariance structure of GRF through suitable functions. Under the hypothesis of second-order stationarity and isotropy it is defined as in Eq. (2.13).

$$\gamma_j(h) = \frac{1}{2} Var\left[\varepsilon_j(\mathbf{u}+h) - \varepsilon_j(\mathbf{u})\right] = Var\left[\varepsilon_j(\mathbf{u})\right] - C_j(h) \tag{2.13}$$

Therefore, for an isotropic and homogenous random field, considering that for $h \to 0$, $C_j(h) = Var(\varepsilon_j)$ the semivariogram results as in Eq. (2.14),

$$\gamma_j(h) = C_j(0) - C_j(h) = Var(\varepsilon_j) \cdot \left[1 - \rho_j(h)\right] \tag{2.14}$$

where $\rho_j(h)$ denotes the spatial correlation coefficient between $\varepsilon_j(\mathbf{u}+h)$ and $\varepsilon_j(\mathbf{u})$; see Cressie (1993) for more details.

In fact, estimation of correlation usually develops in three steps: (1) computing the empirical semivariogram (assuming a common semivariogram for different events, that is, invariant through earthquakes, allows to neglect the subscript *j* in the following equations); (2) choosing a functional form; (3) estimating the correlation parameters by fitting the empirical data with the functional model.

Empirical semivariograms are computed as a function of site-to-site separation distance, with different possible estimators. The classical estimator is the method-of-moments (Matheron, 1962) which is defined for an isotropic random field in Eq. (2.15),

$$\hat{\gamma}(h) = \frac{1}{2 \cdot |N(h)|} \cdot \sum_{N(h)} \left[\varepsilon(\mathbf{u}+h) - \varepsilon(\mathbf{u})\right]^2 \tag{2.15}$$

where N(h) is the set of pairs of sites separated by the same distance h, and $|N(h)|$ is the cardinal of N(h).

To compute the semivariogram, it may be useful, when dealing with earthquake records, to define tolerance bins around each possible h value. The selection of distance bins has important effects: if its size is too large, correlation at short distances may be masked; conversely if it is too small, empty bins, or bins with samples small in size, may impair the estimate. A rule of thumb is to choose the maximum bin size as a half of the maximum distance between sites in the dataset, and to set the number of bins so that there are at least 30 pairs per bin (Journel and Huijbregts, 1978).

The method-of-moments estimator is unbiased; however it can be badly affected by atypical observations (Cressie, 1993). Therefore, Cressie and Hawkins (1980) proposed a more robust estimator (less sensitive to outliers), as in Eq. (2.16).

$$\hat{\gamma}(h)=\frac{1}{2}\left\{\left[\frac{1}{|N(h)|}\sum_{N(h)}\left|\varepsilon(\mathbf{u}+h)-\varepsilon(\mathbf{u})\right|^{0.5}\right]^{4}\Bigg/\left(0.457+\frac{0.494}{|N(h)|}\right)\right\} \tag{2.16}$$

The fitting analytical model, under stationary and isotropic hypotheses, may be of different kinds, for example, exponential, Gaussian, or spherical (Goovartes, 1997). In particular, the exponential model, which is the most common one, is described in Eq. (2.17) where c_0 is defined as the nugget, and represents the limit value of the semivariogram when h is zero because of variations at distances smaller than the sampling interval and measurement errors, which causes a discontinuity at the origin (Matheron, 1962); c_e is the sill, or the population variance of the random field (Barnes, 1991); and b is the range defined as the intersite distance at which $\gamma(h)$ equals the sill. For the exponential model, the sill is asymptotic and it is possible to define a practical range as the separation distance at which $\gamma(h)$ equals 95% of the sill.

$$\gamma(h)=c_0+c_e\cdot\left(1-e^{-3\cdot h/b}\right) \tag{2.17}$$

The goodness of fit of a model can be determined via several criteria that have been proposed in the geostatistical literature. Studies dealing with earthquake data sometimes use visual or trial and error approaches in order to appropriately model the semivariogram structure at short site-to-site distances (Jayaram and Baker, 2009a). In this thesis experimental semivariograms are fitted visually, although using the least squares estimation as a starting point (to follow).

2.2.3.2. Semi-empirical models based on multi-event European datasets

The estimation of the correlation starts from the characterization of residuals of empirical data with respect to a GMPE. To this aim, subsets of the European Strong-motion Database and the Italian Accelerometric Archive datasets were considered. The ground motions and related information were provided by authors of Akkar and Bommer (2010) and Bindi *et al.* (2010) GMPEs for ESD and ITACA datasets, respectively. In particular, subsets of data used to fit these GMPEs; i.e., only free field records from earthquakes for which more than one record was available have been considered.

ESD subset is comprised of 480 records from 87 events recorded between 1973 and 2003, and characterized by moment magnitude from 5 to 7.6, and the closest horizontal distance to the vertical projection of the rupture (i.e., Joyner-Boore distance, R_{jb}) from 0 to 100 km. The number of considered recordings for the ITACA

subset is 1112 from 162 events over the 4-6.9 magnitude range (moment or local), and R_{jb} up to 196 km. Characteristics of the datasets, with respect to explanatory variables of the considered prediction equations (magnitude, distance and local site conditions) are shown in Fig. (2.6). ESD is a smaller database of stronger and closer to the source records from European events, while ITACA is a denser dataset of Italian earthquakes within a lower magnitude range and a broader distance range. A limited number of records (150 from 19 events) are in common between the two sets of data. In Fig. (2.7) the distributions of data pairs as a function of separation distance bins (4 km width for ESD and 1 km for ITACA) are also shown.

To compute the empirical semivariogram, normalized intra-event residuals are obtained for a single earthquake j and a generic site p as $\varepsilon_{pj}^{*}=\varepsilon_{pj}/\sigma_p$ where σ_p is the standard deviation of the intra-event residual at the site p (in the study the intra-event standard deviation is common for all sites consistent with GMPEs used to compute residuals). In this case Eq. (2.14) becomes Eq. (2.18), where the superscript represents an empirical estimate.

$$\hat{\gamma}\left(h\right)=1-\hat{\rho}\left(h\right) \tag{2.18}$$

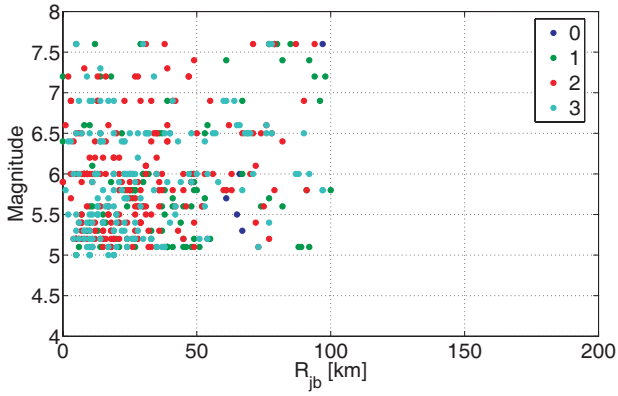

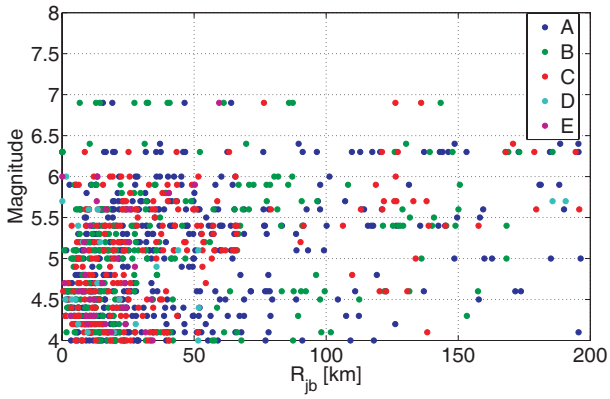

Figure 2.6 ESD subsets with respect M, Rjb, and local site conditions: rock (3), stiff soil (2), soft soil (1), and very soft soil (0) (up); and ITACA strong-motion subsets with respect M, Rjb and local site conditions (down) according to Eurocode 8 (2004)

Eq. (2.18) shows that standardization enables to not estimate the sill, as it should be equal to one. This applies if standardization is carried out using the true population's variance. With earthquake data, the sample variance or the standard deviation provided by the GMPE can be used to obtain standardized residuals[3]. Another option is to use the sample variance as an estimate of the true variance (e.g., Jayaram and Baker, 2010a). Goda and Atkinson (2010) used the intraevent standard deviation inferred from the large-separation-distance plateau of the semivariogram, assuming that at those distances residuals are not correlated. In this work, the variance provided by the GMPEs was preferred. In fact, evaluation of possible alternatives for standardization leads to results which seem to be not significantly affected by a choice with respect to another (as discussed later on).

Because geostatistical estimation needs a relatively large number of data to model the semivariogram (i.e., many records to have more than 30 pairs in each h bin), which are not available for individual events in the chosen datasets, all data available from multiple events (and regions) are used herein to fit a unique correlation model. The same isotropic semivariogram with the same parameters for all earthquakes is assumed.

[3] It is usual to use the sample variance as an estimator of the sill for the experimental semivariogram, but this may be improper in some circumstances; see Barnes (1991) for a discussion.

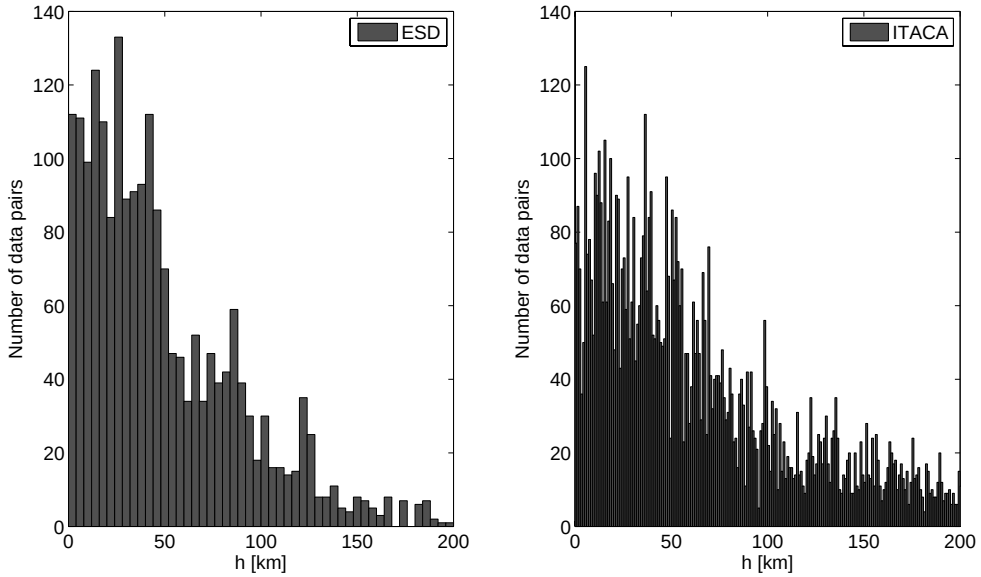

Figure 2.7 Histograms of the number of data pairs as a function of site-to-site separation distance

The experimental semivariogram becomes that of Eq. (2.19), where n_j is the number of records for the *j*th event and $\left|N\left(h\right)\right|$ is the number of pairs in the specific *h* bin. Eq. (2.20) shows how individual events are kept separated in computing the empirical semivariogram. In fact, the differences of residuals of Eq. (2.19) are computed only between pairs of residuals (standardized with the common standard deviation from the GMPE) from the same earthquake, then differences from different earthquakes are pooled. This process is visually sketched in Fig. (2.8) from which it is possible to note that the empirical semivariogram point at h_1 is not the average of experimental semivariograms from different earthquakes, as $\left|N\left(h\right)\right|$ is the number of pairs in the specific *h* bin from all earthquakes.

$$\hat{\gamma}\left(h\right)=\frac{1}{2\cdot\left|N\left(h\right)\right|}\sum_{N(h)}\left[\varepsilon^{*}_{pj}-\varepsilon^{*}_{qj}\right]^{2} \tag{2.19}$$

$$N\left(h\right)=\left\{\left(j,\varepsilon^{*}_{pj},\varepsilon^{*}_{qj}\right):\left\|\varepsilon^{*}_{pj}-\varepsilon^{*}_{qj}\right\|=h;\quad p,q=1,\ldots n_j;\ \ j=1,\ldots k\right\} \tag{2.20}$$

2.2.3.3. Proposed model

For the European subset, each bin has 4-km width, as it also allows having at least 30 pairs per bin and no empty bins until the half of the maximum distance between pairs in the dataset. Both estimators (classical and robust) were used; no significant difference was found in the shape of the fitted semivariogram. Of the three basic models (Gaussian, spherical and exponential), the exponential model provided the best fit at the small separation distances (where the correlation is expected to be strong). Least square method (LSM) was used as a starting point to fit the semivariogram. Because LSM minimizes the fitting error over the whole distance interval data, and in order to give more importance to the small separation distances, LSM has been applied until a limit separation distance (of the same order of magnitude of the range where correlation is expected to disappear). LSM results are then used as a reference to manually fit a model in the empirical semivariogram.

This approach was used to estimate correlation of both PGA and PGV. Because the chosen GMPE refers to geometric mean of horizontal components, the correlation was estimated for this IM. Assuming that there is no nugget effect (as this study does not investigate variations at a smaller scale with respect to that of the tolerance), the only parameter to estimate is the range *b* whose results equal to 13.5 km for PGA and 21.5 km for PGV, as shown in Fig. (2.9).

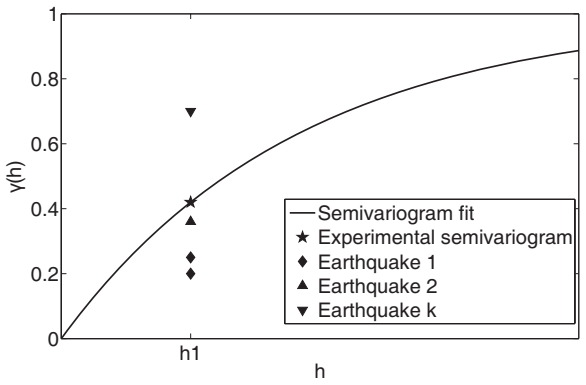

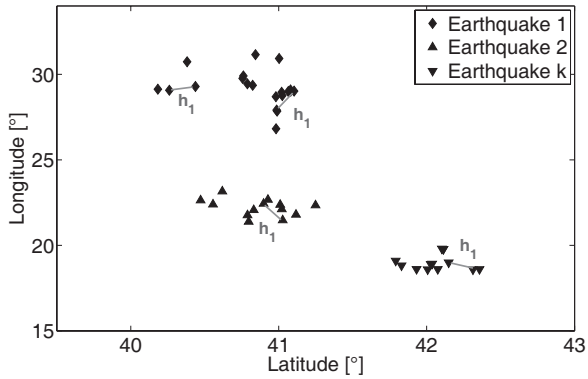

Figure 2.8 Pooling standardized intra-event residuals of multiple events (up) to compute experimental semivariogram (down)

It should be noted that in Esposito *et al.* (2010) the proposed methodology was used to estimate the correlation of the PGA (horizontal and vertical components) intraevent residuals starting from a less recent GMPE, the Ambraseys *et al*. (2005a,b), and also the dataset was not exactly the same. However, the resulting range was quite similar, 12 km and 18 km horizontal and vertical components, respectively.

For the Italian dataset, the spatial correlation ranges of residuals obtained from the Bindi *et al.* (2010) GMPE were 11.5 km and 14.5 km for PGA and PGV, respectively (Fig. 2.10). In this case, because of the denser dataset, it was possible to consider 1-km bin width; however, it seems that estimates are not significantly dependent on such size. In fact, exponential model for PGA obtained with a bin width of 4-km is characterized by a range of 13.5 km.

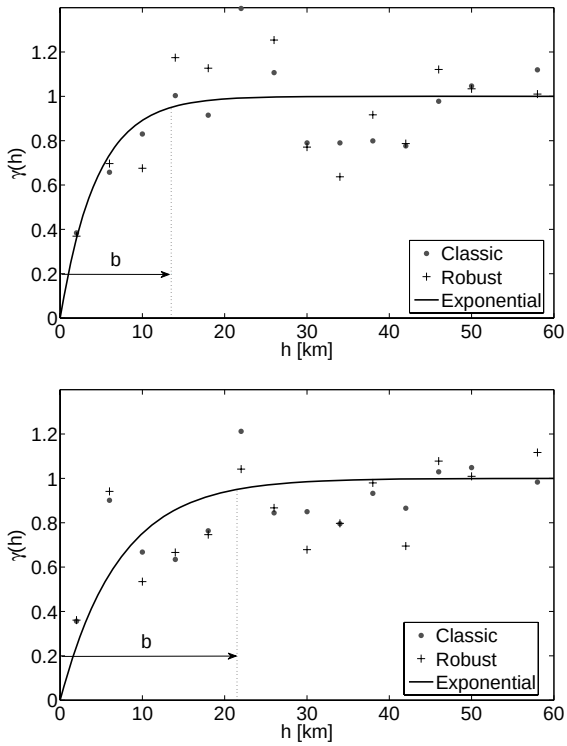

Figure 2.9 ESD empirical semivariogram and fitted exponential model for PGA (up) and PGV (down) considering a bin width of 4 km

In both cases of ESD and ITACA correlation ranges are higher for PGV than for PGA. In fact, the acceleration time history shows a significant proportion of relatively high frequency, while velocity records shows substantially less high-frequency motion and are likely to yield higher correlations (e.g., Kramer, 1996). This seems to be consistent with past studies of ground motion coherency (Zerva and Zervas, 2002). In fact, the coherency describes the degree of correlation between amplitudes and phases angles of two time histories at each of their component frequencies. Considering that coherency decreases with increasing distance between measuring points and with increasing frequency, it may be reasonable to expect more coherent ground motion, as velocity that corresponds to low frequency exhibits more correlated peak amplitudes.

In principle, residuals model what is not explained by the covariates of the GMPE, therefore, because datasets are different, differences in the results between ESD and ITACA may be legitimate[4]. However, for a given IM, practical ranges are definitely

[4] One may argue that the larger ranges found for ESD with respect to ITACA are an effect of different distribution of magnitude in the two datasets. However, the proposed correlation models does not incorporate dependency on magnitude also based on the findings of Jayaram and Baker (2009).

comparable and probably the differences are not significant, although the latter is difficult to assess because the estimation methodology does not provide the statistics of the range, which would allow quantitatively to assess differences by means, for example, of hypothesis tests.

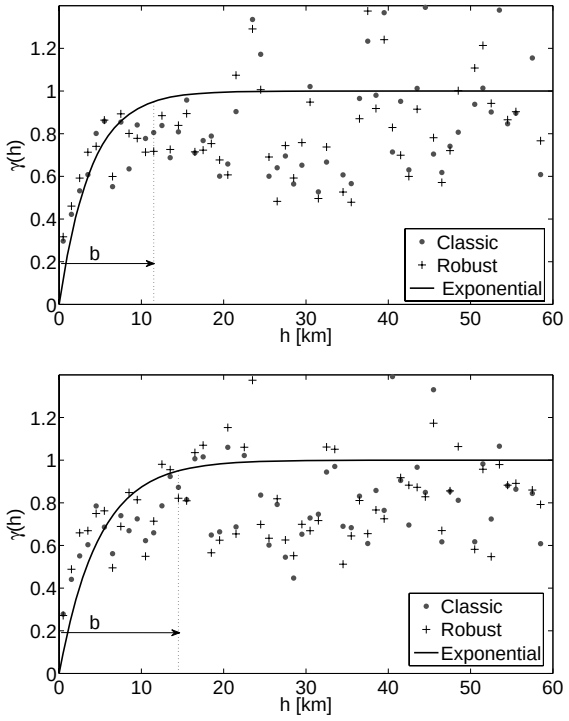

Figure 2.10 ITACA empirical semivariogram and fitted exponential model for PGA (up) and PGV (down) considering a bin width of 1 km

Another important point regards the different possibilities to obtain standardized residuals. As suggested in Goda and Atkinson (2010), positive correlations among intra-event residuals may lead to underestimated intra-event sample variance in GMPEs. Hence, intraevent standard deviations inferred from the large separation distance plateau of the semivariograms were used to estimate practical ranges of correlation in the two subsets. In particular, intra-event residuals without any standardization were used to estimate the sill (population variance) under the assumptions that at large-separation distance those residuals are not correlated. The resulting estimates are practically the same (less than 10% differences) with respect to those of the GMPEs. This is also because there are relatively few data at short

separation distances in the datasets. As a result, it was possible to infer that, at least in the considered case studies, the GMPEs variance can be used for the standardization.

The same approach has been used to estimate spatial correlation for spectral acceleration (Sa) in order to evaluate a possible dependency of the correlation length on the period Sa refers to. Preliminary results obtained from ITACA dataset are shown in Appendix A.

2.2.3.4. Regional hazard

Developed correlation models can be used, for example, to obtain the exceedance probability of the IM in a region and in a time interval of interest. The hazard integral of Eq. (2.3) provides such annual rate of joint exceedance in a region, if the same assumptions of site-specific hazard analysis are retained (McGuire, 2004).

As an example, regional hazard was developed considering as a source the Paganica fault on which the 2009 L'Aquila (central Italy) earthquake originated, and the Bindi *et al.* (2010) GMPE under the assumption that all the sites have the same stiff soil local site conditions. PGA and PGV hazards, considering ranges of 11.5 km and 14.5 km respectively, were computed for a characteristic earthquake of moment magnitude 6.3, and occurrence rate on the source $\nu = 1/750$ (Pace *et al.*, 2006).

In Fig. (2.11), surfaces are a function of IMs (as in traditional hazard curves) and exceedance areas (A*), which are fractions, between 2.5% to 25%, of a region of 2500 km^2 around the fault. Referring for example to PGA, entering the plot with a set of two A* and PGA values, the surface returns the mean annual rate of exceedance of that PGA value over an area at least equal to A*.

For comparison, hazard considering uncorrelated intra-event residuals was also computed. For both PGA and PGV, correlation does not always provide higher rates with respect to the independent case. In fact this is because, in the simulated case, the *n* sites constituting the A* exceedance region are not necessarily adjoining. Given that *im** is exceeded (not exceeded) at a given site, correlation increases the probability of having neighbouring sites exceeding (not exceeding) *im** as well.

If an alternate hazard criterion is considered, an example is that *im** has to be exceeded at exactly *n* points constituting A* , the joint hazard for correlated residuals is always higher with respect to the independent case (Fig. 2.12). This seems also consistent with the results of Sokolov and Wenzel (2011).

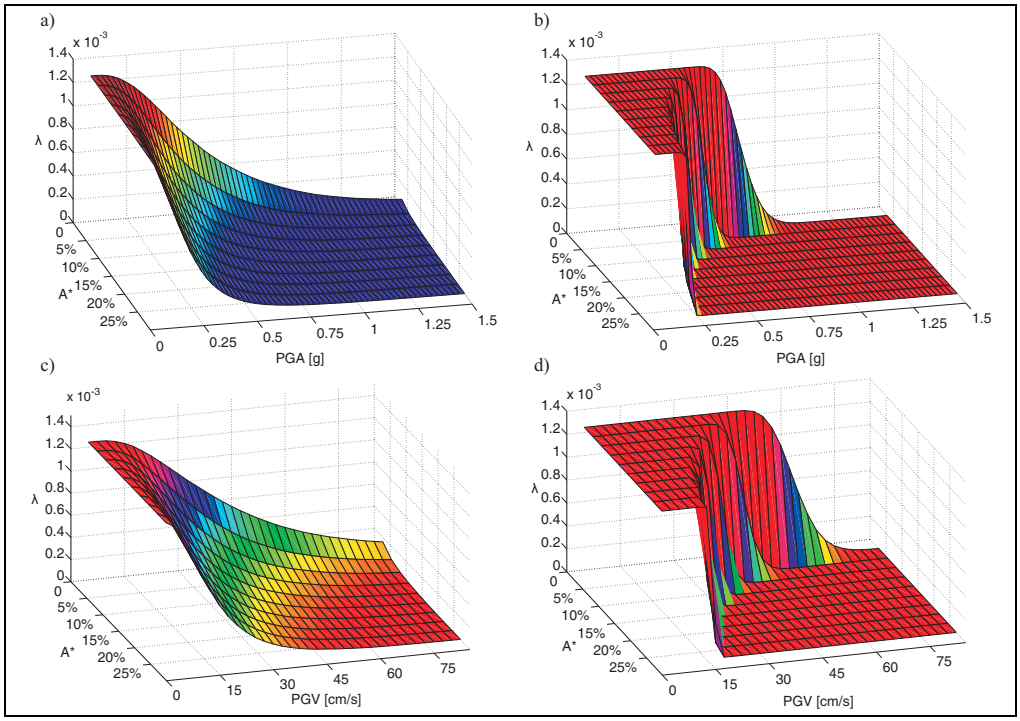

Figure 2.11 *Regional* hazard surface considering: correlated residuals (a and c) and independent residuals (b and d) for PGA and PGV

2.2.4. Spatial cross-correlation of intensity measures

The performance of spatially distribute systems may be conditional upon the failure of many components within the system each of which is sensitive to different IMs, id est each component may respond differently to the input ground motion. In particular some elements of a gas system, such as regulator stations, are more sensitive to PGA respect to pipelines whose seismic behavior is closely related to PGV.

As shown previously each IM is spatially correlated but the hazard assessment of a system, since it is characterized by different IMs, has to take into account the possibility of the existence of a cross-correlation between IMs in order to model the joint distribution of different random fields. Therefore when considering the spatial distribution of multiple ground motion parameters, it is necessary to evaluate both autocorrelation and cross-correlation properties. Jayaram and Baker (2010b) demonstrated that spectral acceleration at different fundamental periods are spatially cross-correlated but until now, this represents the unique preliminary study available

on this topic. Further research on the characterization of the joint distribution of different IMs in multiple points is still needed.

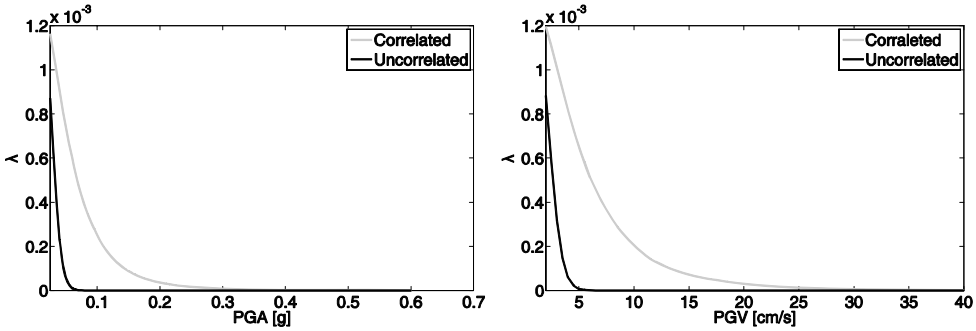

Figure 2.12 *Regional* hazard curve considering correlated and independent residuals for PGA (left) and for PGV (right)

2.2.5. Site amplification

Site conditions may influence the amplitude of ground shaking at the ground surface: sites near the source of a large earthquake are characterized by high levels of ground shaking that may produce significant damages. Although seismic waves travel through the rock for the majority of their trip from the source to the ground surface, the final part of the trip is through soil, which characteristics may influence the nature of shaking at the ground surface. The soil tends to act as a "filter" to seismic waves attenuating or amplifying the motion.

Since soil conditions may differ over short distances, levels of ground shakings may vary dramatically also within a small area. Generally site effects represent local ground response effects, basin effects and the influence of surface topography on ground motion. Local ground response refers to the influence of relatively shallow geologic materials on (nearly) vertically propagating body waves. The term basin effects refers to the influence of two- or three-dimensional sedimentary basin structures on ground motions, including critical body wave reflections and surface wave generation at basin edges. Site effects due to surface topography (i.e., topographic effects) can amplify the ground shaking that would otherwise be expected on level ground along ridges or near the tops of slopes. Details about amplification due to those effects can be found in Kramer (1996).

Depending on the extend of the information that are available to define the site characteristics across a region, several different approaches could be considered for the purposes of characterizing the strong motion amplification due to local geology. There are essentially two general types (Kramer and Stewart, 2004):

- GMPE-based site amplification: each site can be characterized according to the site classification scheme adopted and modeled within the GMPE. The site class becomes a fixed parameter of the site in question and can be used directly within the strong ground motion evaluation. The key advantage of the GMPE-based approach is that it requires a minimum amount of information within the site characterization. In most cases each site need only be categorized according to Eurocode classes, NEHRP classes or the 30-m shear wave velocity, V_{s30}, (see Tables 2.1). There are several shortcomings to this particular approach. Actual conditions at strong motion recording sites are highly variable with respect to local geotechnical conditions, possible basin effects and surface topography may occur, and hence estimates from attenuation relationships necessarily represent averaged values across the range of possible site conditions. Moreover, it is possible that the set of strong motion records used for deriving the GMPE will not adequately sample all the site classes of interest. This is the case for many existing European models, which may only derive amplification factors for NEHRP classes B, C, D (rock, stiff soil and soft soil), which broadly correspond to Eurocode 8 classes A, B, and C (Akkar and Bommer, 2010).
- Site amplification factor: site amplification factors represent for a given ground motion intensity measure, the ratio of that parameter for a given site category to the value of the parameter for a reference category (usually rock). Site amplification factors are generally inferred from strong motion recordings or are derived from analyses using engineering models of wave propagation (Kramer and Stewart, 2004). However, site condition remains relatively crudely represented with amplification factors, quantified only by site conditions that affect the categorization per the classification scheme. For example, in the HAZUS technical manual (FEMA, 2004) soil amplification factors are given according to NEHRP site class (A to E) and spectral acceleration on class B rock. As with the GMPE-based approach, code-based approach has several advantages in terms of simplicity and relatively minimal requirements in terms of the site classification but this approach is limited to site categories for which the code supplies such factors. An additional limitation is that design codes are extremely unlikely to provide amplification factors for IMs other than PGA or spectral acceleration limiting the extension of the code-based site amplification approach to less common IMs. A more complex alternative to describe the site amplification

is the model produced by Choi and Stewart (2005). It was derived from 1828 observed strong motion records taken from 154 active shallow crustal earthquakes. The amplification factor was determined from the ratio of observed spectral acceleration to expected acceleration calculated for the same event using an existing GMPE. A variation on this approach has been presented by Walling *et al.* (2008) where the amplification factors are calculated using a 1D equivalent linear analysis model of site amplification, applied to a synthetic time history generated by point source stochastic simulation. Both approaches may be implemented either directly as a single site amplification model, or indirectly via the GMPEs that adopt it as their site amplification function.

It is important to note that the approach used by Walling *et al.* (2008) could be used to characterize a generic site amplification model on the basis of one-dimensional modeling tools based on geotechnical profiles produced by microzonation study for the region of interest (if it is available). In this way amplification factors, instead of being generic or characteristic for a particular site class, are defined in order to be specific to the sites for the application in question.

2.3. Permanent ground deformation hazard

Geotechnical hazards induced from earthquakes have been the subject of a considerable amount of researches in the last decades. A substantial body of literature on pipeline systems has been produced on this topic. Although PGD hazards are usually limited to small regions within the pipeline network, their potential for damage is very high since they impose large deformation on pipelines. The relative impact of the various earthquake induced effects on a pipeline system, as a gas system, depends on the geological conditions in which surface faulting and the other collateral effects occur and the coincidence of these regions with the buried infrastructure. In fact where these phenomena coincide with the network, relatively high pipeline damage rates are observed but in localized areas.

The principal forms of permanent ground deformation are surface faulting, landsliding, seismic settlement and lateral spreading due to soil liquefaction. There are many models available that have the intent to relate the degree of deformation (PGD) and the probability of occurrence of each geotechnical hazard to the strength of ground motion but the main limiting factor of many models is the requirement of very detailed geotechnical data that could make difficult the implementation of those models for many lifeline systems. Therefore it may be preferable to consider simpler

models, as the approach implemented in HAZUS (FEMA, 2004) that may be implemented in the widest variety of applications.

In the following sections, the most important earthquake induced effects for gas systems are presented and for each geotechnical hazard, HAZUS methodology will be illustrated.

Table 2.1 Site Classification According to Eurocode 8 (2004)

Class	Stratigraphy	V_{s30} (m/s)
A	Rock or rock-like geological formation, including at most 5m of weaker material at the surface.	> 800
B	Deposits of very dense sand, gravel or very stiff clay, at least several tens of metres in thickness, characterised by gradual increase of mechanical properties with depth	360 – 800
C	Deep deposits of dense or medium-dense sand, gravel or stiff clay with thicknesses several tens to many hundreds of metres	180 – 360
D	Loose-to-medium cohesionless soil (with or without some soft cohesive layers), or of predominantly soft-to-firm cohesive soil.	< 180
E	A soil profile consisting of a surface alluvium layer with V_s values of type C & D, and thicknesses varying between about 5m and 20m, underlain by stiffer material with V_{s30} > 800 m/s	-
S_1	Deposits consisting of, or containing a layer at least 10 m thick, of soft clays/silts with high plasticity index (PI > 40) and high water content	< 100
S_2	Deposits of liquefiable soils, of sensitive clays, or any other soil profile not included in types A – E or S_1	-

2.3.1. Liquefaction

Liquefaction is a term used to describe a variety of complex phenomena involving soil deformations characterized by the generation of excess pore-water pressure under undrained loading conditions. During earthquake ground shaking, induced cyclic shear creates a tendency in most soils to change volume by rearrangement of the soil-particle structure. In loose soils, this volume change tendency is to compact or densify the soil structure. For soils such as fine sands, silts and clays, permeability is

sufficiently low such that undrained conditions prevail and no or insignificant volume change can occur during the ground shaking. To accommodate the volume decrease tendency, the soil responds by increases of pore-water pressure and corresponding decreases of intergranular effective stress. In general, more compressible soils such as plastic silts or clays do not generate excess pore-water pressure as quickly or to as large an extent as less compressible soils such as sands. Therefore, silty and clayey soils tend to be less susceptible than sandy soils to liquefaction-type behaviours.

Soil liquefaction has caused significant damage to buried lifelines in past earthquakes. Zonation of liquefaction hazard is therefore of particular importance to lifeline earthquake engineers. Therefore the first step of liquefaction hazard evaluation is the determination of liquefaction susceptibility. For a given soil, liquefaction susceptibility can be judged according to various historical, geological, compositional or soil state criteria. Once it has been evaluated, the next stage is to determine the likelihood that an earthquake will cause a disturbance strong enough to initiate the phenomenon (i.e. the probability of liquefaction). The criteria necessary to determine liquefaction susceptibility and the condition require to trigger liquefaction are complex and beyond the scope of this study. More details can be found in Kramer (1996).

In HAZUS methodology, susceptibility classes are categorized on the basis of deposit type, age and general distribution of cohesionless sediments (see Appendix B for the classification scheme). Based on the analysis of Youd and Perkins (1978), at each susceptibility class corresponds a conditional probability of liquefaction for a given value of PGA and a proportion of map unit susceptible to liquefaction as expressed by the Eq. (2.21)

$$
\begin{aligned}
&P[liquefaction] = \frac{P[Liq \mid PGA = a]}{K_M K_W} P_{ml} \\
&K_M = 0.0027M^3 - 0.0267M^2 - 0.2055\mathrm{M} + 2.9188 \\
&K_W = 0.022\mathrm{d}_w + 0.93
\end{aligned}
\tag{2.21}
$$

where $P[Liq \mid PGA = a]$ is the conditional probability for a given susceptibility category at a specified level of peak ground acceleration; K_M is the moment magnitude (M) correction factor; K_W is the groundwater correction factor as a function of the water depth d_w (in feet); and P_{ml} is the proportion of map unit susceptible to liquefaction (see Appendix B for more details).

Alternatively, if more geotechnical information is known for the site of interest, as the effective overburden stresses, the probability of liquefaction may be determined

from the Liao *et al.* (1988) empirical model. If not, the simpler approach of HAZUS can be preferred.

Given that liquefaction is likely at a particular location, the last step is to predict the amount of permanent ground deformation associated to liquefaction. The ground failure phenomena associated to liquefaction that may induce pipe damage are generally lateral spread and settlement.

2.3.1.1. Lateral spreading

Lateral spreads develop when a loose saturated sandy soil deposit is liquefied and occur near abrupt topographic features (i.e., free-faces) and on gently sloping ground underlain by liquefied soil. Earthquake ground-shaking affects the stability of sloping ground containing liquefiable materials by causing seismic inertia forces to be added to gravitational forces within the slope and by shaking-induced strength reductions in the liquefiable materials. The ground movement is primarily horizontal since vertical component is typically small.

The potential for PGD to induce pipe damage is related to the amount of ground movement, the length and width of the PGD zone as well as the pattern of deformation (O'Rourke and Liu, 1999). Predicting the amount of ground displacement due to lateral spread is a challenging problem. Nevertheless there are a number of studies available, both analytical and empirical. A review of these studies may be found in (O'Rourke and Liu, 1999). Nevertheless the simple relation proposed by HAZUS may be considered as a first order estimate on the amount of displacement associated with lateral spreading. The amount of lateral displacement in inches is calculated via the Eq. (2.22):

$$\begin{aligned} &E\left[PGD\right] = K_{\Delta} \cdot E\left[PGD \,|\, \left(PGA/PL_{SC}\right) = a\right] \\ &K_{\Delta} = 0.0086M_W^3 - 0.0914M_W^2 + 0.4698M_W - 0.9835 \end{aligned} \tag{2.22}$$

where $E\left[PGD \,|\, \left(PGA/PL_{SC}\right) = a\right]$ is the expected PGD for each susceptibility category under the normalised level of shaking defined by $PGA/PGA(t)_{\,|\,SC}$ where $PGA(t)_{|\,SC}$ is the threshold PGA. The factor K_{Δ} is a displacement correction term.

The primary advantage of the HAZUS methodology is the simplicity and the dependence on few site specific factors. If the ground conditions can be better constrained for the site in question, other empirical models, as Bardet *et al*. (2002), Youd *et al.* (2002), could alternatively be applied.

2.3.1.2. Seismic settlement

Settlement is a result of the dissipation of excess pore pressure generated by the rearrangement of loosely compacted saturated soils into a denser configuration during shaking. Such dissipation produces volume decreases (termed consolidation or compaction) within the soil that is manifested at the ground surface as settlement.

Volume changes may occur in both liquefied and non-liquefied zones with significantly larger contributions to settlement expected to result from liquefied soil. Densification may also occur in loose unsaturated materials above the ground water table. Spatial variations in material characteristics may cause such settlements to occur differentially. Differential ground settlement may also occur near sand boil manifestations due to liquefied materials being removed from the depths of liquefaction and brought to the ground surface.

Despite being a commonly observed liquefaction phenomenon, there are fewer established models that are used for the estimation of ground settlement. In the HAZUS methodology a characteristic settlement is attributed to each susceptibility class, thus making the expected settlement a product of the liquefaction probability and the characteristic settlement. The actual values of the characteristic settlement were determined from the process described by Tokimatsu and Seed (1987) (see Appendix B) that suggest characteristic values for volumetric settlement to use for the characterization of seismic input of a spatially distributed system.

The HAZUS methodology represents the most widely applicable, in spite of the relative crudeness of the model. Alternative models, as Pradel (1998) and Takada and Tanabe (1988), can be taken into account if detailed site data are available.

2.3.2. Landslide

Landslides are mass movements of the ground which may be triggered by ground shaking. There are different schemes to classify landlslides. Based on the different effects on pipelines, Meyersohn (1991) established three types of landslides as shown in Fig. (2.13).

The first type includes rock fall and rock topple, which can cause damage to above-ground pipelines by the direct impact of falling rocks. The second type includes flow and debris flow in which the transported material behaves as a viscous fluid. For loss estimation purposes, this type of landslide is part of the liquefaction potential assessment rather than the landslide potential. The last type includes earth slump and earth slide, in which the earth moves as a block. They usually develop along natural slopes, river channels and embankments. Because pipelines often cross such zones, the following will focus on this type of landslide.

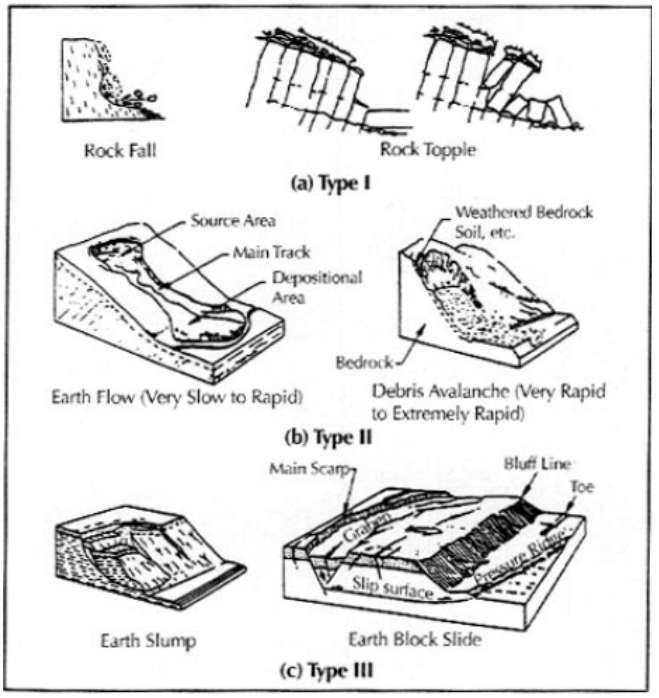

Figure 2.13 Types of landslides (Meyersohon, 1991)

The HAZUS approach for the characterization of slope displacement mirrors, in concept, that of liquefaction displacement. First landslide susceptibility has to be evaluated. Susceptibility is characterized by the geologic group, slope angle and critical acceleration. The acceleration required to initiate slope movement is a complex function of slope geology, steepness, groundwater conditions, type of landsliding and history of previous slope performance. The relationship proposed by Wilson and Keefer (1985) is utilized in the methodology where landslide susceptibility is selected from a ten point scale and assigned on the basis of geology, slope angle and the position of groundwater with respect to the level of sliding (essentially a wet/dry distinction). The description for each geologic group and its associated susceptibility is given in Appendix B. The groundwater condition is divided into either dry condition (groundwater below level of the sliding) or wet condition (groundwater level at ground surface). For each susceptibility class, a critical acceleration is defined; hence, if PGA exceeds the critical acceleration then a landslide is observed. The probability of a landslide occurring is modified by a term to determine the percentage of the map area having a landslide susceptible deposit due to the conservative nature of the Wilson and Keefer (1985) correlation. The calculation of expected ground displacement in HAZUS is relatively simple and it is given by the Eq. (2.23):

$$E\left[PGD\right] = E\left[d \mid a_{is}\right] \cdot a_{is} \cdot n$$
$$n = 0.3419M_W^3 - 5.5214M_W^2 + 33.6154M_W - 70.7692 \tag{2.23}$$

where $E\left[d \mid a_{is}\right]$ is the expected displacement factor, which is a function of the induced acceleration (a_{is}) and n is the number of cycles. Note that the induced peak ground acceleration within the slide mass, a_{is}, represents the average peak acceleration within the entire slide mass. For many applications a_{is} may be assumed equal to the accelerations predicted by the peak ground acceleration attenuation relationships being used for the loss estimation study (FEMA, 2004).

Alternative models exist, in particular the empirical relations suggested by Saygill and Rathje (2008) displacement may be the simplest extension of the slope displacement calculation already implemented in HAZUS. The ground displacement is functions of the critical acceleration K_c and PGA (in g) and it is given by the Eq. (2.24):

$$\ln\left(PGD\right) = a_1 + a_2\left(\frac{K_c}{PGA}\right) + a_3\left(\frac{K_c}{PGA}\right)^2 + a_4\left(\frac{K_c}{PGA}\right)^3 + \ldots$$
$$\ldots a_5\left(\frac{K_c}{PGA}\right)^4 + a_6 \ln\left(PGA\right) \tag{2.24}$$

2.3.3. Faulting

An active fault is a discontinuity between two portions of the earth crust along which relative movements can occur. The extent of faulting is linked closely with earthquake magnitude. In most earthquakes, the fault rupture plane does not have a surface expression; the surface fault trace is usually only observed for large earthquakes occurring at shallow depth but even for earthquakes without a surface fault expression, coseismic strains induced in the epicentral region may still be large enough to cause damage to buried pipelines. Faults can be classified according to the movement of the two sides of the fault relative to each other, in particular the principal types of fault movement include strike-slip, normal-slip and reverse slip as shown in Fig. (2.14).

In a strike-slip fault the predominant motion is horizontal, which may deform a continuous pipe in tension or compression depending on the pipe-fault intersectional angle. In normal and reverse the predominant ground displacement is vertical. When the overhanging side of the fault moves downwards, the fault is normal, which deforms a horizontal pipe primarily in tension. When the overhanging side moves upwards, the fault is reverse, this deforms a horizontal pipe primarily in compression.

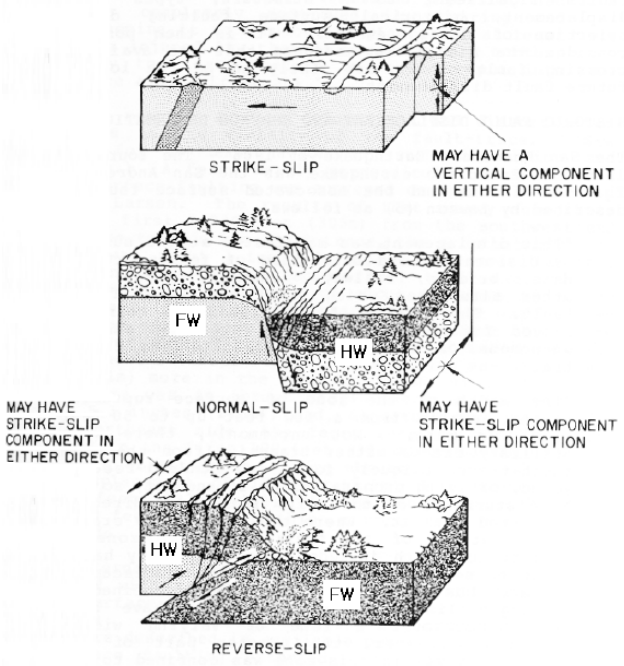

Figure 2.14 Difference types of faulting (Taylor and Cluff, 1977). FW-foot wall; HW-hanging wall

The large permanent ground deformation associated with faulting can present a very severe hazard to structures on or near to active faults. In the case of gas pipelines, crossing active faults is often unavoidable, since pipeline location is dictated by the locations of supply and demand areas. It is therefore useful to be able to estimate the amount of permanent ground displacement that might occur in the event of an earthquake of a given magnitude on a particular fault.

Various empirical relations between fault displacement and moment magnitude have been proposed. Based on a worldwide data base of 421 historical earthquakes, Wells and Coppersmith (1994) selected 244 earthquakes, and developed empirical relationships among magnitude, rupture length, rupture width, rupture area and surface displacement. These expressions (Eq. 2.25-2.27) can be used to predict likely fault rupture characteristics given a specific magnitude of event. Of most interest for the prediction of pipeline damage are the following expressions:

$$\log \bar{D} = -6.32 + 0.90M \quad \textit{for Strike-Slip Fault} \tag{2.25}$$

$$\log \bar{D} = -4.45 + 0.63M \quad \textit{for Normal Fault} \tag{2.26}$$

$$\log \bar{D} = -0.74 + 0.08M \quad \textit{for Reverse Fault} \tag{2.27}$$

where $\bar{D}$ is the average surface fault displacement, in meters, and M is the moment magnitude. According to Wells and Coppersmith, the maximum fault displacement is twice the average fault displacement and it is assumed that the maximum displacement can potentially occur at any location along the fault considering that at the end of the fault displacements must drop to zero. Therefore for the hazard assessment, the fault rupture displacement, as suggested in HAZUS (FEMA, 2004), may be sampled from an Uniform distribution between half the maximum and the maximum displacement.

2.4. Seismic hazard assessment

In the past, researchers have developed several techniques for lifeline risk assessment. The procedure for loss estimation of such systems involves several aspects that make the loss computation though traditional approaches adopted for single structures, theoretically possible but highly impractical (Bazzurro and Luco, 2005). In particular, regarding the hazard assessment, the first and most important aspect stems from the fact that in the same earthquake, ground motion intensities at multiple sites are spatially correlated. Hence the joint hazard of ground shaking at more location and correlation models for the intensity measure of interest should be included in the risk computation. In this case, the use of simulation-based methods may be the approach of choice: multiple scenarios of ground shaking are simulated at all sites of interest though stochastic models that may include spatial correlation. This procedure is conceptually sounder but the estimation of the performance may be high computationally intensive especially when the facility covers a very large area. Moreover lifeline hazard assessment may involve the simulation of several intensity measures (co-simulation) due to the presence of different components (buried and unburied) sensitive to different IMs. Since intensity measures may be cross-correlated, simple sampling methods (e.g. Matrix Decomposition , Davids 1987) applied usually for the simulation of one single spatially correlated IM are not feasible (Weatherill *et al*, 2011). To this aim different simulation methods have to be considered.

In this section available earthquake hazard assessment methods are described with a summary of strengths and limitations when a spatially distributed system is of concern. The formulation adopted for the case study application of L'Aquila gas system is described in the Chapter 5.

2.4.1. Methods

This section briefly describes available hazard assessment methods in terms of their potential to be used for lifeline risk evaluation.

A first way to evaluate seismic risk for spatially distributed system is to use individual scenarios: a particular scenario event (defined generally in terms of magnitude and location) is specified where ground motion is estimated though GMPEs; then losses are estimated conditional on occurrence of that scenario. Focusing on one or few earthquake scenarios no computational effort is required but for many applications, as insurance portfolio planning or risk reduction policy, the knowledge of one or few occurrence earthquake and consequences might be completely ineffective.

In order to consider the effects of all possible earthquakes with different sizes, occurring at different locations with different probabilities of occurrence, probabilistic seismic hazard analysis (PSHA) can be applied. For each site considered, the probability of exceeding different levels of ground motion (e.g. PGV) for a specified period of time is evaluated ("hazard curve"). Generally when this method is applied for multiple sites, individual site hazard and losses curves are combined to obtain the overall lifeline risk assessment and spatial correlation of ground motion among sites is not considered (FEMA, 1999); in this way loss estimation of multiple sites might be underestimated (Bazzurro and Luco, 2005). Anyway it is theoretically possible to extend PSHA formulation accounting for spatial correlation in lifeline seismic risk assessment (Rohades and McVerry, 2001) but it is difficult in practice. Moreover lifeline performance measures are usually not available in closed form function of ground-motion intensities, making the evaluation of risk assessment not possible.

Alternative methods for charactering ground motion and computing resulting losses for spatially distributed systems are simulation-based (Bazzurro and Luco, 2005; Crowley and Bommer, 2006). Monte Carlo simulation (MCS) based approaches involve the probabilistic simulation of many earthquakes in the region of interest, considering all possible scenarios that could occur, and use them for the loss assessment. This approach has the advantages of including in a simple way spatial correlation among sites to evaluate lifeline loss exceedance curves. Nevertheless, conventional MCS may be computationally intensive for large systems and inefficient (Jayaram and Baker, 2010a) considering that large magnitude events that are more important than small-events earthquakes for lifelines risk assessment, are infrequently sampled. Some simulation-based approaches that tend to reduce the number of earthquake scenarios are characterized by the selection of a small set of possible earthquakes that may dominate the hazard in the region of interest (Jayaram and

Baker, 2009b) or represent the total regional hazard in terms of the frequency and distribution of ground motion they causes, i.e. "hazard-consistent" scenarios (Campbell and Seligson, 2003, Lee *et al*., 2005). Those methods have the advantages of including partially spatial correlation among sites (since they are simulation-based methods) while reducing the computational demand. Nevertheless, the identification of the events that dominate the hazard is not easy and the determination of the reduced set of scenarios and their associated hazard-consistent occurrence probabilities is usually based on matching according to a single ground motion parameter, making difficult represents other parameters or induced hazards (e.g. liquefaction). Moreover those procedures do not capture the effect of the uncertainties in ground motion intensities. Jayaram and Baker (2010a) use instead an innovative simulation-based framework based on an efficient sampling method (Important Sampling, IS) and data reduction technique (K-Means Clustering) for developing a small but stochastically representative set of earthquake ground-motion intensity maps. In this framework, IS is used to preferentially sample "important" ground motion intensity maps, involving the probabilistic sampling of earthquake magnitude, rupture locations and GMPE' residuals and K-means is used to identify and combine redundant maps in order to obtain a small set of earthquakes.

Meanwhile non-sampling based approaches have been also developed (Chang and Song, 2007, Kang *et al*., 2008, Song and Ok, 2009, Bensi *et al*., 2009) but those are generally applicable to only specific classes of lifeline systems.

2.4.2. Simulation of spatially cross-correlated ground motion fields

As explained in the section 2.2.4 the computation of joint distribution of spatially correlated IMs needs the availability of spatial cross-correlation models. A simple way to tackle this issue, especially if only two IMs are of concern (for example PGA and PGV for gas systems) is the sequential conditional simulation (Weatherill *et al*, 2011). This technique starts from the assumption that two IMs considered are jointly distributed according to a bivariate Gaussian distribution. This hypothesis for several ground motion intensities has been verified by Jayaram and Baker (2008) and Iervolino *et al.* (2010).

Considering two correlated IMs (e.g. PGA and PGV) which logarithms are distributed as normal random variables with means ($\mu_{\log PGA}$ and $\mu_{\log PGV}$) and standard deviations ($\sigma_{\log PGA}$ and $\sigma_{\log PGV}$) and correlation coefficient ρ, the conditional PDF of one variable ($\log PGV$) given a known value of the other

($\log PGA = z$) is normally distributed characterized by the conditional mean $\mu_{\log PGV|\log PGA,M,R}$ and standard deviation $\sigma_{\log PGV|\log PGA}$ as reported in Eq. (2.28)

$$\begin{cases} \mu_{\log PGV|\log PGA,M,R} = \mu_{\log PGV|M,R} + \rho\sigma_{\log PGV}\dfrac{z-\mu_{\log PGA|M,R}}{\sigma_{\log PGA}} \\ \sigma_{\log PGV|\log PGA} = \sigma_{\log PGV}\sqrt{1-\rho^2} \end{cases} \tag{2.28}$$

Moreover assuming that each IM considered in multiple sites is modelled as a GRF, whose at least one spatial correlation model is known, the conditional simulation of those IMs can be realized following those steps: 1) simulation of the unconditional means of the two IMs from the specified GMPEs for each site 2) evaluation of residual terms for the first IM (e.g. PGA) according to the own spatial correlation model 3) evaluation of residual terms of the second IM (e.g. PGV) for each site according to the normal distribution whose parameters are described by Eq. (2.28).

This approach has the advantage to avoid making assumptions about the structure of the cross correlation between the two IMs. Moreover since the spatial simulation is made only for one IM, it can be conditioned upon the ground motion parameter for which the spatial correlation model is available. The secondary IM (or IMs) is simulated then on the basis of his correlation to the first IM. The only requirement of this procedure is the availability of correlation coefficients between different IMs. Several studies in literature have been tackled this issue: Inoue and Cornell (1990), Backer and Cornell (2006) and Baker and Jayaram (2008) are only some examples.

Chapter 3 – SYSTEM CHARACTERIZATION AND FRAGILITY ANALYSIS OF GAS NETWORKS

3.1. Natural Gas System

Natural gas is considered among the world's most important resource. The process and systems involved are highly complex and capital-intensive. The natural gas system can be subdivided essentially into two major parts (as shown in Fig. (3.1)):

- Production/Processing
- Transmission/Distribution

Production facilities consist of onshore facilities (production field) or offshore (marine-water) platforms. The former is an area encompassing a group of oil and gas pools and wells (oil, gas and condensate wells). The natural gas that comes from oil wells is typically referred to as 'associated gas'. The 'associate gas' can exist separate from oil (free gas), or dissolved in the crude oil (dissolved gas). The natural gas that comes from gas and condensate wells, where there is little or no crude oil, is termed 'non-associated gas'. Gas wells typically produce raw natural gas, while condensate wells produce free natural gas along with a semi-liquid hydrocarbon condensate.

In Europe gas supply essentially comes from four sources outside of domestic production; production within the Europe accounts for around a third, and imports come from the following four countries: Russia (46% of imports), Norway (27%), and Algeria (20%), and to a lesser extent Nigeria (less than 8%). Proportions of supply sources vary from member state to member state for obvious geographic reasons. The dominance of Algerian gas in the mix of Mediterranean states (Italy, France, and also Portugal) contrasts with Russia's dominance in Central Europe, notably in the new member states and Germany. The rest comes from internal production, which rose to 33% in 2005 (Nies, 2008).

The production facility is complemented by a gathering facility, which is a flow-line network (surface pipeline) and by process facilities that transport and control the flow of oil or gas from the wells to the main storage facility, the processing plant or the shipping point. There are two types of gathering systems, radial and trunk line.

The radial type brings all the flow-lines to a central header, while the trunk-line type uses several remote headers to collect fluid. The latter is mainly used in large fields. The gathering line consists of low pressure, low diameter pipelines that transport raw natural gas from the wellhead to the processing plant. The natural gas must be purified before it can be transported. Therefore, after its extraction, the natural gas is processed in order to obtain pipeline quality gas, namely dry natural gas. The gas is treated to remove any contaminants, water, and dust or petroleum liquids. The processing can be done at the wellhead and at centralized processing plant.In the production and the processing facility, the gas is treated through a chemical and a heating process. In offshore development, instead, field platforms or floating vessels are used for the production and extraction process.

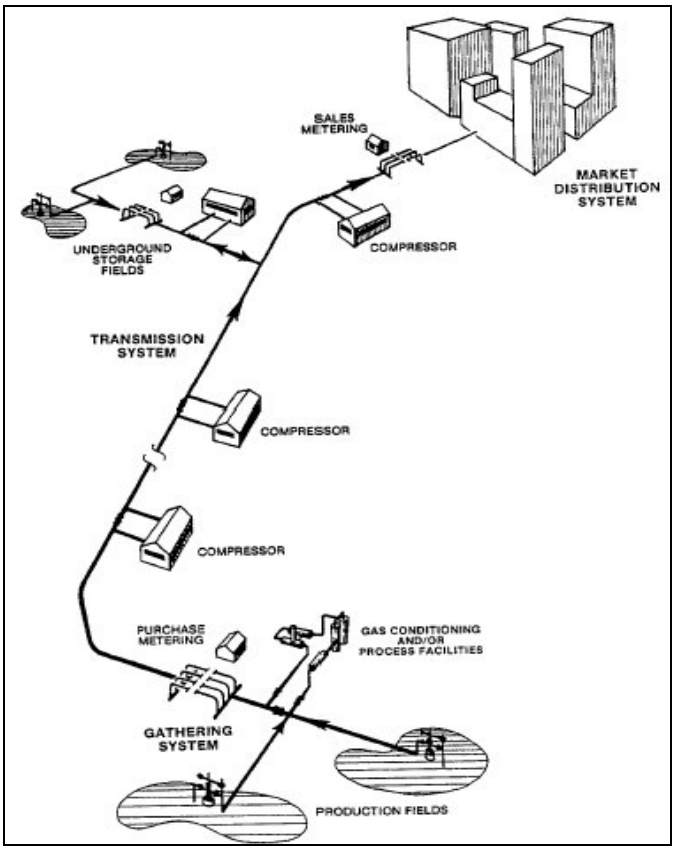

Figure 3.1 Scheme of a gas system

After the separation from water and sediments, gas is placed in storage areas. From there the resource can be pumped through pipelines to the loading terminals

where is ready to be transported. Storage facilities are usually of two types: underground storage facilities (depleted gas reservoirs, aquifers, salt caverns); and storage tanks for Liquefied Natural Gas (LNG) that includes pipes and electric components.

The gas transmission pipelines use compressors to force the gas through the pipe; when the natural gas enters into the compressor station, it is compressed by a turbine, a motor, or an engine to ensure that the flowing of the natural gas, through any pipeline, remains pressurized. The turbine operates a centrifugal compressor that, using a fan, compresses and pumps the natural gas through the pipeline. Natural gas engines are also used to power some compressor stations. Compressor stations usually contain scrubbers and filters that capture any undesirable particles or liquids that might be still contained in the natural gas flowing through the pipeline.

Before reaching a major metropolitan area, the natural gas is diverted through intermediate stations (metering/pressure reduction stations) where the pressure is reduced, measured, and sold to the local gas company. Metering/Pressure Regulator Stations contain metering equipments for monitoring and managing the natural gas in their pipes, including the reduction of the gas pressure before its distribution into the pipe system. The natural gas company distributes the natural gas through an underground network of smaller pipelines called "mains." Smaller lines called "services" connect the mains to the end-users. Along the distribution system there are other intermediate stations (regulator stations) where gas pressure is reduced as required for the gas to arrive to the end-user.

Therefore there are three major types of pipelines used in three different systems: 1) the gathering system connects the wellhead to the treatment plant and it is characterized by low pressure and diameter pipelines; 2) the transportation system transports gas from the treatment plant to the distribution systems, often across long distances and it is characterized by high pressure and large diameter pipelines; 3) the distribution system that connects regulator stations to the city, communities and it is characterized by low pressure and small-diameter pipelines. Moreover pipeline systems may include a great number of valves along their entire distributed network. These valves work like gateways: they are open to allow the flow of the natural gas and they can be closed to stop the gas flow along a certain section of pipe. In addition for the safe and continuous conveyance of gas fuels, control and communication systems are critical and vital to guarantee an effective and timely emergency response. In particular, Supervisory Control and Data Acquisition, SCADA, which stands for sophisticated communications systems that take measurements and collect data along

the pipeline network (usually in a metering or compressor stations and valves) and transmit them to centralized control stations. This enables a quick reaction to equipment malfunctions, leaks, or any other unusual activity along the pipeline. Some SCADA systems incorporate the ability to remotely operate certain equipment along the pipeline, including compressor stations, allowing engineers in a centralized control center to immediately and easily adjust flow rates in the pipeline.

Note that methodologies illustrated in this thesis focus on the systems components that belonging to the transmission and distribution part. As explained in Franchin *et al.* (2011), system components may be classified essentially in "point-like" components (critical facilities) or "line-like" (network) components respect to the geometric point of view and the approaches used for the characterization and definition of the vulnerability. According to this classification production and treatment plants may be considered as "critically facility", i.e. single site-facilities whose importance for the functionality of the system (or generally more systems if they are interconnected with other networks) makes them critical, justifying a detailed description and analysis. Therefore stations, storage facilities and pipelines are considered "line-like" components, and the vulnerability methodology explained below will be referred to these components.

3.1.1. Past earthquake effects on system components

According to (Eguchi, 1987), past earthquakes have caused significant damage to pipeline system networks.

For above-ground components of pipeline systems, such as buildings and storage tanks, inertial forces resulting from ground shaking are a major concern. According to (EERI, 1986), damage to tanks has been quite common throughout past earthquakes as in the 1975 Imperial Valley earthquake and the 1985 Chile earthquake. Reports from past earthquakes show little information on above ground facilities (intermediate stations), yet the small number of incidents associated to these components tends to indicate a good behaviour of these support facilities during an earthquake. The anchorage of subcomponents is especially a crucial point, as unanchored equipment can lead to the rupture of electrical connections or the tipping and sliding of mechanical parts.

For buried pipelines, major problems seem to be most related to faulting, landslides, and liquefaction induced deformation. The first sign of damages to buried pipelines is the 1906 San Francisco earthquake, which resulted in significant fires through the city, due to the rupture of water lines needed by fire-hydrants. Regarding

the causes of damage, according to (O'Rourke and Liu, 1999), the zones of lateral spreading accounted for only 5% of the built-up area affected by strong ground shaking, yet approximately 50% of all pipeline breaks occurred within one city block of these zones: this fact demonstrate the high impact of ground failure on pipelines damage. However significant damage to the gas pipeline system due to ground shaking have been also observed in four earthquakes : the 1933 Long Beach, 1952 and 1954 Kern County, 1971 San Fernando and 1994 Northridge earthquakes (O'Rourke and Palmer, 1996). According to O'Rourke and Palmer (1996) damages to gas transmission and supply lines followed these earthquakes occurred primarily in the form of ruptures of oxy-acetylene girth welds in areas which lack of significant permanent deformation.

3.2. Physical characteristics and fragility analysis

To estimate earthquake damage to a natural gas system, given knowledge of ground shaking (or ground failure), earthquake intensity parameters have to be correlated with system component damage in terms of fragility functions. In fact these relations provide the probability of reaching or exceeding a particular damage state (level of damage) given the level of ground shaking (or ground failure). To this aim the typology classification of each component, damage scale definition and the intensity measures have to be defined. Based on these fragility curves, functionality of each component of the natural gas system can be assessed.

3.2.1. Buried pipelines

Natural gas pipelines are operating at various pressures, depending on their scale:

- Supra-regional transmission pipelines: these pipelines operate at very high pressures (~100 bar) and present large diameters (up to 1.40 m). Such pipelines can cover large area;
- Regional transmission/distribution pipelines: these pipes still operate at high pressure (from 1 to 70 bar) and are used to connect local distribution systems;
- Local distribution pipelines: these smaller pipelines usually operate in the medium (0.1 – 4 bar) or low-pressure (< 0.1 bar) range;

In addition to this classification, the pipeline typologies mainly rely on the following parameters (Gehl *et al.*, 2010):

- material type (usually PVC, HDPE, Cast Iron, Ductile Iron, Steel)
- material strength
- diameter
- wall thickness
- smoothness of coating
- type of connection
- design flow

Fragility curves available in literature are usually based on empirical data collected throughout past earthquakes. The usual practice is to evaluate the Repair Rate, R_R, parameter of a Poisson process model, which is defined as the number of pipeline repairs in an area divided by the length of the pipelines in the same area, with respect to a parameter (i.e. an intensity measure, IM) representative of ground shaking (e.g. PGV or PGA) or ground failure (e.g. permanent ground deformation, PGD). Empirical data is collected from field crews of gas / oil companies operating the pipelines and consists of the following: length of pipes subjected to a given level of ground shaking, and the number of repairs carried out for that segment. This means that this data may be generic characterized for example by some inaccuracies, including omitted address indication, vague damage description and multiple repairs at a single site combined into one record. Moreover no distinction is made between the different kinds of repairs: complete fracture of the pipe, leak in the pipe or damage to an appurtenance of the pipe (ALA, 2001a).Then, based on the data points, a correlation procedure is performed in order to fit a predefined functional form with the empirical data, for example linear models ($R_R = a \cdot IM$) or power models ($R_R = b \cdot IM^c$). Depending on the consistency of the available data, it is possible to build specific models based on various factor such as pipe material, pipe diameter or pipe connections; hence a corrective factor K is usually added to the fragility model in order to account different factors that affect the vulnerability of pipelines. For example, considering a linear model, fragility functions for a generic IM is expressed by Eq. (3.1):

$$R_R = K \cdot a \cdot IM \tag{3.1}$$

As mentioned previously, buried pipelines are very sensitive to permanent ground deformation (resulting from various ground failures), in addition to transient ground deformation due to seismic wave propagation: the characteristics of these physical phenomena are summed up in Tab. (3.1).

Table 3.1Two main types of sollicitations

	Permanent ground deformation	**Transient ground deformation**
Hazard	surface faulting, liquefaction, landslides	R-waves, S-waves
Intensity measure	PGD	PGV, PGA, strain

Wave passage effects are transient vibratory soil deformations caused by seismic waves generated during an earthquake. Wave passage effects cover a wide geographic area and affect pipe in all types of soil. Strains are induced in buried pipe because of its restraint within the soil mass. Among the various seismic parameters used to correlate the ground motion effects to the damage suffered by buried pipeline, PGV has been identified as the one having a more direct physical interpretation (O'Rourke *et al.* 1998). In theory, for vertically propagating shear waves, peak ground strain is directly proportional to peak ground particle velocity (PGV); therefore, PGV is a natural demand description (ALA, 2001a).

Many PGV fragility relations are available in literature, as O'Rourke and Ayala (1993), Eidinger (1998), ALA (2001a), HAZUS (FEMA 1999, 2004). Some of them are expressed in Tab. (3.2)[5] and compared graphically in Fig. (3.2).

Table 3.2 Pipeline fragility curves for PGV

Author	**Fragility relation**	**Notes**
ALA (2001a)	$R_R = K_1 \cdot 0.002416 \cdot PGV$	"backbone[6]" curve (K_1=1)
HAZUS (FEMA, 1999)	$R_R = 0.00003 \cdot PGV^{2.25}$	"ductile pipes" curve

[5] Fragility relations reported in Tab. (3.2) were converted by Tromans (2004): R_R was converted from 1/feet*10^3 to 1/km and PGV from inch/s to cm/s.

[6] Backbone fragility functions represent the average performance of all kinds of pipes in earthquakes. These functions can be used when there is no knowledge of the pipe materials, joint type, diameter, etc.

Eidinger (1998)	$R_R = K_1 \cdot 0.0001658 \cdot PGV^{1.98}$	"best-fit" curve (K_1=1)

As mentioned previously, depending on the availability of data used for the estimation of fragility curves, a corrective factor may be added to the formulation.
As example values of modification factor, K_1 estimated in ALA (2001a) for different combination of pipe material, join type, soil type and pipe diameter are summarized in Tab. (3.3).

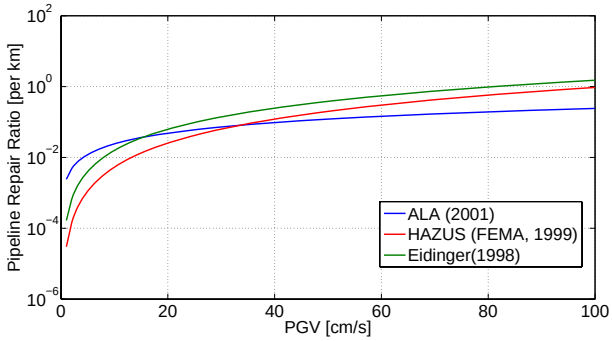

Figure 3.2 Fragility curves expressed in Tab. (3.2)

However, the seismic response of buried pipes is mostly controlled by the amplitude of transient strain induced in the ground by the wave propagation. In case of body waves, S-waves only are considered, since they tend to generate larger ground motion that P-waves. Concerning surface waves, the most significant motions are caused by Rayleigh waves. O'Rourke and Deyoe, (2004) proposed a relation between peak ground strain and R_R introducing also a distinction between the type of wave.

Although using transient ground strain as an intensity measure parameter seems really powerful, the studies carried out so far do not develop fragility functions for the typology directly concerned with gas pipelines: these are usually made of ductile materials, whereas the results of O'Rourke and Deyoe (2004) are mainly relying on brittle segmented pipes, like cast-iron. Therefore PGV represents the best choice to characterize the transient ground deformation hazard since for this parameter a large number of empirical relations, based on a wide range of pipe typologies, is available.
A concise summary of fragility curves for buried pipes due to ground shaking can be found in Tromans (2004) and in Gehrl *et al.* (2010) including the dataset used and the range of applicability for each relation.

Ground failure effects are permanent soil movements caused by such phenomena as liquefaction, landslides and localized tectonic uplifts. These tend to be fairly

localized in a geographic area and potential zones can be identified a priori by the specific geotechnical conditions. Ground failure can be very damaging to buried pipe because potentially large, localized deformations can develop as soil masses deform and move relative to each other. Such deformations can cause pipe segments embedded within the soil to fracture or pull out of place. Permanent ground deformation (PGD) is used as the demand description. The PGD descriptor ignores any variation in the amount of ground displacement and the direction of ground displacement relative to the pipeline. If this level of detail is desired, then site-specific analytical methods should be used instead of area-wide vulnerability functions (ALA, 2001a). There are different PGD fragility relations available in literature, as Eguchi (1983), ALA (2001a), HAZUS (FEMA, 2004).

Table 3.3 Values of modification factor K_1 for PGV fragility curves (ALA, 2001a)

Pipe material	Joint type	Soil	Diameter[7]	K_1
Cast Iron	cement	unknown	small	**1.0**
	cement	corrosive	small	**1.4**
	cement	non corrosive	small	**0.7**
	rubber gasket	unknown	small	**0.8**
Welded Steel	arc welded	unknown	small	**0.6**
	arc welded	corrosive	small	**0.9**
	arc welded	non corrosive	small	**0.3**
	arc welded	all	large	**0.15**
	rubber gasket	unknown	small	**0.7**
	screwed	all	small	**1.3**
	riveted	all	small	**1.3**
Asbestos Cement	rubber gasket	all	small	**0.5**
	cement	all	small	**1.0**
Concrete	welded	all	large	**0.7**
	cement	all	large	**1.0**

[7] For the ALA (2001a) study, the "small" category includes pipes of 30.48 cm diameter, whereas "large" refers to diameter greater than 30.48 cm.

	rubber gasket	all	large	**0.8**
PVC	rubber gasket	all	small	**0.5**
Ductile Iron	rubber gasket	all	small	**0.5**

The empirical fragility proposed by Eguchi (1983) are focused on PGD induced by fault ruptures while vulnerability relation of ALA (2001a), has been estimated from four earthquakes where the liquefaction ground failure was the predominant mechanism. This relation is expressed by Eq. (3.2),

$$R_R = K_2 \cdot 11.223 \cdot PGD^{0.319} \tag{3.2}$$

where PGD is given in *m* and K_2 is the modification factor for different combination of pipe material and join type summarized in Tab. (3.4). A concise summary of fragility relations for permanent ground deformation can be found in O'Rourke and Liu (1999) with more developments given by ALA (2001a).

As stated before, empirical relations for the fragility of pipelines are based on the recorded number of repairs during past earthquakes, and no distinction is really made between damage states. As a result, all fragility relations for pipelines are given for a single "damage state", e.g. the repair rate per unit length of pipe.

Table 3.4 Values of modification factor K_2 for PGD fragility curves (ALA, 2001a)

Pipe material	**Joint type**	**K_2**
Cast Iron	cement	**1.0**
	rubber gasket	**0.8**
	mechanical restrained	**0.7**
Welded Steel	arc-welded, lap welds	**0.15**
	rubber gasket	**0.7**
Asbestos Cement	rubber gasket	**0.8**
	cement	**1.0**
Concrete	welded	**0.6**
	cement	**1.0**
	rubber gasket	**0.7**
PVC	rubber gasket	**0.8**

Ductile Iron	rubber gasket	**0.5**

However, according to HAZUS (FEMA, 2004), two damage states (summarized in Tab. 3.5) are considered: leaks and breaks and the type of repair or damage depends on the type of hazard: a damaged pipe because of ground failure is likely to present a break (it is assumed 80% breaks and 20% leaks), whereas ground shaking may induce more leak related damages (e.g. 20% breaks and 80% leaks). These percentages are accepted in the reviewed publications that are interested in making such distinction even if these values do not result from a specific argumentation. Then, using a Poisson probability distribution and the repair rate R_R, one can assess the probability of having n pipe breaks / leaks in a pipe segment of length L though the Eq. (3.3):

$$P\left(N=n\right)=e^{-R_R\cdot L}\cdot\frac{\left(R_R\cdot L\right)^n}{n!} \tag{3.3}$$

Therefore, assuming that a pipe segment fails (flow rupture) when it has a least one break along its length, the probability of failure is given by the Eq. (3.4):

$$P_f=1-P\left(N=0\right)=1-e^{-R_R\cdot L} \tag{3.4}$$

Finally, using the HAZUS assumption and considering the type of hazard, it is possible to assess the probability to have a pipe break or a pipe leak along the length of the segment

Table 3.5 Damage states for pipeline components

Damage state	Damage description
leakage	at least one leak along the pipe length
failure	at least one break along the pipe length

3.2.2. Storage facilities

Storage facilities are usually of two types: underground storage facilities (depleted gas reservoirs, aquifers, salt caverns); and storage tanks for Liquefied Natural Gas (LNG) that includes pipes and electric components.

Underground storage facilities are used for storing gas to balance seasonal variations in demand. They may be classified as: 1) seasonal supply reservoirs designed to be filled during the 214 day non-heating season (mostly gas/oil fields and

aquifers); 2) high-deliverability sites for 151-day heating season (mostly salt cavern reservoirs). These facilities are located hundred meters below the surface. They are usually natural geological reservoirs, such as depleted oil or gas fields or water-bearing sands on the top and impermeable cap rock.

Aside from underground storage facilities, natural gas is usually stored while in its liquefied state (LNG) in specific LNG tanks: these facilities are designed to insulate the gas from any heat ingress, using "auto-refrigeration" techniques. LNG will stay at near constant temperature if kept at constant pressure. As long as the steam (LNG vapour boil off) is allowed to leave the tank, in a safe and controlled manner, the temperature will remain constant. This vaporisation loss is collected from the tank and either reabsorbed as a liquid, sent to the gas output line connecting to the national gas grid, or used as fuel on the site. The LNG tanks would be of a full containment design. In a full containment system two tanks are employed, an inner tank which contains the stored liquid, and an outer tank which provides security in the event of any loss of containment or leak from the inner tank. Inner tanks are usually made of a nickel-steel alloy, whereas the outer tanks are a pre-stressed concrete construction (Gehl *et al.*, 2010). Storage tanks may be classified according to:

- Shape
- Capacity
- Dimension
- Material
- Construction type
- Style of roof system (Steel)
- Anchored or unanchored[8]
- Back up power

Past studies on the vulnerability of storage tanks usually propose PGA as the earthquake descriptor used to define the fragility curves. This seems to be a sound a choice as this acceleration-driven parameter is appropriate to account for the inertia forces inherent to these large and usually tall structures and the liquid contents within.

[8] Anchored means equipment designed with special seismic tie downs and tiebacks while unanchored means equipment with manufactures normal requirements.

Regarding fragility curves, empirical relations are also quite common, such as O'Rourke and So (2000), HAZUS (FEMA, 2004) and ALA (2001a). During past earthquakes, at each storage facility subjected to a given level of ground shaking, the proportion of damaged tanks has been evaluated. Observations may give some details about the type of failure, which is then translated into a damage state, DS , Eq. (3.5) defines the general form of a damage function for the storage facility:

$$P(DS \geq j) = \Phi_j\left(x\right) \tag{3.5}$$

where x reprents the intensity measure (IM) considered, $P(DS \geq j)$ is the probability of DS being in damage state j or higher, $\Phi_j\left(\cdot\right)$ is the cumulative distribution function of a normal random variable with mean $\ln(\mu_j)$ and standard deviation β_j .

An analytical approach can be found in the study of Iervolino *et al.,* (2004) where numeric analyses on dynamic models of unanchored steel tanks have been performed. The results (μ and β of the fragility function) are displayed as a response surface according two effects: the fluid height-over-radius ratio and the friction coefficient between the tank and the baseplate. This method is interesting, as it allows for the vulnerability assessment of all structures belonging to the "tank" typology. Yet, this study was only applied to one specific damage state (failure by elephant's foot buckling), and other sets of response surfaces should be needed for an exhaustive evaluation of the vulnerability of storage tanks.

Fragility curves from the literature, whether they are empirical or analytical, usually propose the same number of damage states and very similar definitions (O'Rourke and So, 2000; ALA, 2001a; FEMA, 2004). The detailed damage states used by HAZUS (FEMA, 2004) are summarized in the Tab. (3.6).

For each damage state, the HAZUS methodology proposes fragility curves accounting also for the fragility of the equipment needed for the tank facilities to function properly (i.e. electric power, tank, elevated pipes, electrical/mechanical component) using the logic fault-tree shown in Fig. (3.3).

Table 3.6 Damage states for tank farms defined in HAZUS (FEMA, 2004)

Damage state	Damage definition
None	No damage to tank or I/O pipes
Slight / minor	Damage to roof, minor loss of contents, minor damage to piping, but no elephant's foot buckling

Moderate	Elephant's foot buckling with minor loss of content
Extensive	Elephant's foot buckling with major loss of content, severe damage
Complete	Total failure, tank collapse

The global damage state is based on the individual damage state of its components and using the fault-tree analysis and the fragility parameters of the sub-components (lognormal distributions which parameters are summarized in Tab. 3.7), fragility curves for tank farms, with anchored or unanchored components are obtained. Tab. (3.8) shows the parameters of the corresponding lognormal distributions.

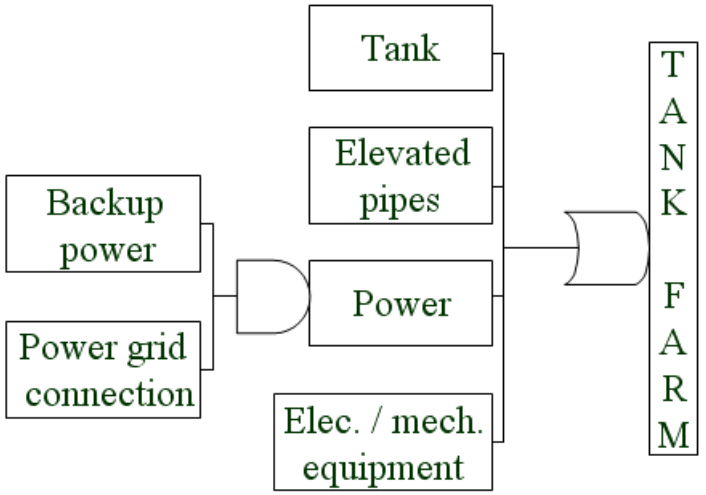

Figure 3.3 Fault-tree analysis proposed by HAZUS (FEMA, 2004) to assess the vulnerabiltiy of tank farms

Note that tank farms may be vulnerable also to PGD if they are located in liquefiable or landlisde soils.In HAZUS (FEMA, 2004) is mentioned that damage functions due to ground failure for these components are assumed to be similar to those described for buildings, unless specified otherwise.

In particular it is assumed that for lateral spreading, a lognormal damage function with a median of 60 inches and a dispersion of 1.2 is assumed for the damage state of at least extensive and 20% of this damage is assumed to be complete. For vertical settlement, a lognormal curve with a median of 10 inches and a dispersion of 1.2 is assumed for the damage state of at least extensive and 20% of this damage is assumed

to be complete. For fault movement or landslide, a lognormal curve with a median of 10 inches and a dispersion of 0.5 is assumed for complete damage state.

Table 3.7 Fragility curves of components (anchored or unanchored) of tank frams components, according to HAZUS (FEMA, 2004)

Components	**Damage state**	**Anchored**		**Unanchored**	
		μ(g)	**β**	**μ(g)**	**β**
Electric Power (Backup)	minor moderate	0.80 1.00	0.60 0.80	0.20 0.40	0.60 0.80
Loss of commercial Power	minor moderate	0.15 0.30	0.40 0.40	0.15 0.30	0.40 0.40
Electrical/ Mechanical Equipment	moderate	1.00	0.60	0.60	0.60
Steel tank	minor moderate extensive complete	0.30 0.70 1.25 1.60	0.60 0.60 0.65 0.60	0.15 0.35 0.68 0.95	0.70 0.75 0.75 0.70
Elevated pipes	extensive complete	0.53 1.00	0.60 0.60	0.53 1.00	0.60 0.60

Table 3.8 Fragility parameters for tank farms, according to HAZUS (FEMA, 2004)

Typology	**Damage state**	**μ(g)**	**β**
Tank farm with anchored components	slight / minor	0.29	0.55
	moderate	0.50	0.55
	extensive		
	complete	0.87	0.50
Tank farm with	slight / minor	0.12	0.55

unanchored components	moderate	0.23	0.55
	extensive	0.41	0.55
	complete	0.68	0.55

3.2.3. Stations

Four different types of stations exist in Gas System:

- Compression Stations: the natural gas enters into the compressor station, where it is compressed by a turbine, a motor, or an engine to ensure that the flowing of the natural gas, through any pipeline, remains pressurized. The turbine operates a centrifugal compressor that, using a fan, compresses and pumps the natural gas through the pipeline. Natural gas engines are also used to power some compressor stations. Compressor stations usually contain scrubbers and filters that capture any undesirable particles or liquids that might be still contained in the natural gas flowing through the pipeline.

- Metering /Pressure Reduction Stations: these stations contain metering equipments for monitoring and managing the natural gas in their pipes, including the reduction of the gas pressure before its distribution into the pipe system.

- Regulator Stations: at regulator stations gas pressure is reduced as required for the gas to arrive to the end-user.

- Metering Stations: metering stations are only measurement points.

Considering that stations mean the building and the equipments inside they may be classified with respect to:

- Building typology
- Anchored or unanchored subcomponents
- Existence of SCADA system
- Electrical and mechanical component

- Existence of back up power
- Kiosk Solution
- Buried equipment
- Equipment inside or near by the buildings

Processing facilities are mostly vulnerable to PGA, sometimes PGD, if located in liquefiable or landslide zones. Therefore, damage states and fragility curves for these components are defined and associated with either PGA or PGD (FEMA, 2004).

3.2.3.1. Compressor stations

This type of station is a facility which supplies gas with energy to move along the transmission lines. Compressor stations are also used in storage facilities to compress the gas when it is fed into the pipeline. Each station contains one or more centrifugal or reciprocating compressor units, and auxiliary equipment for purposes such as generating electricity or cooling discharge gas and SCADA system that controls the station with all the equipments. Two or more compressors in a station can be used either in parallel or in series (FEMA 233, 1992).

Regarding fragility analysis, in HAZUS (FEMA, 2004) damage algorithms are assumed to be similar to those described for pumping plants of oil systems. In particular compressor stations are categorized as having either anchored or unanchored subcomponents and a total of five damage states are defined (as shown in Tab. 3.9). As for tank farms, fragility curves for these components are based on the probabilistic combination of subcomponent damage functions using Boolean expressions of the fault tree analysis to describe the relationship of subcomponents with the component. Note that the Boolean logic is implicitly presented within the definition of a particular damage state. In general, the Boolean combinations do not produce a lognormal distribution, so a lognormal curve that best fits this probability distribution is determined numerically.

Table 3.9 Description of damage states for gas compressor (FEMA, 2004)

Damage state	**Description**
No	No damage
Slight/Minor Damage	Slight damage to building or full loss of commercial power and backup power for few days (< 3 days)

Moderate Damage	Considerable damage to mechanical and electrical equipment or considerable damage to building or loss of electric power and of backup for 7 days.
Extensive Damage	Building being extensively damaged, or the pumps badly damaged beyond repair.
Complete damage	Building collapsed

Table 3.10 Fragility curves for stations components (FEMA, 2004)

Components	**Damage state**	**Anchored components**		**Unanchored components**	
		μ(g)	**β**	**μ(g)**	**β**
Electric Power (Backup)	minor moderate	0.80 1.00	0.60 0.80	0.20 0.40	0.60 0.80
Loss of commercial Power	minor moderate	0.15 0.30	0.40 0.40	0.15 0.30	0.40 0.40
Vertical/ Horiz. Pump	extensive	1.25/1.60	0.60	1.25/1.60	0.60
Electrical/ Mechanical Equipment	moderate	1.00	0.60	0.60	0.60
Building	minor moderate extensive complete	0.15 0.40 0.80 1.50	0.80 0.80 0.80 0.80	0.15 0.40 0.80 1.50	0.80 0.80 0.80 0.80

3.2.4. Other components

Regarding pressure reduction stations and SCADA systems, no quantitative fragility curves are available in literature

3.3. Combined Damage due to Ground Failure and Ground Shaking

In order to evaluate the damage induced by the combination of ground failure and ground shaking hazard, this section describes the general formulation that can be

adopted. Regarding facilities (tank farms, stations) the combined damage state probability (due to occurrence of ground failure and ground shaking) is found using the principle of probability of a union of events.

Considering the hypothesis of independent events according to (FEMA, 2004) Equation (3.6) summarizes this operation:

$$P^C\left[DS \geq j\right] = P^S\left[DS \geq j\right] + P^F\left[DS \geq j\right] - P^S\left[DS \geq j\right] \cdot P^F\left[DS \geq j\right] \tag{3.6}$$

where S an F indicate the earthquake hazard, ground shaking and ground failure respectively, j is the particular damage state, and C indicates the combined probability for the damage state due to occurrence of ground failure or ground shaking.

Table 3.11 Fragility curves for gas compressor stations, according to HAZUS (FEMA, 2004)

Typology	Damage state	μ(g)	β
Anchored components	Minor	0.15	0.75
	Moderate	0.34	0.65
	Extensive	0.77	0.65
	Complete	1.50	0.80
Unanchored components	Minor	0.12	0.60
	Moderate	0.24	0.60
	Extensive	0.77	0.65
	Complete	1.50	0.80

Considering that the probability for the damage state due to occurrence of ground failure depends on the triggering of the ground failure phenomena, and $P^F\left[DS \geq j\right]$ is explicated as:

$$P^F\left[DS \geq j\right] = \phi\left(\frac{\ln\left(PGD_F\right) - \ln\left(\mu^F{}_j\right)}{\beta^F{}_j}\right) \cdot p_F \tag{3.7}$$

where p_F is the probability of ground failure occurrence and it is assumed a lognormal damage function characterized by median $\square^F{}_j$ and standard deviation $\square^F{}_j$.

Moreover considering that four are the principal forms of ground failure, i.e. surface faulting , landsliding , and volumetric settlement and lateral spreading due to liquefaction, the Eq. (3.6) may be generalized as in Eq. (3.8):

$$P^C\left[DS \geq j\right] = P\left(\bigcup_{k=1}^{n} E_k\right) = \sum_{k=1}^{n} P\left(E_k\right) - \sum P\left(\cap two\ events\right) + \sum P\left(\cap three\ events\right) + \ldots\ldots + \left(-1\right)^{n+1} P\left(E_1, E_2, \ldots, E_n\right) \quad (3.8)$$

where n indicates the numer of earthquake hazard and $P\left(E_k\right)$ is the damage state probability due to the k-th earthquake hazard.

One issue that may yet be unresolved when modeling geotechnical hazard for applications such as this, is if multiple effects are possible. In most application it is assumed that, for a given site, permanent displacement due to liquefaction, slope displacement and faulting are mutually exclusive. In this case in the Eq. (3.8) all products referring to ground failure phenomena are equal to zero. Depending on the nature of the models used to characterize the ground failure, this assumption may be valid for many applications. For liquefaction, however, it is possible that both lateral spreading and volumetric settlement may be observed at a particular site. This issue is not widely addressed in relevant literature on the subject, and may therefore need to be explored further in the case study applications.

Regarding pipelines, the combined fragility function (in terms of repair ratio) for a particular damage state j is generally evaluated hypothesizing that the earthquake hazards are mutually exclusive, as defined by the Eq. (3.9):

$$R_R{}^C = a_j \cdot R_R{}^S + b_j \cdot R_R{}^F \quad (3.9)$$

where a_j and b_j are the proportion of leaks and breaks with respect to the expected number of pipe repairs, e.g. 0.2 and 0.8 for j=1 (break) and 0.8 and 0.2 for j=2 (leak) according to values suggested by HAZUS. Moreover the combined hazard due to ground failure at the site is generally assumed to be the maximum of the three types of ground failure. This means that PGD value should refer to the maximum of all possible types of permanent displacement at a site. These assumptions are generally used in many applications due to the nature of empirical fragility curves.

3.4. L'Aquila gas distribution system

In the L`Aquila Region the gas is distributed via a 621 km pipeline network, 234 Km of that with gas flowing at medium pressure (2.5-3 bar) and the remaining 387 Km with gas flowing at low pressure (0.025-0.035 bar) (Fig. 3.4).

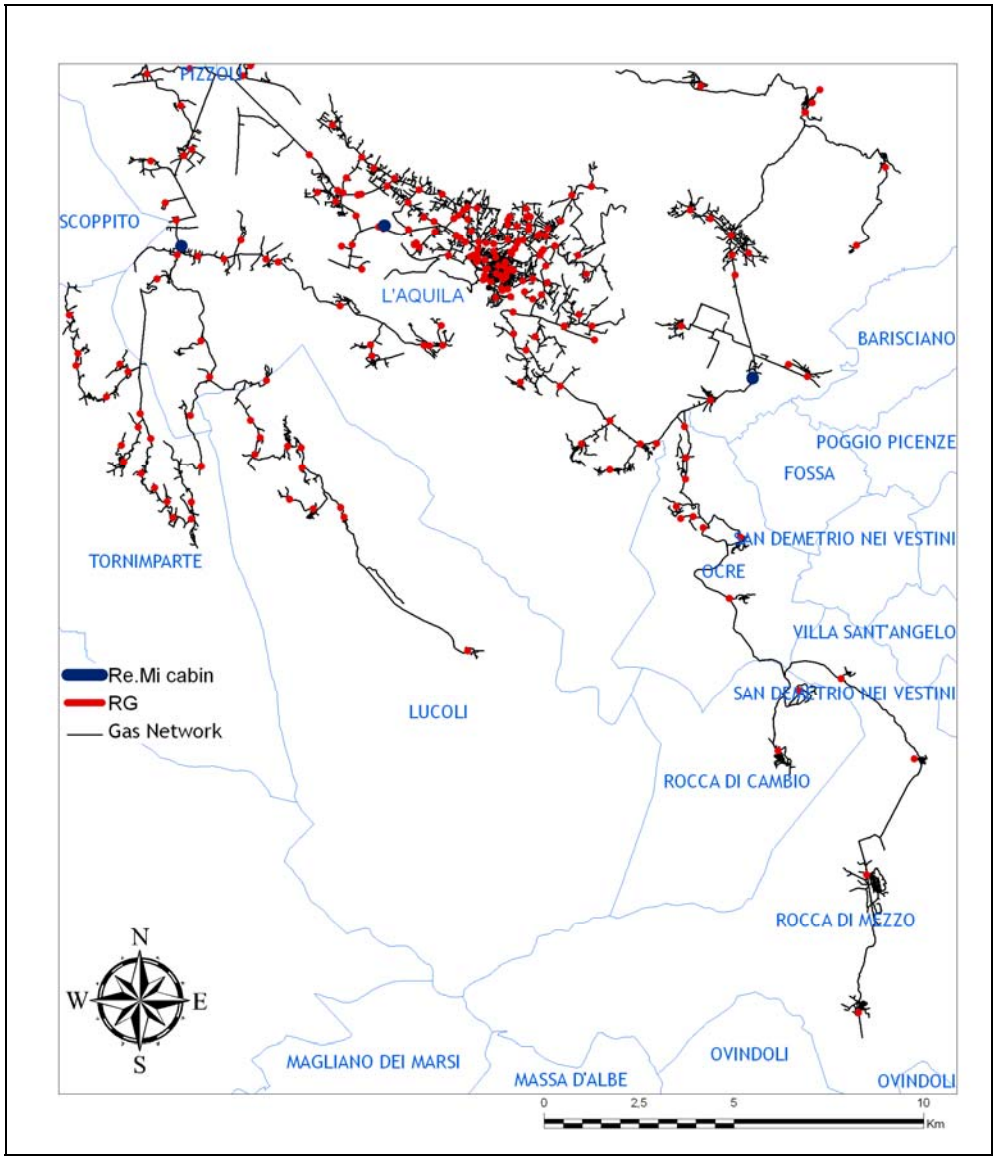

Figure 3.4 L'Aquila gas network

The medium-pressure distribution network is connected to the high pressure transmission network (operated by SNAM at national level) through three M/R stations (referred to as Re.Mi "REgolazione e MIsura" stations in Italian) providing gas to about 42300 customers in five municipalities (L'Aquila, Lucoli, Tornimparte, Ocre, Rocca di Cambio e Rocca di Mezzo). The three M/R stations are cased in one-story reinforced concrete structures with steel roofs (Fig. 3.5) hosting internal regulators and mechanical equipment (heat exchangers, boilers and bowls) where the gas undergoes the following processes: (1) gas preheating; (2) gas-pressure reduction and regulation; (3) gas odorizing; (5) gas-pressure measurement.

Figure 3.5 Metering/Pressure Reduction Stations external view (up) internal view (down)

The pipelines of the medium and low pressure distribution networks are either made of steel or HDPE (*High Density Polyethylene*) according to the pressure level (Tab. 3.12). The Maximum Service Pressure, MOP [bar], is the parameter adopted for classifying the pipelines accounting for the pressure of the gas flowing in the distribution network. The MOP is defined as the maximum allowed pressure of the gas inside the pipeline, expressed in bar. The MOP accounts for both the physical and the mechanical properties of the gas system components and is evaluated according to the Eq. (3.10):

$$MOP = \frac{20 \cdot MRS}{C(SDR - 1)} \tag{3.10}$$

where *MRS* is the Minimum Required Strength, *SDR* is the Standard Dimension Ratio and *C* is a safety factor.

Table 3.12 Pressure Classification and allowed material for pipelines according to the Italian Standards (D.M. 24/11/84 e s.m.)

Pressure Class	**Maximum Service Pressure MOP [bar]**	**Material (D.M. 24/11/84 e s.m.)**
1	MOP >24	Steel
2	12 < MOP ≤24	Steel
3	5 < MOP ≤ 12	Steel
4	1.5 < MOP ≤ 5	Steel; HDPE
5	0.5 < MOP ≤1.5	Steel; HDPE
6	0.04 < MOP ≤ 0.5	Steel; HDPE
7	MOP ≤ 0.04	Steel; HDPE

For HDPE pipes, the Minimum Required Strength *MRS* is the long-term hydrostatic capacity [MPa] (rounded according to the standards ISO 3:1973 and ISO 497:1973) with 97.5% probability to be exceeded in every HDPE specimen. The Standard Dimension Ratio, *SDR*, is a method of dimensionally rating gas pipelines; the SDR is the ratio of pipe external diameter to wall thickness (e.g. a SDR 11 means that the external diameter of the pipe is eleven times the wall thickness). The safety factor C is a coefficient that accounts for both the service conditions and the properties of the gas system components (usually C=1.25). HDPE pipes have nominal

diameters ranging from 32 to 400 mm, whereas diameter of steel pipes is usually between 25 and 300 mm. Moreover different types of in-line valves are found along the pipeline network (mainly gate valves, butterfly valves, check valves, ball valves). The transformation of the medium distribution pressure into the low distribution pressure (LP) is operated via 300 Reduction Groups (RGs). Generally along the low pressure network (in some cases also along medium distribution pressure network), there are several demand nodes (IDU, "Impianto di Derivazione Utenza" in Italian) consisting of buried and not buried pipes and accessory elements to supply natural gas to utilities. Moreover, depending on the type of final client of the network and whether there is an IDU system, there are three types of RG (as shown in Fig. 3.6): (a) GRM, Reduction Groups and Measure along medium distribution pressure (MP) network and direct connected to large users (e.g., industrial facilities); (b) GRU, Reduction Groups smaller than GRM for medium pressure users connected to a medium pressure IDU system; (c) GRF, Final Reduction Group connected to low pressure network. It is worth noting that all the components contained in both the L'Aquila M/R stations and reduction groups are unrestrained, and therefore especially seismically vulnerable. The 300 reduction groups, that in the L`Aquila gas distribution allow for the transformation of the medium distribution pressure into the low distribution pressure are either buried, sheltered in a metallic kiosk or housed within/close to a building (Fig. 3.7).

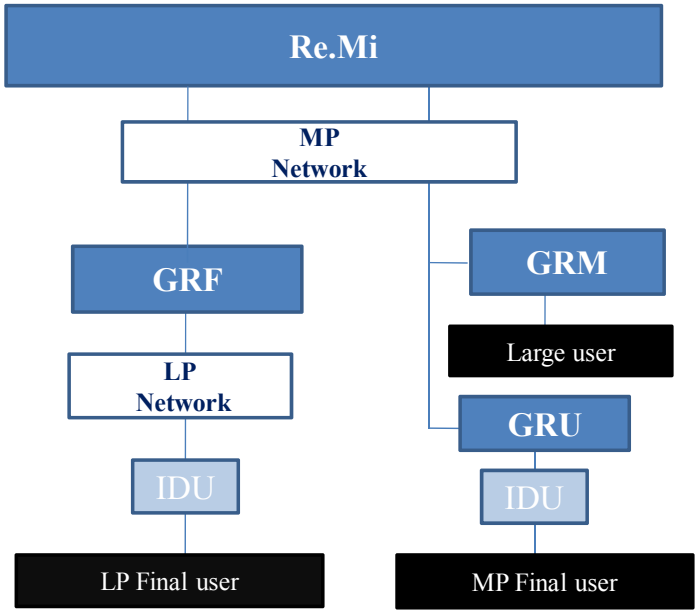

Figure 3.6 L'Aquila Gas system flow chart

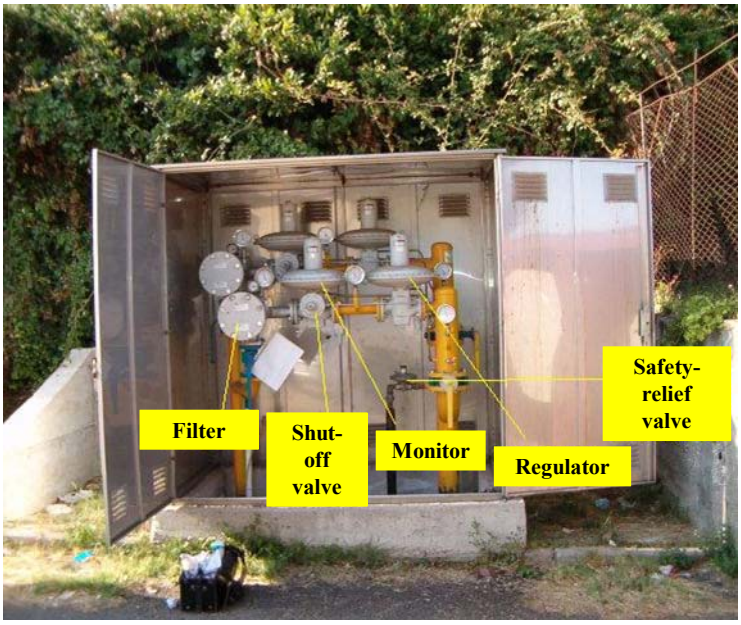

Figure 3.7. Reduction group in L`Aquila housed in a metallic kiosk

3.4.1. Description of database

The following sections provide an overview of the GIS databases available for the gas distribution network and a summary of the mechanical and geometric properties.

3.4.1.1. High Density Polyethylene pipelines

Data available for the HDPE (Italian acronyms PEAD, "Politilene ad Alta Densità") pipelines and their GIS representation are described in Tab. (3.13).

Nominal Dimensions *DN* (mm) for the HDPE pipelines in L`Aquila are: 32; 40; 50; 75; 90; 110; 125; 140; 160; 180; 200; 400. The nominal external diameter, d_n, the minimum average external diameter, $d_{em,min}$, the maximum average external diameter, $d_{em,\max}$, and the maximum deviation in circularity for the HDPE pipelines are correlated to the nominal dimension *DN* according to UNI EN 1555-2 standard. The minimum thickness e_{min}, for the HDPE pipelines is related to the Nominal Dimension *DN* and to the Standard Dimension Ratio *SDR*. In conformity with the UNI EN 1555-2 Standard the Standard Dimension Ratio *SDR* is related to the *MOP* and *MRS* according to Eq. (3.10).

Table 3.13 Description of database for HDPE pipelines

Component	Topology	Field Name	Type	Field Description
HDPE Gas pipelines	Line	MATERIAL	T ext	Material
		DN	Double	Nominal Dimension
		PRESSURE_CLASS	Integer	Pressure Classification
		DIAMETER_EXTmax_MM	Double	Max External Diameter [mm]
		DIAMETER_EXTmin_MM	Double	Min External Diameter [mm]
		THICK_MM	Double	Thickness [mm]
		DEPTH_M	Double	Depth [m]
		LENGTH_M	Double	Pipe length [m]
		CONNC_TYPE	Text	Joint Type
		YIELD_MPA	Double	Yield stress (MPa)
		YIELD_ELONGATION	Double	Yield Elongation (%)
		ULT_ ELONGATION	Double	Ultimate Elongation (%)
		CONS_YEAR	Double	Construction year

Regarding the mechanical and material properties HDPE pipelines of the L`Aquila gas system are PE100 types. The Design Strength, σ_s, for PE100 pipelines is σ_s=8 MPa. The Design Strength for a certain application is the ratio between the Minimum Required Strength, MRS, and the safety factor, C. For PE100 pipelines, MRS=10 MPa and C=1.25. Tab. (3.14) shows further mechanical properties for PE100 pipelines. Tab. (3.15) shows material properties for PE100 pipelines.

Table 3.14 Mechanical Properties of HDPE pipelines

Mechanical Properties	Symbol	Units	Value	Testing condition	Testing Protocol
Yield strength	-	[MPa]	23	*at 23 C°*	ISO 527
Yield elongation	-	%	9	*at 23 C°*	ISO 527
Ultimate elongation	-	%	≥350	*e < 13 mm v=100 mm/min* *e ≥ 13 mm v=25 mm/min*	EN 638
E modulus (tension)	-	MPa	900	*at 23 C°*	ISO 527
E modulus (flexure)	-	MPa	1200		DIN 54852 Z4

Table 3.15 Material Properties of HDPE pipelines

Material Properties	Symbol	Units	Value	Testing Conditions	Testing Protocol
Density		[Kg/m^3]	958	at 23 C°	ISO 1183
Viscosity		[cm^3/g]	≥360		ISO 1628-3
Fluidity Index	MFR190/5	[g/10 min]	0.22	at 190 C° weight 5kg	ISO 1133
Fluidity Index	MFR 190/21.6	[g/10 min]	6.6	at 190 C° weight 21.6 kg	ISO 1133
Minimum required strength	MRS	[MPa]	>10		ISO TR 9080
Slow crack growth resistance	SGC	[h]	>1000	*σ=4.0Mpa; 80 °C; >165h*	EN 33479
Rapid Crack propagation	RCP	[bar]	>25	*Specimens ∅=110x10*	ISO DIS 13477

3.4.1.2. Steel pipelines

Data available for the steel pipelines and their GIS representation are described in Tab. (3.16).

Table 3.16 Description of database for steel pipelines.

Component	Topology	Field Name	Type	Field Description
HDPE Gas pipelines	Line	MATERIAL	Text	Material
		DN	Double	Nominal Dimension
		PRESSURE_CLASS	Integer	Pressure Classification
		DIAMETER_EXT_MM	Double	Nominal External Diameter [mm]
		THICK_MM	Double	Thickness [mm]
		DEPTH_M	Double	Depth [m]
		LENGTH_M	Double	Pipe length [m]
		CONNC_TYPE	Text	Joint Type
		YIELD_N_MM2	Double	Yield strength [N/mm^2]
		ELONGATION	Double	Elongation [%]
		TENSILE_N_MM2	Double	Ultimate Tensile Strength [N/mm^2]

		CONS_YEAR	Double	Construction year

Nominal Dimensions *DN* (mm) for the steel pipelines in L`Aquila are: 25; 32; 50; 65; 80; 100; 150; 200; 250; 300. The nominal external diameter, d_n, the nominal wall thickness, e_n, and the nominal mass are correlated to the nominal Dimension DN according to the UNI EN 10208-1 Standard. Tab. (3.17) shows the mechanical properties of the steel pipelines for the L`Aquila gas system (in conformity with the UNI EN 10208-1 Standard).

Table 3.17 Mechanical properties of steel pipelines

Steel Quality	**Yielding strength [N/mm^2]**	**Ultimate Tensile Strength [N/mm^2]**	**Elongation [%]**
L235GA	235	370-510	23
L245GA	245	415-555	22
L290GA	290	415-555	21
L360GA	360	460-620	20

3.4.1.3. Stations

Data available for Re.Mi.cabins and RGs are described in Tab. (3.18) and Tab. (3.19).

Table 3.18 Description of database for Re.Mi cabins

Field Name	**Type**
CODE	Integer
NAME	Text
LOCATION	Text
ADDRESS	Text
CONTRUCTION YEAR	Integer
REMOTE ALARM	Text
TELEMETRY	Text
SECOND REDUCTION	Text
ODORIZING SYSTEM	Text
INPUT PRESSURE (PRE-HEATED)[BAR]	Integer
MEASUREMENT PRESSURE [BAR]	Double
OUTPUT PRESSURE [BAR]	Double
FLOW (QIMP)[SMC/H]	Integer
RELIEF VALVE	Text
BUILDING	Text

GROUND	Text
FENCE	Text

3.4.2. Vulnerability assessment

As mentioned previously for pressure reduction stations (Re.Mi. and RG) no quantitative fragility curves are available in literature.

In the configuration where support equipment (e.g. regulators) is sheltered within a building, a solution is to treat these facilities as a common building. Thus, one can use fragility curves for low-rise reinforced concrete or masonry structures to assess the vulnerability. Another approach is to consider these facilities as systems and to aggregate the fragility of each component into a global systemic vulnerability based on a fault tree analysis. The fault tree decomposition follows a logic structure with AND/OR operators that indicate how to aggregate the fragilities of two connected components. Using the basic rules of system reliability it is possible to build up the global probability of failure of the processing facility and to account for the fragility of both the building and the components within.

Table 3.19 Description of database for Regulator stations

Field Name	**Type**	**Field Description**
ALLOGGIAME	Text	Housing
ANNOCOSTRU	Integer	Construction Year
FACTYP1020	Text	Gas System Component
INSONORIZZ	Text	Soundproofing
LINEE	Text	Lines
PMASSIMAIN	Double	Maximum Pressure
PMINIMA	Double	Minimum Pressure
PORTATANOM	Double	Nominal Flow
PUSCITA	Double	Exit Pressure
RECINZIONE	Text	Fence
TELEALLARM	Text	Remote Alarm
TELEMISURA	Text	Telemetry
TERRENOPIA	Text	Ground Typology
TIPOGRUPPO	Text	Reduction group type
UBICAZIONE	Text	Location

To this aim, in collaboration with the network operator, a fault tree analysis of Re.Mi station and RG has been performed. The fault-tree decomposition has been applied to Re.Mi cabins in order to identify which sub-component is critical with respect to seismic fragility. All sub-components are considered to be not anchored and simply supported on the ground (with the exception of bowls located in a separated area that are ceiling-mounted). The Re.Mi. station is decomposed in the following sub-components:

- Building
- Regulators
- Mechanical equipment (heat exchangers, boilers and bowls)

To compute the global fragility curve of the whole plant the fault tree shown in Fig. (3.8) has been formulated:

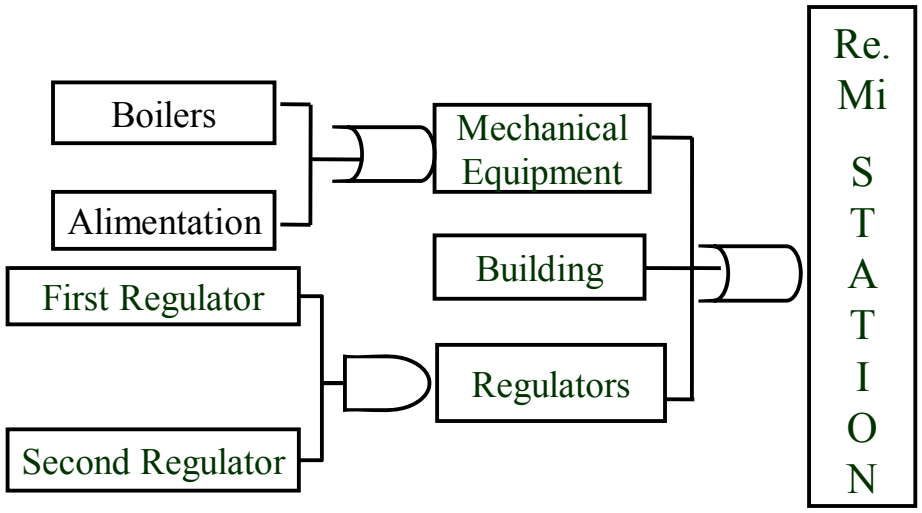

Figure 3.8 Fault tree analysis of a Re.Mi station

Since gas supply has to be maintained at all times, two installations are mounted in parallel where each installation is characterized by a regulator and a monitor. The monitor is a safety device that has to be able to prevent the outlet pressure from exceeding safe thresholds in the case of complete failure of the regulator, taking over the function of the primary, normally active regulator. During normal operation the monitor is fully open and if the pressure becomes equal to the setpoint of the monitor, the monitor will close to constrain the pressure.

According to experts' experience, two damage states have been indentified: Complete and Extensive that corresponds to a complete loss of functionality of the system (no gas supply).

Tab. (3.20) summarizes the damage states and the description.

Table 3.20 Damage states for the Re.Mi cabin

Damage state	**Description**
Complete	Building collapse
Extensive	Extensively damaged building, or both regulators damaged, or badly damaged boilers/heat alimentation

In particular, when boilers break down the gas flow is ensured since the freezing stops the system.RGs are decomposed, instead, in the following sub-components:

- Regulators
- Masonry housing (when it is present)

To compute the global fragility curve of the whole plant the fault tree shown in Fig. (3.9) has been formulated.

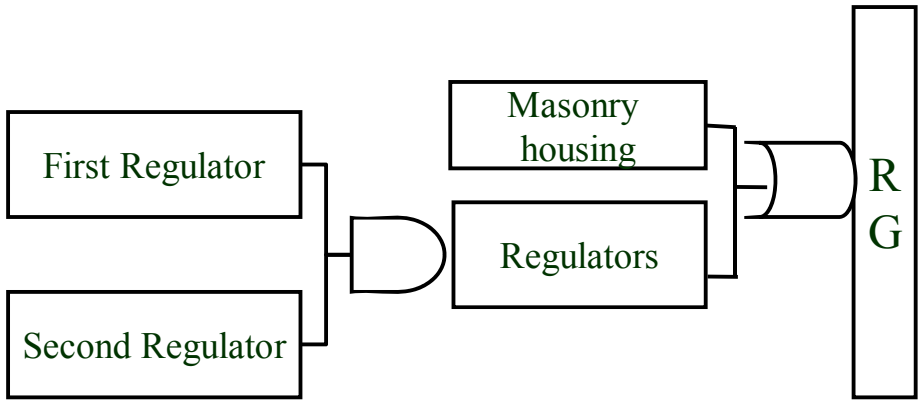

Figure 3.9 Fault-tree analysis of a Reduction Group

In the most of cases the safety device is ensured by the presence of shut-off valves that are able to block the gas flow. When the pressure exceeds a maximum value the valve closes. Also in this case two damage states have been identified that Tab. (3.21) summarizes.It is important to note that some RGs do not have the second regulator and this fact implies a higher vulnerability.

Table 3.21 Damage states of the Reduction Group

Damage state	**Description**
Complete	Building collapse (mansory housing)
Extensive	Extensively damaged housing, or both regulators damaged.

These preliminary results represent the first attempt for the developing of new fragility curves. Further research is needed in order to propose new fragility curves. However, as first approximation fragility curves of compressor stations of HAZUS (FEMA, 2004) will be used for the seismic analysis of the case study.

Regarding pipelines, fragility curves available in literature have been validated through an analysis of the damages occurred on the gas network following the 6th April L'Aquila earthquake by processing technical reports from Enel Rete Gas describing the repairs and replacements activities following the seismic event. In particular the ground shaking induced damage to the gas distribution network was analyzed to obtain the repair rate (number of repairs per km) as a function of the level of ground shaking experienced, expressed in terms of PGV. Results shows that the trend is somehow comparable with existing pipeline-fragility curves (see Appendix C for more details); although the fragility curves seems to be conservative on respect to the observed damage, it must be highlighted that the scatter associated with the empirical fragility relations is quite high since those fragility curves have been obtained combining data from different kinds of pipes (e.g. ALA 2001a).

Chapter 4 – SYSTEMIC VULNERABILITY ANALYSIS

4.1. Systemic Vulnerability analysis

Vulnerability assessment of a gas network can be measured generally in two perspectives:

- Connectivity reliability between node pairs where the main goal is related to determine the probability of the existence of a path connecting the source and the demand node when the links and the nodes are subjected to random failure events or in terms of serviceability defined by the aggregate functionality of facilities (nodes) composing the system, i.e. the number of distribution nodes which remain accessible from at least one supply node following the earthquake; in this case individual failures of each component do not influence other components vulnerability but change the topology of the network;
- Flow-performance reliability includes consideration of the network capacity, e.g. maintaining minimum head pressure related to leakages from two particular points of the network or related to a demand node or determining flow discharge of the network that quantifies the undelivered flow related to i -th distribution demand node related to leakages.

Moreover an extra vulnerability could be considered when the failure of one element is dependent on the failure of elements in the other networks. This regards inter-dependent networks such as gas and electricity network that are interconnected through the gas fired power plants that need fuel from gas pipeline systems to generate electricity.

Depending on the goal of the analysis, the performance of the system may be evaluated though the use of performance indicators that express numerically either the comparison of a demand with a capacity quantity, or the consequence of a mitigation action, or the assembled consequences of all damages.

4.1.1. Connectivity analysis

4.1.1.1. Functional modeling

Gas systems are networks that can be modeled as a graph composed by the set of nodes connected by edge links amongst each other. The way these connections are formed dictates how the vulnerability of each element influences the vulnerability of the network as a whole.

A graph G = (X, A) is a collection of points or vertices (node) x_1, x_2 … x_n (denoted by the set X) and a collection of lines (edge/branch) a_1, a_2 … a_n (denoted by the set A) joining all or some of these points. Graph can be divided into directed graph and undirected graph. If the lines in A have direction, which is usually shown by an arrow, they are called arcs and the resulting graph is called a directed graph (Christofides, 1975). Moreover a graph is said to be strongly connected if for any two vertices x_i and x_j, there is at least one path going to vertices x_i and x_j. For a strongly connected graph, vertex x_j is reachable from vertex x_i and vice versa for any x_i and x_j, the strong component containing a given vertex x_i is unique and x_i will appear in the set of vertices of one and only one strong component. Considering a gas network. This system is strongly connected if the gas flows in one direction between every two positions. The network is weakly connected if the gas flows in both directions between every two positions. The network is disconnected if there is no possible way for the gas to flow from one point to another.

These systems can be classified in two different types namely tree or loop. The tree type pipeline system happens where the pipeline system is not in the loop condition. While for the loop type system, the pipeline system contains loops. It is much easier to solve the calculations for the tree type system compare to the loop type pipeline system. This is due to the looped nature, flow and direction of each pipe cannot easily be calculated. Usually the tree type is used for the distribution level of the network since it has the task of reaching as close as possible to the end user.

Different graph theory algorithms and numerical methods exists, each of them solve different problems. Dijkstra's algorithm solves the shortest path problem for a directed graph with non negative edge weights. For example, if the vertices of the graph represent gas wells and edge weights represent distances between pairs of wells connected by a pipeline, this algorithm can be used to find the shortest route between two gas wells. The Depth First Search algorithm instead is used to determine which nodes are reachable from a given node. More details on graph theory algorithms can be found in Christofides (1975).

Graph theory is very useful to represent the network computation of any topology and to check the connectivity of the gas network systems.

4.1.1.2. Connectivity evaluation

In the seismic vulnerability assessment the general aim of a connectivity analysis is to determine if after the seismic event a demand node is accessible from at least on supply node. To this aim nodes should be distinguished considering their functionality. The nodes are generally treatment plant, storage tanks, stations and end user demand node. Moreover for the underground pipeline network construction, T-junction, and joints represent other nodes since in that place the failure probability is fairly high. The deliver line between the structures is the side of graph.

In order to compute performance indicators, that are used to provide a measure of the impact of the earthquake on the systemic vulnerability, it is important to designate which nodes in the network are sources and which are demand node. All the nodes that do not belong to either of these two classifications are considered transmission nodes. Directions of the flows are presumably from sources to demand node. In the case of gas transportation/distribution network the source node is represented by the gas treatment plant; moreover if it is possible to determine the intermediate response to the shortage of the gas in the system, the storage tanks must also be considered as source nodes in the graph representation. Nodes that are connected directly with customers are considered demand nodes.

It is important to note that if only the transportation (or distribution) part of the gas supply network is of concern, node functionality changes. In particular considering only the distribution network, regulator stations becomes source nodes.

4.1.2. Flow analysis

In a flow-based analysis the network performance is measured evaluating the satisfied customer demand after the earthquake event respect to that before the earthquake. In the case of gas network, for the purpose of calculating pipe flows and nodal pressure, Newton Nodal method in steady state condition and flow equations may be used respect to different pressure levels. A network is in a steady state when the values of the quantities characterizing the flow of gas in the system are independent of time and the system is described by a set of nonlinear algebraic equations (Osiadacz, 1987). In steady state analysis, the pressure of the nodes and the flow rate in the pipes must satisfy the flow equations and the value of load node and source node must fulfill the two Kirchhoff's laws, which are the Kirchhoff's first law and Kirchhoff's second law.

Common flow equations can be expressed in a general form (Osiadacz, 1987). For any pipe k, the pipe flow equation from node *i* to node *j* can be expressed as in Eq. (4.1):

$$\phi\left[\left(Q_n\right)_k\right] = K_k\left(Q_n^{m_1}\right)_k \tag{4.1}$$

where $\phi\left[\left(Q_n\right)_k\right]$ is the flow function for the pipe k, K_k is the pipe constant, $\left(Q_n\right)_k$ is the flow in the pipe k and m_1 is the flow exponent. The low pressure version of the equation is:

$$\phi\left[\left(Q_n\right)_k\right] = K_k\left(Q_n^2\right)_k = p_i - p_j \tag{4.2}$$

where p_i is the pipeline inlet pressure and p_j is the pipeline outlet pressure. The medium and high pressure version of the equation is:

$$\phi\left[\left(Q_n\right)_k\right] = K_k\left(Q_n^{m_1}\right)_k = p_i^2 - p^2{}_j \tag{4.3}$$

where m_1 is equal to 1.848 for medium pressure pipes and 1.854 for high pressure pipes.

Note that taking account of the fact that a change of the flow direction of the gas stream may take place in the network Eq. (4.2) and (4.3) should be rearranged respectively as:

$$\left(Q_n\right)_k = S_{ij}\left(\frac{S_{ij}\left(p_i - p_j\right)}{K_k}\right)^{0.5} \tag{4.4}$$

$$\left(Q_n\right)_k = S_{ij}\left(\frac{S_{ij}\left(p_i - p_j\right)}{K_k}\right)^{1/m_1} \tag{4.5}$$

where $S_{ij} = 1$ if $p_i > p_j$ and $S_{ij} = -1$ if $p_i < p_j$.

Details on Newton Nodal method and selection of flow equations can be found in Osiadacz (1987).

4.1.3. Inter-dependencies

Interdependencies that are likely to exist in service lifelines can be classified as physical, geographical, logical and cyber (Rinaldi *et al.*, 2011).

Physical dependencies between two systems exist if the state of each is dependent on the material output(s) of the other. For example gas transportation network depends

on electricity because of compressor station backup system. At the same time power network depends on gas system for fuel production. Examples of possible physical inter-dependencies for gas systems with other networks can be found in Esposito and Iervolino (2011c).

Infrastructures are geographically interdependent if a local environmental event can create state changes in all of them, affecting components across multiple infrastructures due to physical proximity (physical disaster propagation). Geospatial interdependency is the relationship that exists entirely because of the proximity of components. For example structural interaction in buried pipelines, especially in the case of being constructed in same ditch (water from the broken water pipe will degrade the transmission performance of the fiber-optics of telecommunication system in the proximity of the water pipe).

Cyber interdependencies are relatively new and include the reliance on telecommunications for supervisory control and data acquisition (SCADA) systems and information technology for e-commerce and business systems. For example a loss of the SCADA system in the electrical power grid will not by itself shut down the grid, but the ability to remotely monitor and operate the breakers is lost.

Two systems are logically interdependent if the state of each depends on the state of the other via a mechanism that is not a physical, cyber, or geographic connection. Logical interactions exist in infrastructures, which are linked through financial markets. A possible logical dependency is the impact that oil futures have on natural gas prices and ultimately the natural gas infrastructure via changes in infrastructure investment.

Several researchers have proposed different types of interdependency simulation models. Dueňas-Osorio *et al*. (2007) proposed a very simple model for interdependent lifeline systems in which the interdependency was determined by geographical immediacy. In particular, the study focuses on the dependence of a water system on the power grid. Adachi and Ellingwood (2008) evaluated the probability of lost functionality of a component whose serviceability depends on the behavior of another network, though the use of a fault tree analysis. A fault tree model in fact illustrates how the functionality of the primary and supporting systems are integrated. More recently Hernandez-Fajardo and Dueňas-Osorio (2011) have introduced an interdependence definition that allows a clear characterization of coupling links between interdependent systems; in particular interdependent failure propagation and evolution are modeled to include cascading effects from network interactions into fragility assessment.

4.2. Performance indicators

Within the seismic reliability analysis of a gas network it is needed to assess the performance of the whole system and its components when subjected to a seismic hazard. The quantitative measure of this performance is given by Performance Indicators (PIs), that express numerically either the comparison of a demand with a capacity quantity, or the consequence of a mitigation action, or the assembled consequences of all damages Therefore PIs are introduced to provide a measure of the impact of the earthquake on the systemic vulnerability and to quantify the degree to which the system is able to meet established specifications and/or customer requirements following an earthquake event.

Depending on the goal of the vulnerability analysis (connectivity or flow reliability) different PIs may be evaluated. Moreover as explained in Franchin *et al.* (2011), PIs can be categorized according to the object they refer to. Thus one has:

- Component level PIs
- System level PIs

In the following section some examples of performance indicators from the literature will be given. At the system level, the adaptation and use of two serviceability performance indicators, originally defined for the water supply system, namely the System Serviceability Index (Wang *et al*. 2010) and the Serviceability Ratio (Adachi and Ellingwood, 2008), is proposed. At the component level, the use of the Damage Consequent Index (Wang *et al*. 2010), originally defined for water pipes, is proposed to assess how the pipelines damage can impact on the system serviceability of gas systems.

4.2.1. System's performance indicators

- **System Serviceability Index** (Wang *et al*, 2010)

The System Serviceability Index (SSI), originally defined by Wang *et al*. (2010) for a water supply system, is proposed as a system performance indicator for the gas network. The SSI is a relative index that compares the serviceability of the utility network, in terms of customer demand satisfaction, before and after the earthquake. It is expressed by the following equation:

$$SSI = \frac{\sum_{i=1}^{n} Q_i}{\sum_{i=1}^{n_0} Q_i} \tag{4.6}$$

where n and n_0 are respectively the number of satisfied demand nodes after and before the earthquake and Qi is the demand (flow) at the i-th node.

- **Serviceability Ratio** (Adachi and Ellingwood, 2008)

The Serviceability Ratio (SR), originally defined by Adachi and Ellingwood (2008) for a water supply system, is proposed herein for a gas network. This index is directly related to the number of distribution nodes in the utility network, which remain accessible from at least one supply facility following the earthquake. It is computed as:

$$SR = \frac{\sum_{i=1}^{n} \left(w_i X_i \right)}{\sum_{i=1}^{n} w_i} \tag{4.7}$$

where SR is the serviceability ratio of the system defined on the domain [0,1], w_i is a weighting factor assigned to the distribution node i and X_i represents the functionality of facility i, which is modeled as the outcome of a Bernoulli trial (X_i = 1 if facility is accessible from at least one supply facility), and n is the number of distribution nodes.

- **Connectivity Loss** (Poljanšek *et al*., 2011)

Connectivity Loss (CL) measures the average reduction in the ability of sinks (gas-fired power plants) to receive flow from sources (gas fields and LNG terminals) counting the number of the sources connected to the i-th sink in the original (undamaged) network $N^i_{source,orig}$ and then in the damaged network $N^i_{source,dam}$. It is expressed by the following equation:

$$CL = 1 - \left\langle \frac{N^i_{source,dam}}{N^i_{source,orig}} \right\rangle_i \tag{4.8}$$

4.2.2. Component performance indicators

- **Damage Consequence Index** (Wang *et al.*, 2010)

The use of the Damage Consequence Index, DCI, originally defined for water system, is proposed herein for a gas network. DCI measures how the damage on a single pipe impacts on the overall system serviceability, by identifying critical links that significantly affect the system seismic performance. The Damage Consequences Index (DCI) is expressed as:

$$DCI_i = \frac{E\left[SSI\right] - E\left[SSI \mid L_i\right]}{1 - E\left[SSI\right]} \tag{4.9}$$

where $E\left[SSI\right]$ is the expected value of SSI defined in Eq. (4.6) and $E\left[SSI \mid L_i\right]$ is the conditional value of SSI that considers only the *i*-th damaged pipes. DCI_i measures the reduction of SSI given that the *i*-th pipe is damaged.

Chapter 5 – PROBABILISTIC SEISMIC RISK ASSESSMENT OF L'AQUILA GAS DISTRIBUTION NETWORK

5.1. Framework

The proposed methodology for the evaluation of seismic performance of gas networks is herein applied to L'Aquila gas distribution system and it consists of five major steps:

1. Seismic hazard assessment of L'Aquila region considering as source the Paganica fault on which L'Aquila (central Italy) 2009 earthquake was originated though the simulation of probabilistic scenarios earthquakes of strong motion parametrs on a regular grid that covers the region of interest.
2. Evaluation of the PGD hazard, in particular focusing on the effects induced by landlside, in order to estimate the seismic demand due to geotechnical hazard.
3. Seismic demand evaluation at each facility and distributing elements within the network to obtain the failure probability though the use of appropriate fragility curves.
4. Systemic vulnerability analysis though the use of a connectivity algorithm to integrate the damage of facilities and distributing elements into the damage of the system.
5. Probabilistic risk assessment of the case study using Monte Carlo simulation in terms of mean functionality and annual exceedance curve.

The methodology presented has been tested via the implementation of the case study in the OOFIM software developed in a Matlab environmental (Mathwork, 2010) by the University of Rome "La Sapienza" . The software, created in relation of the objectives of the Syner-G project, adheres to the OBJECT-ORIENTED Paradigm (OOP) where the problem is described as a set of objects, "software containers" grouping together related procedures and data. Data elements are called attributes of an object. Procedures which operate on data specific for an object are called methods. Objects are instances (concrete realizations) of classes (abstract models) that are used

to model the system. Fig. (5.1) shows the classes implemented in the OOFIM software at the time of release (April 2011) of the deliverable 2.1 (Franchin *et al.*, 2011) of Syner-G project, in which the object-oriented modeling and software development are described.

The first class, *Analysis*, contains the analysis methods required to evaluate the overall impact of wave propagation hazard on an infrastructure, and acts upon the *Enviroment* class. This latter class is composed of two classes, the *Infrastructure* and the *Hazard*. The *Enviroment* is the portion of physical space that needs to be considered in evaluating the impact of the hazard on the Infrastructure. The *Hazard* class is an abstract class, generalization of the *Natural* class that contains environmental hazards such as the seismic one. The *Seismic* hazard, in turn, is modeled as the composition of three classes: one class for seismo-generic sources, one for ground-motion prediction equations and one for the description of events. The *Infrastructure* class is the generalization of the *Physical* class made up of two classes: the *Network* class and the *Inhabited Area* class. The *Network* class is an abstract class, generalization of all types of networks. Note that, as shown in the figure, the classes interact with each other (i.e. they are associated). Association means that an object from a class can call the methods from another class. In physical terms this means that the object describing the set of buildings in a neighborhood (object from the *Inhabited Area* class) can "ask" to the object electric power network (from the corresponding class) whether there is still electric power fed to the neighborhood after the seismic event. *Network* class is composed of two classes: EPN (electric power network) and WSS (water supply system) which are the only systems implemented in the software at the time of release of the deliverable 2.1. These systems are made up of nodes and links connecting them; therefore WSS and EPN classes are the composition of the corresponding node and link classes. More details on the object-oriented modeling and specification of the classes implemented in the software can be found in Franchin *et al.* (2011).

For the purpose of the thesis the programme has been equipped with the *GAS* class, focusing on the components of a gas distribution system, in order to evaluate seismic performance of the L'Aquila gas distribution network. The gas distribution system class, illustrated in Fig. (5.2) is the composition of node and link abstract classes, of which the first is the generalization of *Pipe* class, while the second is the generalization of *FinalNode*, *GasSource* and *Station* classes. In particular the *FinalNode* class is the generalization of *IDU* class that represents the node directly connected with customers (demand node) and *Joint* class that represents nodes used to reproduce the geometry of the system but characterized by a demand equal to zero.

The *Station* class is represented by regulator stations while the *Source* class is represented by Metering/pressure Reduction stations (M/R) that are used to connect the distribution medium-pressure network to the high-pressure transmission lines.

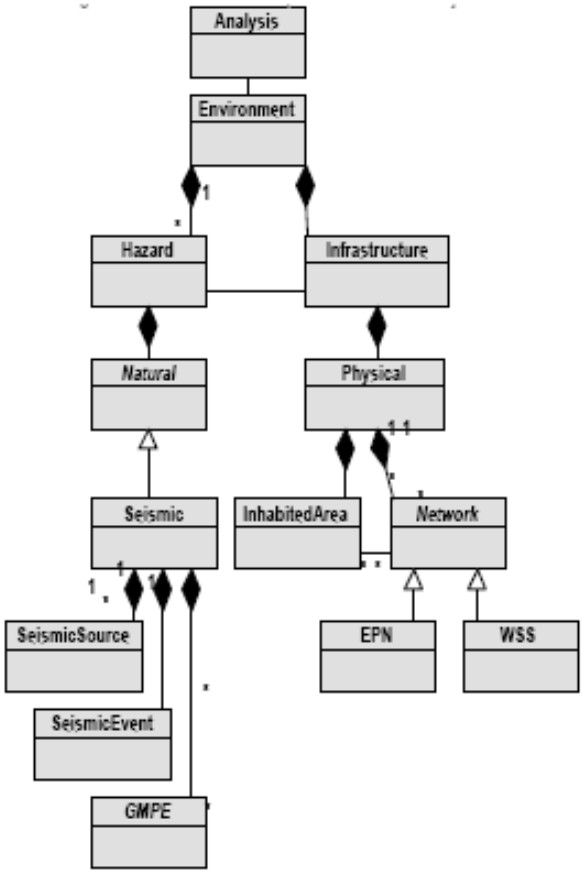

Figure 5.1 Classes implemented in the OOFIM software at the time of release of the deliverable 2.1 (Franchin *et al.*, 2011)

Each class is characterized by attributes and methods. Attributes refer to properties that describe the whole system and each component. For example for the gas distribution system class, possible attributes may be related to the number of links and nodes presented in the system, the list of vulnerable sites and the corresponding intensity measures, or the connectivity and adjacency matrix used for the evaluation state by state of connectivity performance measures. Possible attributes for link and nodes instead may be related to geographical coordinates, site class, material and other data necessary as input to compute fragility and system component performance measures. Methods, instead, may be related for example to the computation of flow in

all pipes and nodes or accessibility of demand nodes or fragility of links and nodes if they are considered vulnerable.

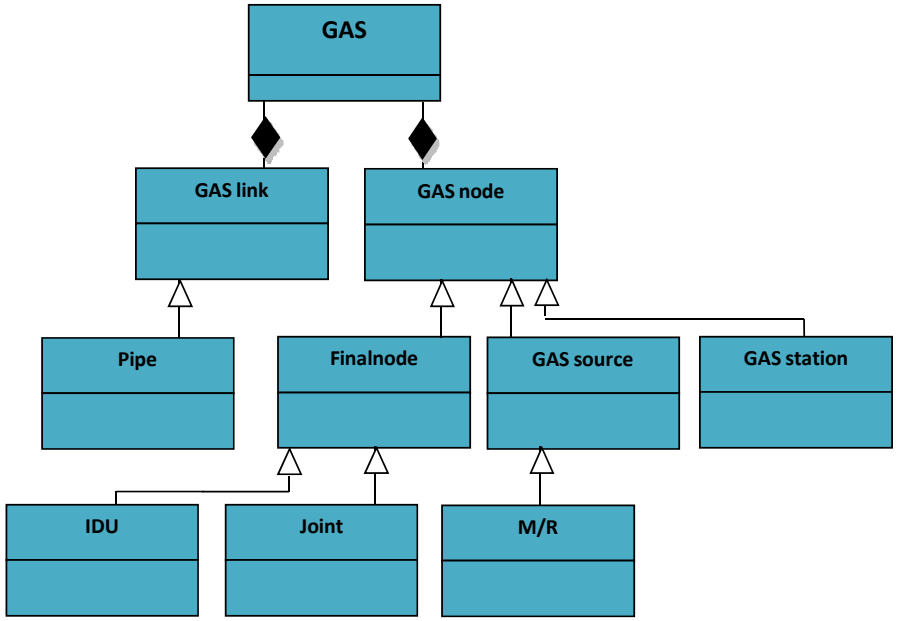

Figure 5.2 Class diagram for the gas distribution network

5.2. Case study

Part of the L'Aquila gas system has been selected for the evaluation of seismic performance. In particular the area selected is characterized by one M/R station, 12 regulator stations and pipelines at medium pressure either made of steel and HDPE as shown in Fig. (5.4). The function of a gas network at medium pressure is to provide end-users with gas where, in this case considering only the MP network, end-users are represented by the regulator stations. The implementation of the selected network in the software imply the identification of nodes and links of the *GAS* class, i.e. the M/R station, regulators groups and joints are nodes while pipes are links. To this aim 39 nodes (1 source, 12 RG stations and 26 joints) and 38 links have been identified and all data necessary for the evaluation of seismic vulnerability have been imported in the software. Nodes and links represent the vulnerable sites for which the seismic demand has to be computed.

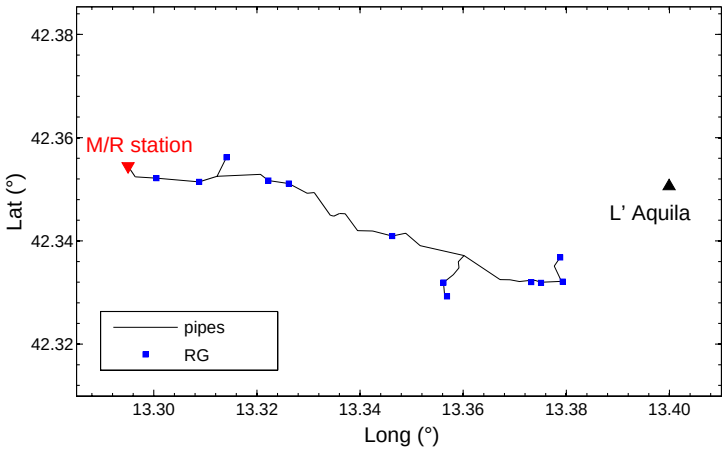

Figure 5.3 Case study

5.2.1. Seismic hazard assessment

Probabilistic hazard scenarios have been simulated for the region covering the gas network. An overview of the procedure implemented in the software according to the proposed methodology to generate the hazard input for each scenario is shown in Fig. (5.4). The process is essentially divided into four separate stages:

- generation of the seismic source
- calculation of ground motion on rock
- calculation of the cross-correlated ground motion
- site and geotechnical characterization

The seismic source needs to be defined in terms of magnitude, geographical extent and mechanism. The latter may refer only to a parameter describing the fault type (normal, strike-slip, reverse) or may be a focal mechanism (strike, dip and rake) characteristic to the source in question. In this case the Paganica fault (normal fault type) on which L'Aquila (central Italy) 2009 earthquake was originated is used as source for the generation of seismic event computed for a characteristic earthquake of moment magnitude M_w 6.3 and occurrence rate of $\nu = 1/ 750$ (Pace *et al.*, 2006). Data on geographical extent of the source are summarized in Tab. (5.1).

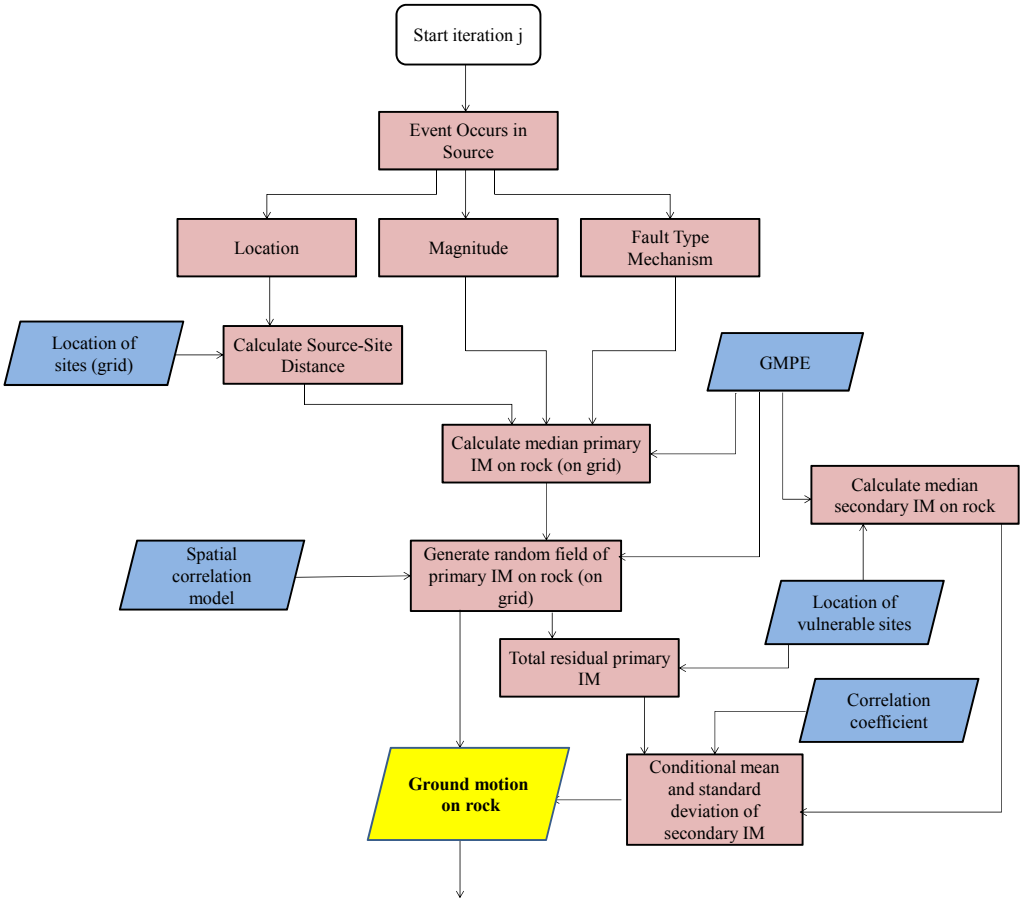

Figure 5.4 Overview of Seismic Hazard Simulation Procedure: inputs (blue), outputs (yellow) and process (red).

The epicenter of the source is sampled as a point within the source model, with every location assumed equally probable. In this case the source is defined as a mesh of points prior to the simulation process and each point is sampled randomly with replacement from the mesh. More details on the approach used for the generation of rupture events can be found in Weatherill *et al*. (2011).

Table 5.1 Geographical extent of the Paganica fault (Chioccarelli and Iervolino, 2010)

	V_{fault} 1	V_{fault} 2	V_{fault} 3	V_{fault} 4
Longitude (°)	13.424	13.552	13.465	13.336
Latitude (°)	42.405	42.293	42.238	42.351
Depth (km)	0.600	0.600	11.800	11.800

The strong ground motion is attenuated away from the source using a GMPE. In particular strong motion is evaluated on a regular grid covering the gas network. An intensity measure for which a spatial correlation model is available is selected as the "primary IM", i.e. the intensity measure chosen to generate a GRF and to obtain the "secondary IM" though the conditional sequential simulation (following the procedure described in the section 2.4.2). The regular grid that cover the region of interest is identified based on the correlation structure of the primary IM, i.e. a grid with a subdivision that is adequately smaller of the IM correlation length (i.e. the *range*).
For each site of the grid the means of primary IM from the specified GMPE are calculated and the residual sampled from a random filed of spatially correlated Gaussian variables according to the own spatial correlation model. Note that the grid depends on the extension of the study region but in general its nodes do not coincide with any of the sites of the gas network components. The number of its nodes is independent of the number of vulnerable components. In this way the evaluation of the number of nodes of the grid is related to the spatial correlation of the primary IM and it is independent of the refinement in the modeling of the network. The value of the primary IM at each site of the network (i.e. the vulnerable sites) is then obtained interpolating the grid values. The resulting ground motions correspond to a "rock" site, corresponding to Eurocode 8 class A.

Then for each site conditional mean and conditional covariance of the secondary IM are simulated using the formulation in Eq. (2.29). The secondary IMs are then determined by sampling a vector of Gaussian variables described by the conditional mean and covariance of each IM upon the primary IM. For the case study PGA has been chosen as primary IM and since gas network components of the case study (pipelines and stations) are vulnerable to PGV and PGA (as discussed in section 3.2), PGV has been chosen as secondary IM. The GMPE used for the evaluation of strong motion is Akkar and Bommer (2010) and spatial variability has been modeled using correlation models provided by Esposito and Iervolino (2011a).

The third stage of the process is to determine the hazard at the soil site, given the hazard for the assumed rock condition that has been calculated by the previous stage. To scale the hazard to the site condition an amplification factor needs to be applied. The amplification factor can be determined in several different ways, depending on the data available. As discussed in section 2.3 there are advantages and disadvantages to the use of code specified amplification factors and those inherent within particular GMPEs. For the case study site condition effects are followed according to the ground motion prediction equation based amplification factors.

Regarding geotechnical hazards, the modeling approach of HAZUS has been largely adopted. For the case study, thanks to a process jointly developed by Department of Hydraulic Engineering, Geotechnical and Environmental and Department of Structural Engineering of University of Naples, "Federico II", the landslide potential of L'Aquila region, according to the HAZUS (FEMA, 2004) procedure has been performed (more details can be found in Appendix D).

Therefore, in order to evaluate PGD hazard though the OOFIM software, the program has been also equipped with the *Landslide* class including attributes and methods according to the HAZUS procedure. The process of estimating site amplification and landslide hazard implemented in the software is shown in Fig. (5.5). As discussed in section 2.3.2 the probability of landsliding is determined for each site using the susceptibility class and the PGA on surface. If PGA is exceeded by the value of critical acceleration determined for each susceptibility class using the HAZUS classification, then displacement occurs at the site, otherwise no permanent displacement is considered. If displacement occurs then the displacement (PGD) is calculated though a displacement model. Since the HAZUS estimator of PGD is deterministic alternative models that better constrain the uncertainty, whilst retaining practicality for use with common intensity measures should be used. In this case the Saygill and Rathje (2008) empirical model has been used. In Tab. (5.2) all data input for the seismic hazard characterization of the case study are summarized.

5.2.2. Seismic vulnerability assessment

To estimate earthquake damage, given knowledge of ground shaking (and ground failure), earthquake intensity parameters have to be correlated with system component damage in terms of fragility functions. To this aim the typology classification of each component, damage scale definition and the intensity measures have to be defined. Based on these fragility curves, functionality of each component of the case study can be assessed. The case study consists essentially of pipelines and stations (M/R and regulator stations). In particular for buried pipelines ALA (2001a) fragility relations, in terms of PGV and PGD, have been selected for each pipe typology (steel and HDPE). Regulator stations have been not considered vulnerable since no quantitative fragility curves are available in literature. Also for the M/R station, no quantitative fragility curves are available in literature but since some authors (Chang and Song, 2007; Song and Ok, 2009) assume the M/R station owns the same fragility property as compressor stations, these fragility curves have been adopted in order to evaluate the implications of this assumption in terms of seismic performance.

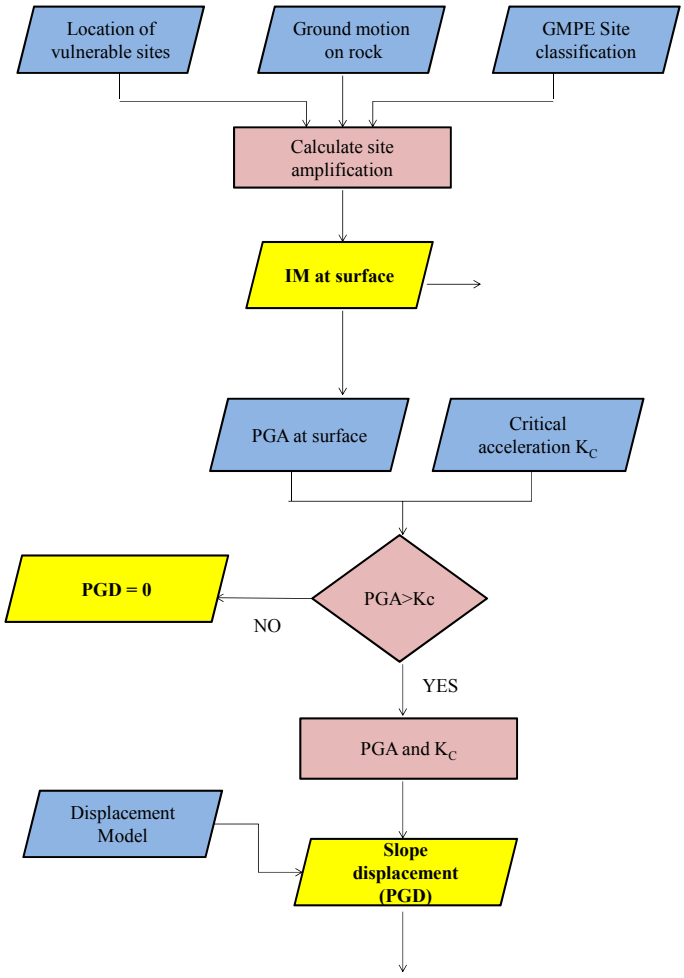

Figure 5.5 Overview of the process of defining site amplification and landslide hazard

Damage states considered for the evaluation of seismic vulnerability are strictly related to the objective of the analysis and then to the level of functionality that is considered. In this case the system is considered functional if demand nodes (regulator groups) continue to provide gas and then if they remain accessible from at least one supply node (M/R stations). Therefore a connectivity analysis has been performed. To this purpose it is assumed that a pipe segment cannot deliver gas when the segment has at least one break, while for the supply node it is assumed that it loses its connectivity when it is in either "extensive" or "complete" damage states. The details about fragility functions and damage states for each component's typology are reported in Section 3.2. As a reminder, the three fragility functions of M/R station and pipelines (steel and HDPE) are summarized in Tab. (5.3).

Table 5.2 Data input for the seismic hazard characterization

Input	Primary IM	Secondary IM	Landslide
IM	PGA	PGV	PGD
GMPE	Akkar and Bommer (2010)	Akkar and Bommer (2010)	-
Spatial correlation model	Esposito and Iervolino (2011)	-	-
Correlation coefficient	-	0.754[9]	-
Site amplification	GMPE	GMPE	-
Critical acceleration map	-	-	Hazus (FEMA,2004)
Displacement model	-	-	Saygill and Rathje (2008)

Table 5.3 Data input for the fragility characterization

Component	Author	Damage state	Fragility relation parameter			
			Ground shaking		Ground failure	
Steel pipelines (small diameter)	ALA (2001a)	Leak	$K_1 = 0.6$		$K_2 = 0.7$	
HDPE pipelines (small diameter)	ALA (2001a)	Leak	$K_1 = 0.5$		$K_2 = 0.8$	
M/R station (Un-anchored)	HAZUS (FEMA, 2004)	Extensive	**μ(g)**	**β**	**μ(inch)**	**β**
			0.77	0.65	10	0.5

[9] The correlation coefficient has been estimated starting from the dataset used for the Akkar and Bommer (2010) GMPE.

5.2.3. System performance evaluation

The quantitative measure of the functionality of the gas network is given by performance indicators to provide a measure of the impact of the earthquake on the systemic vulnerability and to quantify the degree to which the system is able to meet established specifications and/or customer requirements following an earthquake event. For the case study the adaptation and use of the Serviceability Ratio (Adachi and Ellingwood, 2008) and Connectivity Loss (Poljanšek *et al*., 2011) performance indicators are proposed. These indicators are summarized in Tab. (5.4). The process of estimating seismic vulnerability and performance indicators implemented in the software is shown in Fig. (5.6).

Table 5.4 Perfomance indicators adopted

Perfomance Indicator	Parameters	Supply node	Demand node
$SR = \frac{\sum_{i=1}^{n}(w_i X_i)}{\sum_{i=1}^{n} w_i}$	w_i = weight factor related to the nominal flow (m^3/h) of the demand node n= number of demand nodes	M/R station	GR
$CL = 1 - \left\langle \frac{N^i_{source,dam}}{N^i_{source,orig}} \right\rangle_i$	N^i_{source} = number of demand nodes connected to the i-th supply node	M/R station	GR

Probabilistic risk assessment of the case study has been performed using Monte Carlo simulation. The goal of the analysis is to evaluate probability distribution or annual exceedance rate of events defined in terms of performance indicators. Multiple scenarios are simulated at all sites of interest (following the process described in Section 5.2 and shown in figures 5.4, 5.5 and 5.6) and performance indicators are evaluated for each run. This requires the joint distribution of all uncertainties entering the seismic analysis that are due to the randomness in seismic intensity (modeled through magnitude-recurrence laws, ground-motion prediction equations, spatial correlation models, cross-IM correlation models, site amplification models and permanent displacement models) and facility response (modeled through physical damageability of the components). Simulation is a robust way to explore the behavior of systems of any complexity. It is based on the observation of system response to input. Simulation of a set of inputs and evaluation of corresponding outputs allows

determining through statistical post-processing the distribution of the output. In particular the exceedance curve, which provides the annual exceedance rate of various level of the performance indicator, is the product of the exceedance probability curve and the total occurrence rate of earthquakes exceeding the minimum considered magnitude on all sources/faults (n_f) as expressed by Eq. (5.1)

$$\nu_{PI>u} = \sum_{j=1}^{nf} \nu_j \cdot P\left(PI > u\right) \tag{5.1}$$

where $\left(PI > u\right)$ is the probability that the performance indicator exceeds a predefinited level u. This probability can be computed empirically using the MCS approach as follow:

$$\hat{P}\left(PI > u\right) = \frac{1}{n} \cdot \sum_{j=1}^{n} I\left(pi_j > u\right) \tag{5.2}$$

where pi_j is the performance indicator level corresponding to the simulation j, and $I\left(pi_j > u\right)$ is an indicator function which equals 1 if $pi_j > u$ and 0 otherwise.

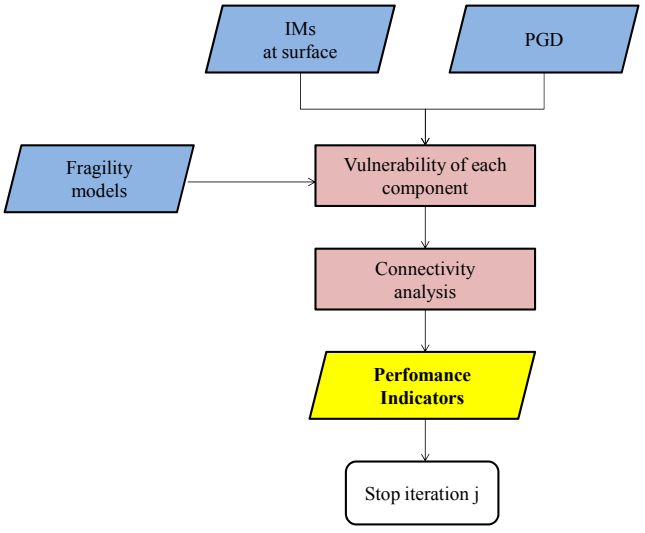

Figure 5.6 Overview of the process of fragility analysis and system performance evaluation

5.3. Risk assessment results

In order to study the effects of different components on risk assessment, five combinations have been identified and listed in Tab. (5.5) and results are presented for the various cases. In the first two cases only the ground shaking effect is considered (transient ground deformation, TGD) assuming or not spatial correlation between intra event residuals of the intensity measures. The third case, instead, has the attempt to verify the severity of damages caused by PGD induced by landslides. Finally the last two cases aim to evaluate the implications of assuming the vulnerability of the M/R station on the seismic system performance.

Table 5.5 Case definitions for risk assessment

Case	Definition
1	TGD and spatial correlations ignored
2	TGD and spatial correlations considered
3	TGD and PGD
4	Case 2 and M/R stations not vulnerable
5	Case 3 and M/R stations not vulnerable

The simulation, of the plain Monte Carlo type, consists of 3000 runs and it has been defined respect to the maximum coefficient of variation (δ) of the system-level performance indicators (CL and SR) that falls below on a target value of 5%, as shown in Fig. (5.7).

5.3.1. Importance of modeling spatial correlations

In order to evaluate the influence of accounting spatial correlation between intra event residuals of primary IM (PGA) the risk assessment has been performed assuming in the first case a correlation coefficient equal to zero, i.e. intra event residual are considered independent and in the second case a correlation length equal to 13.5 km (Esposito and Iervolino, 2011). Fig. (5.8) and (5.9) show the variation of CL indicator and SR indicator respectively with the number of runs in terms of mean (μ) and standard deviation (σ). It is apparent how the risk in terms of connectivity loss is quite underestimated when the spatial correlation is ignored. The expected mean of CL results equal to 0.16 in the first case and 0.18 in the second case. On the contrary, the second indicator, that measures the serviceability of the gas network, is quite overestimated: the expected mean is equal to 0.85 in the first case and 0.81 in the second case.

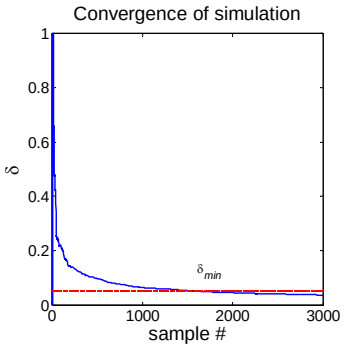

Figure 5.7 Maximum coefficient of variation of the estimated performance indicators (CL, SR) versus number of runs

The influence of spatial correlation is even more pronounced in Fig. (5.10) where exceedance curves are plotted. Note that the annual exceedance rate of various level of the performance indicators has been obtained considering as occurrence rate ν = 1/ 750 (Pace *et al*., 2006).

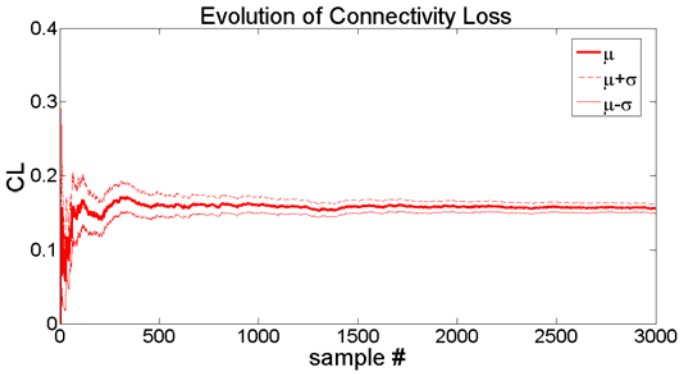

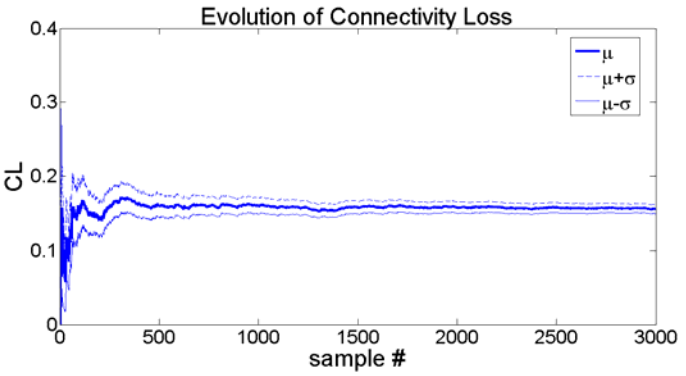

Figure 5.8 Variation of the average connectivity loss considering uncorrelated residuals (up) and correlated residuals (down)

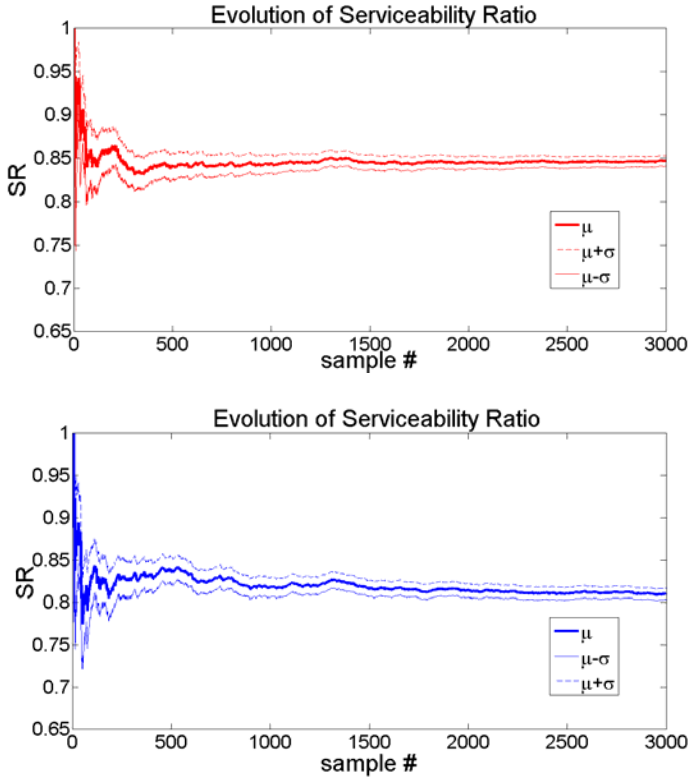

Figure 5.9 Variation of the average serviceability ratio considering uncorrelated residuals (up) and correlated residuals (down)

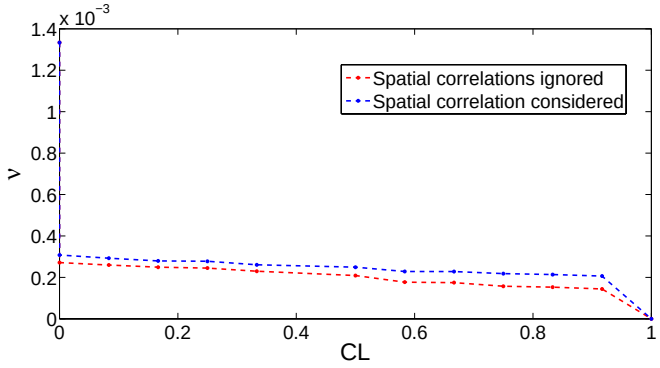

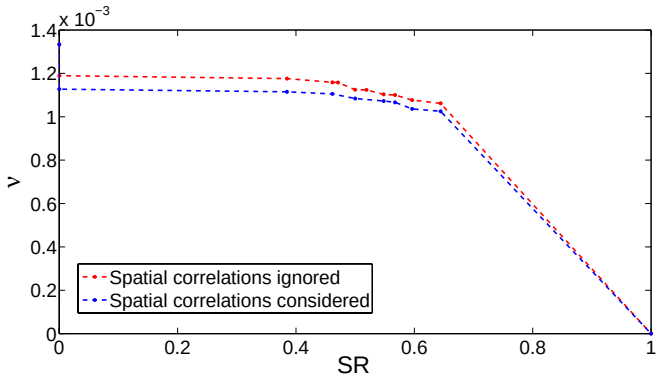

Figure 5.10 Annual exceedance curve of connectivity loss (up) and serviceability ratio (down) considering uncorrelated residuals and correlated residuals

Although past research have shown that risk may be substantially underestimated when spatial correlation is ignored (as also shown in section 2.2.3.4), in this case differences between two cases are not so pronounced; this may be due to the limited extension of the case study.

5.3.2. TGD vs PGD effects

It is recognized that PGD is one of the most pervasive causes of lifeline damage during earthquakes (O' Rourke and Liu, 1999). At the same time, seismic wave, or TGD effects, can also have serious consequences on lifeline performance. Although not as severe locally as PGD, TGD can disturb an entire network as source of system-wide effects. In order to evaluate the contribution of PGD on system performance, performance indicators have been performed considering the combined effect of TGD and PGD due to landlside. Fig. (5.11) shows the variation of performance indicators with the number of runs in terms of mean and standard deviation. It is apparent how the risk in terms of connectivity loss is substantially underestimated when the PGD effect is ignored. In this case the expected mean of CL results equal to 0.59, i.e. it is expected that about the 60% of demand nodes are not connected to the source node (M/R station) while the expected mean of SR is equal to 0.45, i.e. it is expected that only the 45% of demand nodes receive gas after earthquakes accounting for the importance level related to the nominal flow of the RGs.

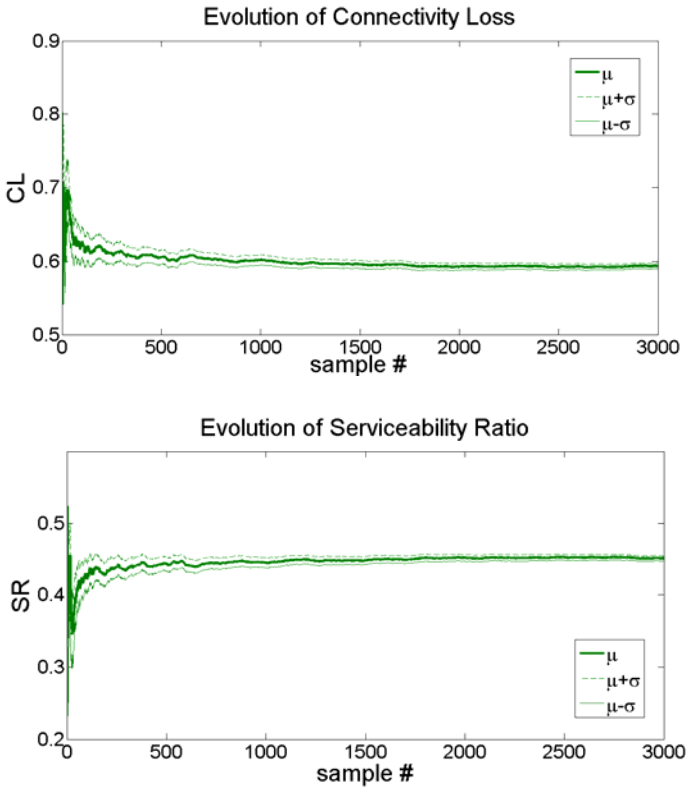

Figure 5.11 Variation of the average connectivity loss (up) and serviceability ratio (down) considering the combined effect of TGD and PGD

Fig. (5.12) shows instead the annual exceedance curve of connectivity loss and serviceability considering only the TGD effects and the combined effects of TGD and PGD. It is important to note that the combined effect of TGD and PGD has an important impact on the probability of exceedance of low values of connectivity loss (and hence high values of serviceability ratio) while for high values of CL (low values of SR) it seems that the contribute of PGD is not relevant. This may be explained considering that high values of connectivity are strongly influenced by the behavior of the M/R station (the source) and pipelines connected to the source node. In fact if the source node is damaged all reduction groups result not connected; moreover at the same time if pipelines that are more close to the source are damaged, a great number of RGs cannot receive gas. Therefore considering that the M/R station is not vulnerable to PGD because the site where the station is located is not susceptible to landlside, and that the most of susceptible sites are in correspondence of pipes from which few RGs depend (as shown in Fig. 5.13), it seems clear that high values of connectivity loss are mostly controlled by TGD effects.

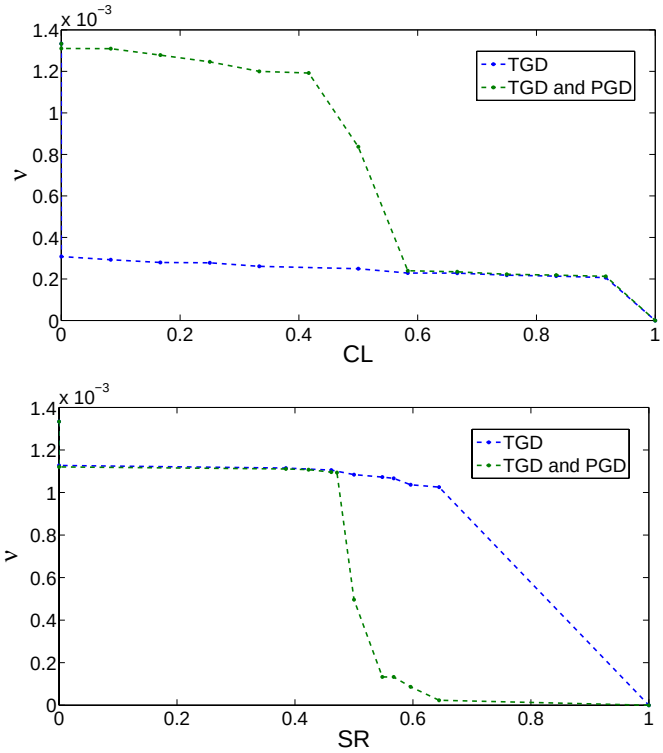

Figure 5.12 Annual exceedance curve of connectivity loss (up) and serviceability ratio (down) considering only the TGD effect and the combined effect of TGD and PGD

Moreover there is another important factor that should be considered to explain these results. To evaluate the critical acceleration map, the methodology of HAZUS (FEMA, 2004) has been used herein (see Appendix D for more details). This methodology is based on the study by Wilson and Keefer (1985) which categorizes landslide susceptibility from lowest to highest. For each susceptibility class, a critical acceleration is defined; hence, if PGA exceeds the critical acceleration then a landslide is observed. As reported in Section 2.3.2, due to the conservative nature of the Wilson and Keefer (1985) correlation, the probability of a landslide occurring should be modified by a term to determine the percentage of the map area having a landslide susceptible deposit. Based on Wieczoreck *et al.* (1985), these percentages have been estimated for the San Mateo County (California) as a function of the susceptibility categories. Since these values have not been validated for L'Aquila region, the probability of a landslide occurring has not been modified. Therefore the contribution of PGD affects results conditioned by this choice. Further consideration must be given to evaluating the probability of slope failure.

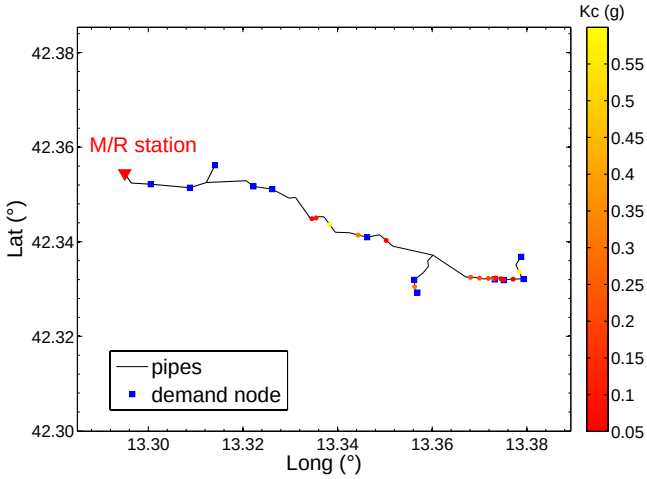

Figure 5.13 Critical acceleration values (Kc) associated to sites susceptible to landlside

5.3.3. Importance of considering vulnerability of M/R station

In addition to PGD and TGD effects, there is another factor that may influence the seismic performance of the gas network. Some authors (Chang and Song, 2007; Song and Ok, 2009) assume the M/R station owns the same fragility property as compressor stations, therefore fragility curves of compressor stations (FEMA, 2004) have been adopted in order to evaluate the implications of this assumption in terms of seismic performance. Fig. (5.14) and (5.15) shows the variation of performance indicators when the M/R station is not considered vulnerable. The risk assessment has been performed considering TGD effects (Fig. 5.14) and the combined effects of TDG and PGD (Fig. 5.15). Results show that the risk in terms of connectivity loss is substantially overestimated when the M/R station is considered vulnerable. In the case of the M/R is not considered vulnerable and accounting for only the TGD effects, the expected mean of CL results equal to 0.05, i.e. it is expected that only the 5% of demand nodes are not connected to the M/R station while the expected mean of SR is equal to 0.95, i.e. it is expected that the 95% of demand nodes receive gas after earthquakes accounting for the importance level related to the nominal flow of the RGs. This means that the seismic behaviour of the M/R station is one of the most important factors that influence the seismic performance of the case study. In the second case where the M/R is not considered vulnerable and accounting for the combined effects of TGD and PGD effects the expected mean of PIs is not substantially underestimated (0.52 respect to 0.59 for CL indicator and 0.53 respect to 0.45 for SR indicator). This may be explained considering that the M/R station is not

vulnerable to PGD and then the seismic behaviour of the M/R station influences only the estimation of damage induced by TGD.

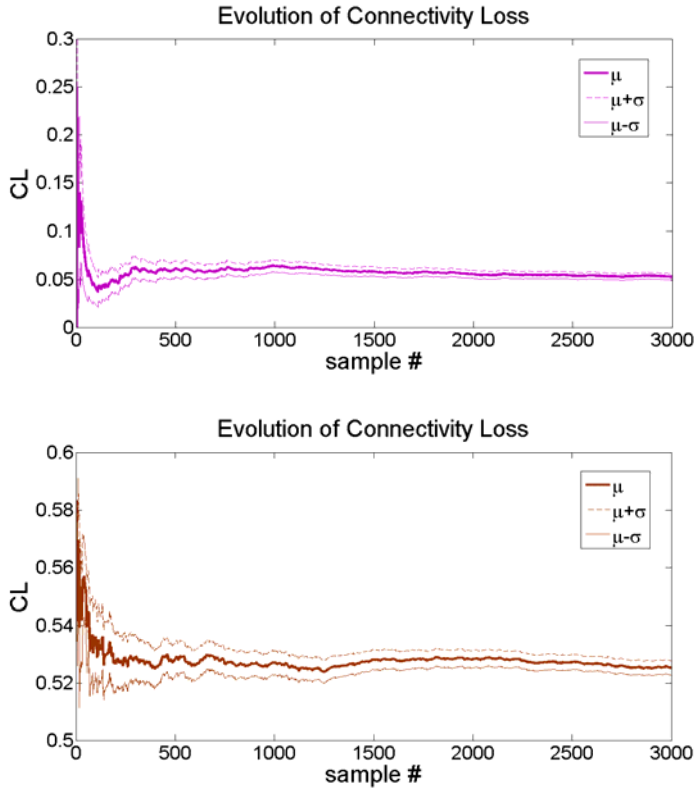

Figure 5.14 Variation of the average connectivity loss considering the M/R station not vulnerable for the TGD case (up) and for TGD and PGD combination case (down)

Fig. (5.16) shows instead the annual exceedance curves of connectivity loss and serviceability ratio considering or not the seismic vulnerability of the M/R station.
The probability of exceedance of the performance indicators is strongly influenced by the seismic behavior of the M/R station when the TGD effects are considered. While comparing the trend of the exceedance curves in case of combined effects of TGD and PGD the influence of the seismic behavior of the M/R station is stronger for high values of CL (low values of SR). This may be explained considering that high values of connectivity are strongly influenced by the behavior of the M/R station (the source) and pipelines connected to the source node that are not vulnerable to PGD while low values of CL (high values of SR) are more influenced by the behavior of pipelines

vulnerable to PGD that are less critical in term of connectivity (i.e. pipes from which few RGs depend).

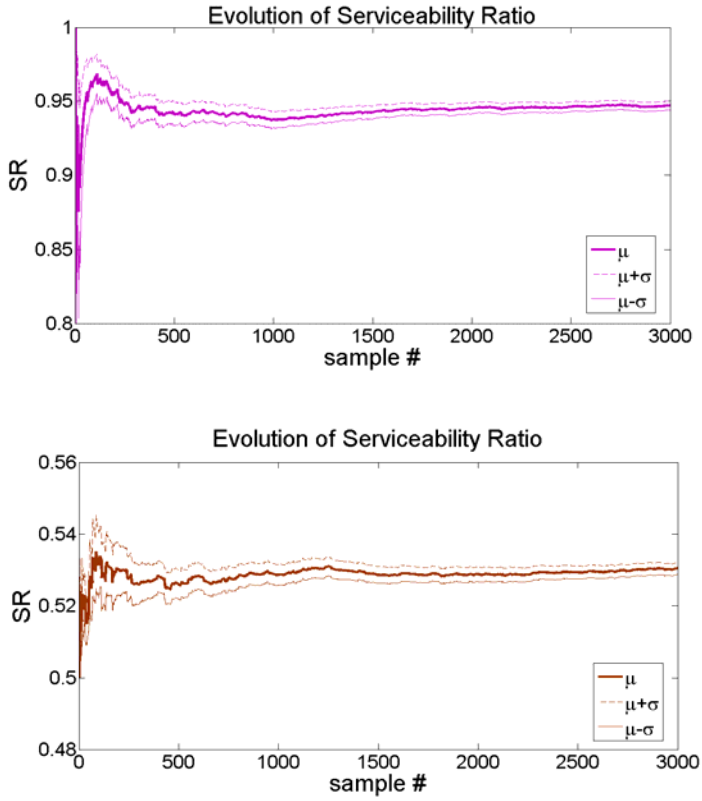

Figure 5.15 Variation of the average serviceability ratio considering the M/R station not vulnerable for the TGD case (up) and for TGD and PGD combination case (down)

Therefore the use of fragility curves of compressor stations as approximation may induce significant errors into the risk calculations. Further consideration should be given to evaluating the fragility of these components.

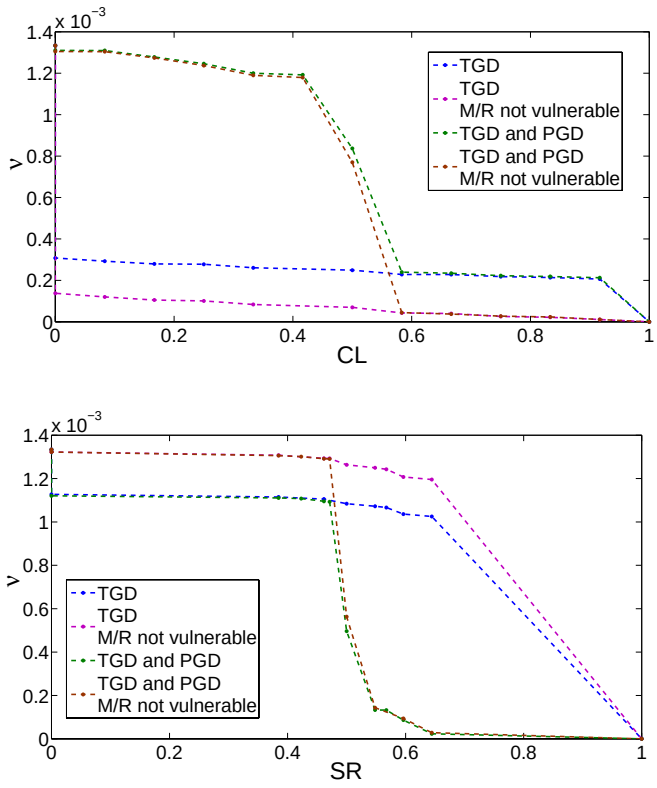

Figure 5.16 Annual exceedance curve of connectivity loss (up) and serviceability ratio (down) considering the influence of the M/R station behavior for the TGD case and for TGD and PGD combination case

Chapter 6 – CONCLUSIONS

6.1. Contribution summary

This study focused on developing a framework for the seismic risk assessment of gas distribution systems investigating the different aspects that are involved. The process make use of probabilistic seismic hazard analysis, empirical relations to estimate pipeline response, fragility curves for the evaluation of facilities vulnerability, performance indicators to characterize the functionality of the gas network. The thesis, in fact, has achieved this goal with special emphasis to the medium and low pressure network of a real system, namely the L'Aquila gas distribution system managed by ENEL Rete Gas s.p.a., for which not only detailed information on the network were retreived, but also data related to damages occurred on the network followed the 2009 L'Aquila earthquake. The important challenge in the seismic risk assessment of a real gas system is to take into account all the aspects of risk. Contributions have been made expecially in the hazard and vulnerability areas.

6.1.1. Wave propagation hazard

Considering that gas networks are essentially located underground, these systems are subjected to both transient ground deformation due to seismic waves, which is felt over a wide geographical area, and ground failure due to geotechnical hazards such as liquefaction and landslide, which determine localized ground failure. In order to characterize the ground shaking hazard of the L'Aquila region, probabilistic scenarios earthquakes have been generated using as source the Paganica fault on which L'Aquila (central Italy) 2009 earthquake was originated, computed for a characteristic earthquake of moment magnitude M_w 6.3 and occurrence rate of $\nu = 1/ 750$ (Pace *et al*., 2006). Strong ground motions, have been evaluated though European ground motion prediction equation and a spatial correlation model. In particular Chapter 2 of this thesis describes how to estimate ground motion including the spatial correlation and how to compute regional hazard analysis. Since correlation models available in literature have been estimated starting from dense observations of different earthquakes outside Europe, in order to characterize spatial correlation fields for the case study, spatial correlation models based on the European Strong-motion Database and the Italian Accelerometric Archive datasets have been estimated for different intensity measures. The correlation decreas with increasing separation between sites

and this correlation structure has been modeled though geostatistical tools. It was seen that the rate of decay of correlation length (i.e. the range) is higher for for PGV than for PGA. In fact, the acceleration time history shows a significant proportion of relatively high frequency, while velocity records shows substantially less high-frequency motion and are likely to yield higher correlations. This seems to be consistent with past studies of ground motion coherency. In fact, the coherency describes the degree of correlation between amplitudes and phases angles of two time histories at each of their component frequencies. Considering that coherency decreases with increasing distance between measuring points and with increasing frequency, it may be reasonable to expect more coherent ground motion, as velocity that corresponds to low frequency exhibits more correlated peak amplitudes. Moreover, Appendix A presents some preliminary results on the spatial correlation analysis of acceleration spectral ordinates. It was shown that the decay rate of correlation, as a function of inter-site distance, tends to increase with structural period. Based on that, a simple linear formula, although preliminary, has beeen provided to model spatial correlation of Sa as a function of frequency.

Since the performance of spatially distribute systems may be conditional upon the failure of many components within the system each of which is sensitive to different intensity measures, the possibility of the existence of a cross-correlation between IMs has been taken into account through the use of the conditional hazard. This technique starts from the assumption that two IMs considered are jointly distributed according to a bivariate Gaussian distribution, and it has the advantage to avoid making assumptions about the structure of the cross correlation between the two IMs.

6.1.2. Geotechnical hazard

For consideration of geotechnical hazards, the modeling approach of HAZUS described in Chapter 2, has been adopted. The principal forms of permanent ground deformation are surface faulting, landsliding, seismic settlement and lateral spreading due to soil liquefaction. Although many models that have the intent to relate the degree of deformation and the probability of occurrence of each geotechnical hazard to the strength of ground motion are available in literature, the main limiting factor of many models is the requirement of very detailed geotechnical data that could make difficult the implementation of these models for the analysis of lifeline systems. Therefore the use of simpler models as those proposed in HAZUS has been taken into account to characterize the geotechnical hazard potential of L'Aquila region. In particular for the case study, thanks to a process jointly developed with specialists the

landslide potential of L'Aquila region has been performed. Results are shown in Appendix D.

6.1.3. Fragility analysis

Regarding vulnerability analysis, in Chapter 3 fragility curves available in literature for the most of gas network components are described. For buried pipelines, a fragility relation is a function that releates pipeline damage rates with different level of seismic intensity. These relations are usually based on empirical data collected throughout past earthquakes. The usual practice is to define damage rates as the number of pipe repirs per unit length of pipeline. Depending on the consistency of the data used for the empirical estimation, fragility curves may provides factors that influence the vulnerability of pipelines such as pipe material, pipe diameter or pipe connections. Since buried pipelines are very sensitive to permanent ground deformation (resulting from various ground failures), in addition to transient ground deformation due to seismic wave propagation , fragility curves are proposed for both phenomena. In paritular PGD is used as the demand description of ground failure and while to correlate the ground motion effects to the damage suffered by buried pipeline, PGV has been identified as the one having a more direct physical. Storage and processing facilities instead are mostly vulnerable to PGA, sometimes to PGD, if located in liquefiable or landslide zones. Therefore, fragility curves for these components are defined and associated with either PGA or PGD. Fragility curves from the literature, whether they are empirical or analytical, usually propose the same number of damage states and very similar definitions. For each damage state, the HAZUS methodology proposes fragility curves accounting also for the fragility of the equipment needed for the facilities to function properly using the fault tree analysis: the global damage state is based on the combination of individual damage state of its components. Unfortunately, there are no exhaustive studies in the literature on seismic behavior of all components making difficult a comprehensive characterization of the case study. Therefore to this aim, seismic vulnerability of pressure reduction stations characterizing the L'Aquila gas network has been investigated through the use of fault tree analysis. Moreover fragility relations for pipeline systems available in literature have been validated through an analysis of the damages occurred on the gas network following the 6th April L'Aquila earthquake by processing technical reports from Enel Rete Gas describing the repairs and replacements activities following the seismic event as described in Appendix C.

6.1.4. Systemic vulnerability and loss

Depending on the goal of the analysis, the performance of the system may be evaluated though the use of performance indicators that represent a quantitative measure of the functionality of the gas providing a measure of the impact of the earthquake on the systemic vulnerability and to quantify the degree to which the system is able to meet established specifications and/or customer requirements following an earthquake event. For the case study the system has been considered functional if demand nodes continue to provide gas and then if they remain accessible from at least one supply node. Therefore a connectivity analysis has been performed in order to integrate the damage of facilities and distributing elements into the damage of the system and the adaptation and use of two performance indicators (Serviceability Ratio and Connectivity Loss) described in Chapter 4, are proposed.

6.1.5. Risk assessment

The methodology presented has been tested via the implementation of the case study in a specific software . The software, created in relation of the objectives of the Syner-G project, adheres to the OBJECT-ORIENTED Paradigm (OOP) where the problem is described as a set of objects, "software containers" grouping together related procedures and data. Data elements are called attributes of an object. Procedures, which operate on data specific for an object, are called methods. Objects are instances (concrete realizations) of classes (abstract models) that are used to model the system. For the purpose of the thesis the programme has been equipped with the *GAS* class, focusing on the components of a gas distribution system, in order to evaluate seismic performance of the L'Aquila gas distribution network.

Probabilistic risk assessment of the case study has been performed using Monte Carlo simulation. The goal of the analysis is to evaluate probability the annual exceedance rate of events defined in terms of performance indicators. Multiple scenarios are simulated at all sites of interest and performance indicators are evaluated for each run.

In order to study the effects of different components on risk assessment, different combinations have been identified.In particular the importance of modeling spatial correlations of ground motion and geotechnical hazard on risk assessment evaluation has been investigated. Results indicate that the system performance estimation may be understimated when the spatial correlation and ground failure effects are ignored.

6.2. Emerging research need

6.2.1. Hazard

Chapter 2 presented a spatial correlation model for PGA and PGV developed using records from datasets characterized by multiple events and regions. One may argue that an unique model may be inadeguate to characterize spatial variability of different earthquake events and regions. For example a dependency of correlation length on magnitude could be an aspect to investigate. However geostatistical estimation needs a relatively large number of data to model the spatial correlation which are not available for individual events in the Italian and European datasets. A possible solution coulb be the use of simulated time histories. Moreover models proposed have been estimated assuming stationarity and isotropy of correlations. Although this hypothesis seems to be reasonable starting from literature results, if hazard assessment of critical facility close to the rupture is required further investigation should be addressed.

It is well recognized that PGD is one of the most pervasive causes of buried pipeline systems damage during earthquakes. Although results shown in Chapter 5 indicate that the risk may be substantially underestimated when PGD effects are ignored, it is important to consider that the conservative methodology suggested in HAZUS has been used herein. This methodology categorizes landslide susceptibility from lowest to highest and for each susceptibility class define a critical acceleration. Hence, if peak ground acceleration exceeds the critical acceleration then a landslide is observed. Due to the conservative nature of the correlation, the probability of a landslide occurring should be modified by a term to determine the percentage of the map area having a landslide susceptible deposit. Some researhers estimated these percentages for the San Mateo County (California) as a function of the susceptibility categories. Since these values have not been validated for L'Aquila region, the probability of a landslide occurring has not been modified. Therefore the contribution of PGD effects results conditioned by this choice. Further consideration must be given to evaluating the probability of slope failure.

6.2.2. Vulnerability

In Chapter 3 fragility curves for gas system components have been presented. As mentioned before, there are no exhaustive studies in the literature on seismic behavior of all components making difficult a comprehensive characterization of the case study. Although a fist attempt has been done, performing fault tree analysis for pressure reduction stations, new fragility curves should be developed. In fact, as shown in

Chapter 5 the use of fragility curves of compressor stations as approximation may induce significant errors into the risk calculations.

Moreover as stated in Chapter 3, empirical relations for the fragility of pipelines are based on the recorded number of repairs during past earthquakes, and do not clarify the proportion of leaks and breaks with respect to the expected number of pipe repairs. However, HAZUS proposes for the two damage states proportions in function of the type of hazard: a damaged pipe because of ground failure is likely to present a break (it is assumed 80% breaks and 20% leaks), whereas ground shaking may induce more leak related damages (e.g. 20% breaks and 80% leaks). Although these percentages are accepted in literature, current fragility relations should be complemented in order to provide better models to describe earthquake effects on pipeline.

Appendix A– PRELIMINARY RESULTS OF SPATIAL CORRELATION ANALYSIS FOR ACCELERATION SPECTRAL ORDINATES FROM ITALIAN DATA

Esposito, S. and Iervoino, I. (2011b). Preliminary results of spatial correlation analysis for acceleration spectral ordinates from Italian data. In *Proceeding, XIV Convegno Nazionale "L'Ingegneria Sismica in Italia"*. September, Bari, Italia.

Abstract

Spatial correlation of peak ground motion amplitudes is required in modeling hazard for risk assessment of spatially distributed systems. In particular when a portfolio of buildings or a transportation/distribution network is of concern, spectral acceleration (Sa) correlation models may be considered in order to evaluate the expected loss in case of seismic events. The estimation of an appropriate spatial correlation model is still a research task in earthquake engineering, because of several issues related to: data, statistical approaches and estimation tools, and tests to evaluate the estimated models. In the presented paper an analysis of the spatial correlation of Sa is carried out using the Italian ACcelerometric Archive (ITACA) dataset. Correlation is estimated on the residuals with respect to a ground motion prediction equation (GMPE) calibrated on the same data considered. Results show that the decay rate of correlation, as a function of inter-site distance, tends to increase with structural period. Based on that, a simple linear formula, although preliminary, is provided to model spatial correlation of Sa as a function of frequency.

A.1.Introduction

Assessment of intraevent spatial correlation of ground motion intensity measures (IMs) has become a relevant topic in seismic risk analysis. The importance of modeling such phenomenon is due to the requirement to extend seismic risk analysis, usually related to site-specific structures, to spatially distributed systems and lifelines. In particular, on the hazard side, probabilistic seismic hazard analysis (PSHA; McGuire, 2004) refers to ground motion prediction equations (GMPEs) to model ground motion which provide probabilistic distribution of the chosen IM conditional on earthquake magnitude, source-to-site distance, and other parameters such as local geological conditions. Since it was demonstrated that GMPEs' residuals of IMs (e.g., peak ground acceleration, peak ground velocity, spectral acceleration) are spatially correlated (e.g., Boore *et al*., 2003; Goda and Hong, 2008; Esposito and Iervolino, 2011a), it is important to have correlation models for hazard assessment of a region. Spatial correlation models available in literature have been empirically estimated mainly on earthquakes outside Europe, such as Northridge (1994) or Chi-Chi (1999). Most of the studies are based on dense observations of single events (e.g., Boore *et al*., 2003; Wang and Takada, 2005; Jayaram and Baker 2009a); a few works have, instead, combined data from multiple events to obtain a unique estimate of correlation (e.g., Goda and Hong, 2008; Goda and Atkinson, 2009; Goda and Atkinson, 2010; Sokolov *et al.,* 2010). Those models depend uniquely on inter-site separation distance and provide the distance limit at which correlation may technically considered to be lost (i.e., distance beyond which IMs may be considered uncorrelated). Moreover, if spectral acceleration (Sa) is of concern, the correlation may depend also on the period Sa refers to.

In Fig. (A.1), several models for spectral acceleration, considering as period 1 sec are shown. The correlation coefficient is expressed by Eq. (A. 1), where *a*, *b,* and *c* are the model parameters, T is the period and *h* is the inter-site separation distance (in km).

$$\rho(h,T) = \max\left\{\left(1\text{-}c(T)\right)+c(T)\cdot \mathrm{e}^{-a(T)\cdot \mathrm{h}^{b(T)}},0\right\} \tag{A.1}$$

The black dotted line in Fig. (A.1) represents the value of distance at which the correlation may technically considered to be lost, i.e. equal to 0.05, or the *practical range* as discussed in the following.

It is clear from the figure that distances at which the correlation is conventionally considered lost is very different for each model considered. In fact, models from different authors provide different results even if estimating correlation for the same IM. This is supposed to depend on several factors such as the dataset used, the GMPE chosen to compute intraevent residuals, and the working assumptions of the estimation.

For example, Sokolov *et al.* (2010), starting from the strong-motion database of TSMIP network in Taiwan, investigated the dependency of spatial correlation on site classes and geological structures, asserting that a single generalized spatial model may not be adequate for all of Taiwan territory. In some cases (e.g., Wang and Takada, 2005; Jayaram and Baker, 2009a) existing GMPEs are used, while, in others (e.g., Goda and Hong, 2008; Goda and Atkinson, 2009; Sokolov *et al*., 2010), *ad-hoc* fit on the chosen dataset is adopted. Generally, regressions analysis used to develop prediction equations does not incorporate the correlation structure of residuals as a hypothesis. Hong *et al*. (2009) and Jayaram and Baker (2010a), evaluated the influence of considering the correlation in fitting a GMPE, finding a minor influence on regression coefficients and a more significant effect on the variance components. Goda and Atkinson (2010), investigated the influence of the estimation approach, emphasizing its importance when residuals are strongly correlated.

In this paper, the evaluation of the spatial correlation of Sa residuals is carried out using the Italian ACcelerometric Archive (ITACA). The analysis of correlation was performed through geostatistical tools pooling data from multiple events to fit a unique model following the same approach of Esposito *et al*. (2010) and Esposito and Iervolino (2011a). The GMPE with respect to which residuals are computed is those of Bindi *et al*. (2011) and only records used to estimate the considered GMPE are employed to estimate spatial correlation.

In the paper, the first part describes the framework adopted to estimate the correlation. The second part provides the working assumptions and a description of the dataset considered. Then, results of the estimation of correlation lengths for spectral acceleration for the eight periods ranging from 0 s to 2 s are given. Finally, an approximated preliminary relationship of the correlation range as a function of period is provided and compared with previous research on the same topic.

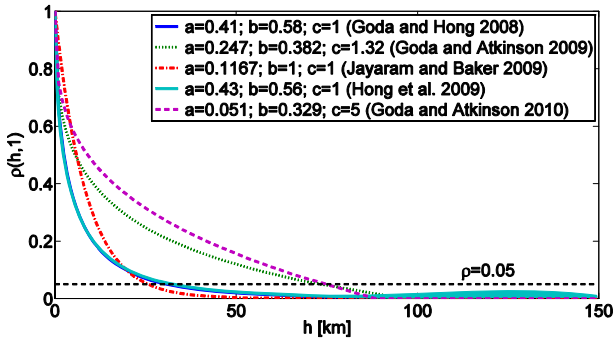

Figure A.1 Some correlation models available in literature for Sa(1s): the black dashed line intersects the curves at the distance at which the correlation is conventionally considered as almost lost (i.e., the correlation coefficient is equal to 0.05)

A.2. Semi-empirical modeling of spatial correlation

A.2.1.Geostatistical analysis

GMPEs model the logs of spectral acceleration for a specific period T, and related heterogeneity, at a site *p* due to earthquake *j* as in Eq. (A.2).

$$\log Sa(T)_{pj} = \overline{\log Sa(T)_{pj}}\left(M, R, \underline{\theta}\right) + \eta_j + \varepsilon_{pj} \tag{A.2}$$

$\overline{\log Sa(T)_{pj}}\left(M, R, \underline{\theta}\right)$ is the mean of the logs conditional on parameters such as magnitude (M), source-to-site distance (R), and others $\left(\underline{\theta}\right)$; η_j denotes the inter-event residual, which is a constant term for all sites in a given earthquake and represents a systematic deviation from the mean of the specific seismic event; and ε_{pj} is the intra-event variability of ground motion. ε_{pj} and η_j are usually assumed to be independent random variables, normally distributed with zero mean and standard deviation σ_{intra} and σ_{inter}, respectively. Then, $\log Sa(T)_{pj}$ is modeled as a normal random variable with mean $\overline{\log Sa(T)_{pj}}\left(M, R, \underline{\theta}\right)$ and standard deviation, σ_T where $\sigma^2{}_T = \sigma^2{}_{intra} + \sigma^2{}_{inter}$.

If the hazard assessment at two or more sites is of concern, the joint probability density function (PDF) for Sa(T) at all locations is required, and it can be modeled with a multivariate normal distribution (Jayaram and Baker, 2008). It is assumed that the logs of Sa(T) form a Gaussian random field (GRF), defined as a set of random variables, one for each site **u** in the study area $S \in R^2$. To any set of *n* sites $\mathbf{u_p}, p = 1, \cdots, n$, corresponds to a vector of *n* random variables that is characterized by the covariance matrix, $\boldsymbol{\Sigma}$, as in Eq. (A.3) where the first term produces perfectly correlated inter-event residuals (Malhotra 2008), while the second term (symmetrical) produces partially correlated intra-event residuals.

$$\boldsymbol{\Sigma} = \sigma^2_{inter} \cdot \begin{bmatrix} 1 & 1 & \cdots & 1 \\ 1 & 1 & \cdots & 1 \\ \vdots & \vdots & \ddots & \vdots \\ 1 & 1 & \cdots & 1 \end{bmatrix} + \sigma^2_{intra} \cdot \begin{bmatrix} 1 & \rho_{12} & \cdots & \rho_{1n} \\ \rho_{21} & 1 & \cdots & \vdots \\ \vdots & \vdots & \ddots & \vdots \\ \rho_{n1} & \rho_{n2} & \cdots & 1 \end{bmatrix} \tag{A.3}$$

In Eq. (A.3), the correlation is heterogeneous as it depends on the pairs of sites considered, and the intra-event variance is homoscedastic as it is constant for all sites (this assumed in most of GMPEs, although some studies have found dependence of intra-event variability on distance, magnitude and non-linear site effects; Strasser *et al*.

2009). If the spatial correlation for intra-event residuals is a function of the relative location of sites, it becomes as in Eq. (A.4), where *p* and *q* are two locations at the end of $\mathbf{h_{pq}}$ (the separation vector between the two sites).

$$\rho_{pq} = \rho\left(\mathbf{h_{pq}}\right) \tag{A.4}$$

Under the hypothesis of second-order stationarity and isotropy of the GRF, correlation depends only on the separation distance h = ||**h**||. Therefore if intra-event residuals may be modeled as a stationary and isotropic GRF, all data available from different earthquakes and regions, therefore deemed homogeneous, are used to fit a unique model (see Esposito and Iervolino 2011a, for more details).

A common tool to quantify spatial variability of georeferenced data is the semivariogram $\gamma_j(h)$ It is used to model the covariance structure of GRF through suitable functions. Under the hypothesis of second-order stationarity and isotropy it is defined as in Eq. (A.5).

$$\gamma_j\left(h\right) = Var\left(\varepsilon_j\right)\cdot\left[1-\rho_j\left(h\right)\right] \tag{A.5}$$

where $\rho_j(h)$ denotes the spatial correlation coefficient between intra-event residuals separated by the distance *h*. The estimation of correlation usually develops in three steps:

- computing the empirical semivariogram[10];
- choosing a functional form;
- estimating the correlation parameters by fitting the empirical data with the functional model.

Empirical semivariograms are computed as a function of site-to-site separation distance, with different possible estimators. The classical estimator is the method-of-moments (Matheron, 1962) which is defined for an isotropic random field in Eq. (A.6), where *N*(h) is the set of pairs of sites separated by the same distance *h*, and |*N*(h)| is the cardinal of *N*(h).

$$\hat{\gamma}\left(\mathrm{h}\right) = \frac{1}{2\cdot\left|N\left(\mathrm{h}\right)\right|}\cdot\sum_{N(\mathrm{h})}\left[\varepsilon\left(\mathbf{u}+\mathrm{h}\right)-\varepsilon\left(\mathbf{u}\right)\right]^2 \tag{A.6}$$

[10] Assuming a common semivariogram for different events, that is, invariant through earthquakes, allows to neglect the subscript *j* in the following equations.

Since this estimator can be badly affected by atypical observations (Cressie, 1993), Cressie and Hawkins (1980) proposed a more robust estimator (less sensitive to outliers). Both estimators will be used in the evaluation of intra-event spatial correlation of Sa(T). To compute the semivariogram it may be useful, when dealing with earthquake records, to define tolerance bins around each possible *h* value. The selection of distance bins has important effects: if its size is too large, correlation at short distances may be masked; conversely if it is too small, empty bins, or bins with samples small in size, may impair the estimate. A rule of thumb is to choose the maximum bin size as a half of the maximum distance between sites in the dataset, and to set the number of bins so that there are at least thirty pairs per bin (Journel and Huijbregts, 1978). The interpretation of experimental semivariograms consists in the identification of a model among the family of functions able to capture and emulate its trend. The three basic stationary and isotropic models are: exponential, spherical, and Gaussian. In particular, the exponential model which is the most common one, is described in Eq. (A.7):

$$\hat{\gamma}(\mathrm{h}) = \frac{1}{2 \cdot \left| N(\mathrm{h}) \right|} \cdot \sum_{N(\mathrm{h})} \left[\varepsilon(\mathbf{u}+\mathrm{h}) - \varepsilon(\mathbf{u}) \right]^2 \tag{A.7}$$

where c_0 is defined *nugget*, i.e. the limit value of the semivariogram when *h* is zero, c_e is the *sill*, or the population variance of the random field (Barnes, 1991) and *b* is the practical range defined as the inter-site distance at which $\gamma(h)$ equals 95% of the sill. Note that the parameter *b* defined in Eq. (A.7), which will be used in the following, does not correspond to the parameter defined in Eq. (A.1). Several goodness-of-fit criteria for finding the best parametric model have been proposed in geostatistical literature. Studies dealing with earthquake data sometimes use visual or trial and error approaches in order to appropriately model the semivariogram structure at short site-to-site distances (Jayaram and Baker, 2009a), where it is significant.

In this work experimental semivariograms are fitted visually, although using the least squares estimation as a starting point.

A.2.2. Estimating correlation on multievent data

Empirical semivariograms are computed starting from normalized intra-event residuals obtained for a single earthquake *j* and a generic site *p* as $\varepsilon_{pj}^{*}=\varepsilon_{pj}/\sigma_p$ where σ_p is the standard deviation of the intra-event residual at the site *p* (in the study the intra-event standard deviation is common for all sites consistent with GMPEs used to compute residuals, to follow). The standardization enables to not estimate the sill, as it should be

equal to one; therefore Eq. (A.5) becomes Eq. (A.8), where the superscript represents an empirical estimate.

$$\hat{\gamma}(h) = 1 - \hat{\rho}(h) \tag{A.8}$$

With earthquake data, standardization can be carried out with the standard deviation provided by the GMPE[11]. Another option is to use the sample variance as an estimate of the true variance (e.g., Jayaram and Baker, 2010a). Moreover Goda and Atkinson (2010) used the intra-event standard deviation inferred from the large-separation-v distance plateau of the semivariogram, assuming that at those distances residuals are not correlated. In this work, the variance provided by the GMPEs was preferred. In fact, evaluation of possible alternatives for standardization leads to results which seem to be not significantly affected by a choice with respect to another (e.g., in Esposito and Iervolino, 2011a). Normalized intra-event residuals from multiple events (and regions) are then pooled to fit a unique correlation model. This because geostatistical estimation needs a relatively large number of data to model the semivariogram (i.e., many records to have more than thirty pairs in each *h* bin), which are not available for individual events in the chosen dataset. Assuming the same isotropic semivariogram with the same parameters for all earthquakes the experimental semivariogram becomes that of Eq. (A.9) where n_j is the number of records for the *j*th event and $\left|N(h)\right|$ is the number of pairs in the specific *h* bin. Eq. (A.10) shows how individual events are kept separated in computing the empirical semivariogram. In fact, the differences of residuals of Eq. (A.9) are computed only between pairs of residuals (standardized with the common standard deviation from the GMPE) from the same earthquake, then differences from different earthquakes are pooled. This process is visually sketched in Fig. (A.3) from which it is possible to note that the empirical semivariogram point at h_1 is not the average of experimental semivariograms from different earthquakes, as *N(h)* is the number of pairs in the specific *h* bin from all earthquakes.

$$\hat{\gamma}(h) = \frac{1}{2 \cdot \left|N(h)\right|} \sum_{N(h)} \left[\varepsilon^*_{pj} - \varepsilon^*_{qj} \right]^2 \tag{A.9}$$

$$N(h) = \left\{ \begin{array}{c} \left(j, \varepsilon^*_{pj}, \varepsilon^*_{qj} \right) : \left\| \varepsilon^*_{pj} - \varepsilon^*_{qj} \right\| = h; \\ p, q = 1, \ldots n_j; \;\; j = 1, \ldots k \end{array} \right\} \tag{A.10}$$

[11] It is usual to use the sample variance as an estimator of the sill for the experimental semivariogram, but this may be improper in some circumstances; see Barnes (1991) for a discussion.

A.3. Dataset

The number of considered recordings from ITACA corresponds exactly to data used to fit Bindi *et al.* (2011) GMPE (except that only earthquakes for which more than one record was available where considered) and it is equal to 763 ground motions from 97 events over the 4-6.9 magnitude range (moment magnitude, M_w). Source-to-site distance is the closest horizontal distance to the vertical projection of the rupture (i.e., Joyner-Boore distance, R_{jb}) and is up to 196 km in the data. Characteristics of the datasets, with respect to explanatory variables of the considered prediction equation (magnitude, distance and local site conditions) are shown in Fig. (A.2).

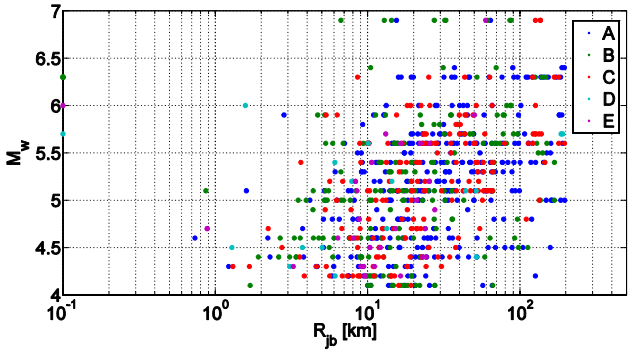

Figure A.2 ITACA strong-motion subsets with respect M_w, Rjb and local site conditions according to Eurocode 8 (2004)

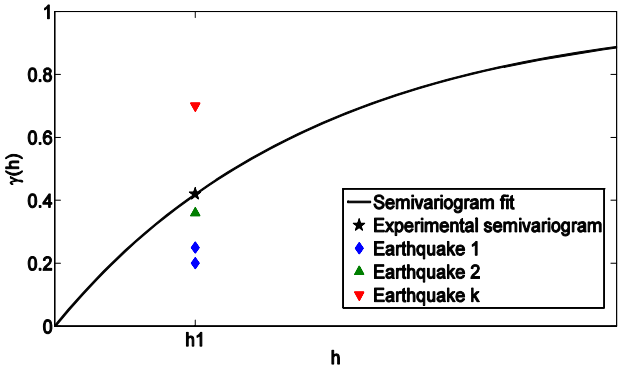

Figure A.3 Pooling standardized intra-event residuals of multiple events (j=1,2,..k) to compute experimental semivariogram

A.4. Spatial correlations of spectral ordinates from ITACA

In order to have a reasonable number of data pairs in the bins (at least 30) and a stable trend of correlation, the experimental semivariograms were obtained using a width of 2 km at seven periods ranging between 0.1 seconds and 2 seconds. In Fig. (A.4) the distribution of data pairs as a function of separation distance bins (2 km) is shown. Because the GMPE used to obtain intraevent residuals refers to geometric mean of horizontal components, the correlation was estimated for this IM. Both estimators (classical and robust) were used; no significant difference was found in the shape of the fitted semivariogram. Of the three basic models (Gaussian, spherical and exponential), the exponential model has been chosen to fit empirical points since this model is widely adopted in the literature. Moreover, the choice of using the same model for all periods allows to compare results and to investigate possible dependency of the model's parameters on the fundamental period. Assuming that there is no nugget effect (as this study does not investigate variations at a smaller scale with respect to that of the tolerance); the only parameter to estimate is the range, *b*. Least square method (LSM) was used as a reference to manually fit the model in the empirical semivariogram in order to give more importance to the small separation distances. In particular, correlation lengths evaluated for spectral acceleration for the seven periods, 0.1 s, 0.2 s, 0.3 s, 0.5 s, 1 s, 1.5 s, 2 s, resulted equal to 11.4 km, 9 km, 13.2 km, 11.9 km, 17.8 km, 25.7 km, and 33.7 km, respectively. In Fig. (A.5) to Fig. (A.11) all estimated exponential models are shown together with data points referring to both classical and robust estimators.

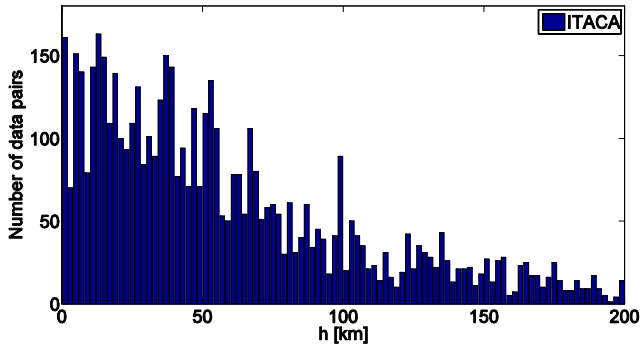

Figure A.4 Histograms of the number of data pairs as a function of site-to-site separation distance

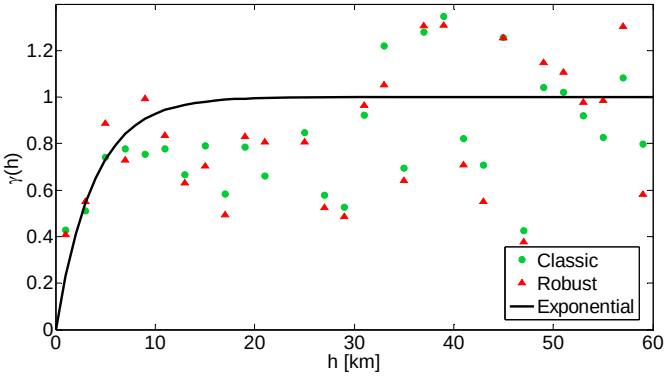

Figure A.5 Empirical semivariogram and fitted exponential model for Sa(0.1 s)

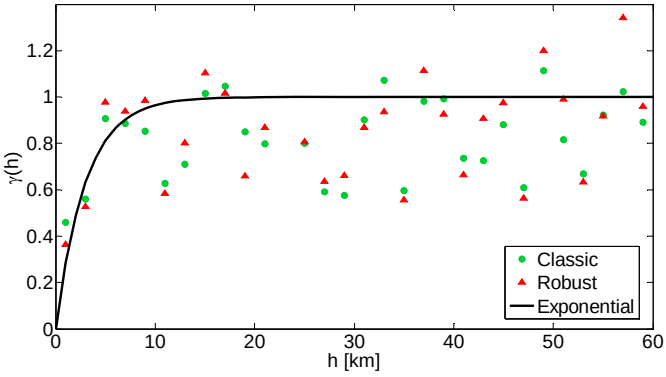

Figure A.6 Empirical semivariogram and fitted exponential model for Sa(0.2 s)

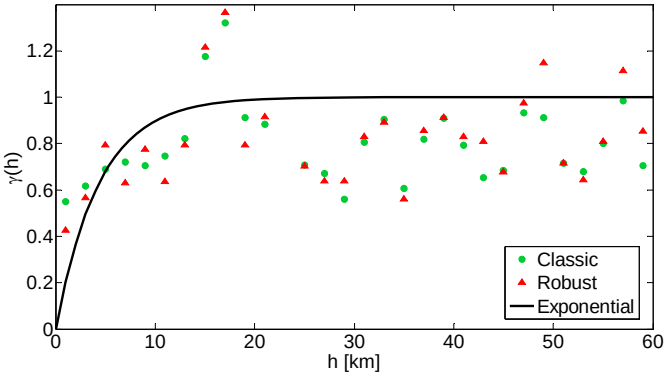

Figure A.7 Empirical semivariogram and fitted exponential model for Sa(0.3 s)

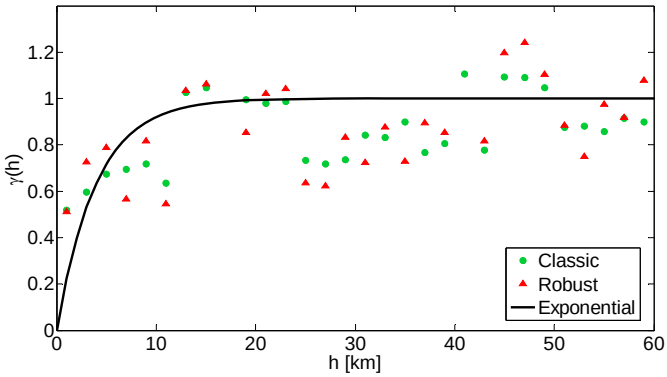

Figure A.8 Empirical semivariogram and fitted exponential model for Sa(0.5 s)

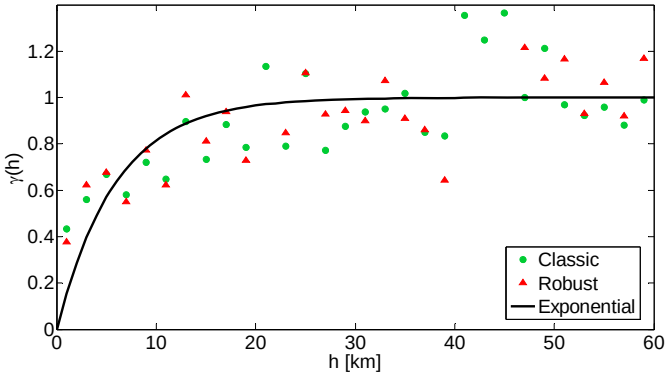

Figure A.9 Empirical semivariogram and fitted exponential model for Sa(1 s)

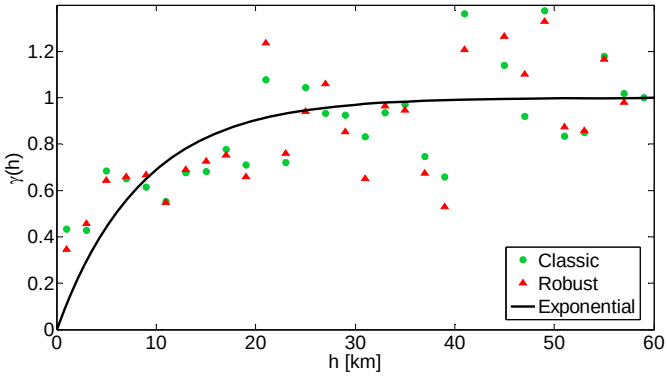

Figure A.10 Empirical semivariogram and fitted exponential model for Sa(1.5 s)

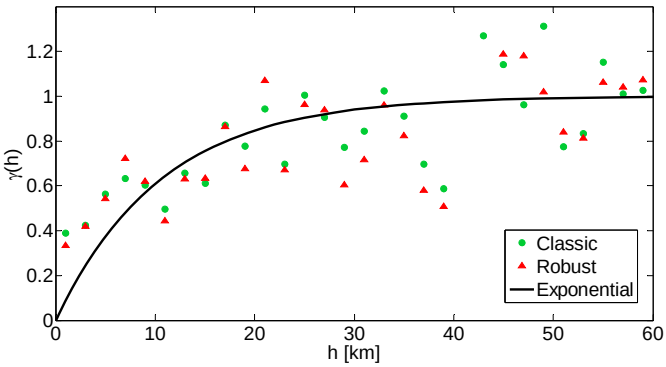

Figure A.11 Empirical semivariogram and fitted exponential model for Sa(2 s)

Results indicate that correlation range tends to increase with period reaching the value of about 40 km for T = 2 s.

It should be noted that in Esposito and Iervolino (2011a) the proposed methodology was used to estimate the horizontal peak ground acceleration (PGA) intra-event residuals' correlation starting from a less recent GMPE, the Bindi *et al.* (2010), and a larger dataset that includes the one used herein. For completeness, their spatial correlation model has been also estimated for horizontal PGA. The resulting range was similar to that of the mentioned study (Fig. A.12); i.e., 10.8 km with respect to 11.5 km, as expected. The slight difference may also be related to the bin width used in the estimation of empirical semivariograms (1 km instead of 2 km considered herein).

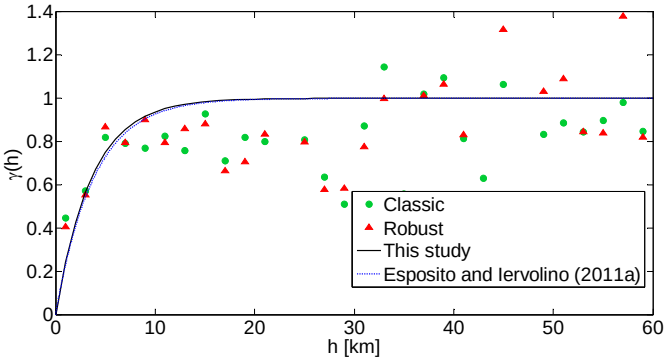

Figure A.12 Empirical semivariogram and fitted exponential model for horizontal PGA compared with Esposito and Iervolino (2011a)

A.5. Discussion

Empirical results demonstrate that correlation length tends to increase with period. Except for high frequencies at which there is no a significant increment. This seems to be consistent with past studies of ground motion coherency (Zerva and Zervas, 2002). In fact, the coherency describes the degree of correlation between amplitudes and phases angles of two time histories at each of their component frequencies. Considering that coherency decreases with increasing distance between measuring points and with increasing frequency, it may be reasonable to expect more coherent ground motion, as spectral acceleration evaluated at high periods exhibits more correlated peak amplitudes. This same issue aspect was also discussed in Jayaram and Baker (2009a) where in all earthquakes analyzed, the estimated ranges increased with period except for some cases.

In Fig. (A.13) estimated ranges have been compared with some correlation lengths available in literature; those models have been chosen considering: Californian dataset from Goda and Hong (2008), "all earthquakes" model from Hong *et al*. (2009), and the "predictive model" based on all earthquakes from Jayaram and Baker (2009a). The range *b* has been obtained evaluating the distance at which correlation is equal to 0.05. Results provided by this study seem to be comparable with ranges estimated in literature in terms of both trend as a function of T, and the estimated value of correlation lengths. This holds generally, except with respect to Goda and Atkinson (2009, 2010) models, in which ranges are larger (never below about 60 km) and the dependence of the correlation on period is not significant. A simple linear predictive model (red dashed line in Fig. A.13) has been estimated using LSM method in order to obtain ranges based on the period of interest. The resulting linear model is expressed by Eq. (A.11).

$$b(T) = 8.6 + 11.6 \cdot T \tag{A.11}$$

Based on this model, the correlation between normalized intraevent residuals separated by *h* is obtained as follows:

$$\rho(h,T) = e^{\left(-3 \cdot h / b(T)\right)} \tag{A.12}$$

derived from Eq. (A.7) and Eq. (A.8) where model parameters c_0 and c_e, the *nugget* and the *sill* respectively, are equal to one. Starting from this predictive model it is possible to get the joint probability density function for Sa(T) at all locations, for which it is required characterizing the covariance matrix, $\boldsymbol{\Sigma}$, expressed in the Eq. (A.3).

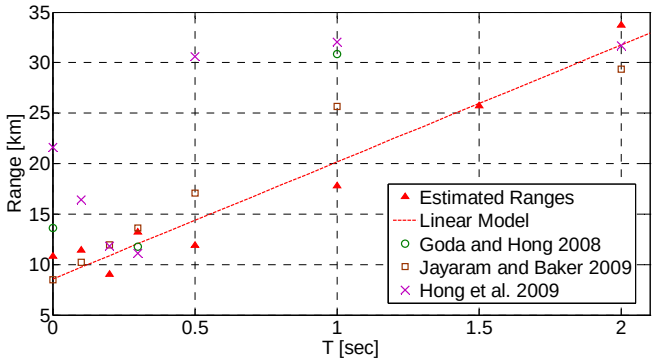

Figure A.13 Estimated ranges in this study compared with some correlation lengths available in literature

A.6. Conclusions

The study presented focused on the assessment of intraevent spatial correlation of spectral acceleration at eight periods ranging between 0 s and 2 s. A subset of the Italian Accelerometric Archive has been used to compute residuals starting from a GMPE calibrated on the same dataset. Consistent with the available literature on the topic, hypotheses of the stationarity and isotropy of the random fields were retained to compute experimental semivariograms of standardized intraevent residuals (with respect to the standard deviation estimated by the GMPE). Moreover, because a relatively small number of records for each earthquake was available, records from multiple events and regions within Italy were pooled to develop a unique model fitted with a large number of observations. Exponential correlation models were calibrated by finding that practical ranges tend to increase with the period. The choice of using the same model (exponential) for all periods allows to compare results and to investigate possible dependency of the parameters on the period the spectral ordinate refers to. Results have been also compared with previous researches finding, generally, a similar trend. Finally a simple linear predictive model has been estimated in order to provide the correlation coefficient between spectral accelerations as a function of structural period.

Appendix B – HAZUS GEOTECHNICAL CLASSIFICATION

B.1. Liquefaction

Table B.1 HAZUS Classification for Liquefaction Susceptibility Category

Type of Deposit	General Distribution of Cohesionless Sediments	Likelihood that Cohesionless Sediments when Saturated would be Susceptible to Liquefaction (by Age or Deposit)			
		< 500 year (Modern)	Holocene (< 11 ka)	Pleistocene 11 – 2 Ma	Pre-Pleistocene > 2 Ma
(a)Continental Deposits					
River Channel	Locally Variable	Very High	High	Low	Very Low
Flood Plain	Locally Variable	High	Moderate	Low	Very Low
Alluvial fan and plain	Widespread	Moderate	Low	Low	Very Low
Marine terraces and planes	Widespread	---	Low	Very Low	Very Low
Delta and fan delta	Widespread	High	Moderate	Low	Very Low
Lacustrine and playa	Variable	High	Moderate	Low	Very Low
Colluvium	Variable	High	Moderate	Low	Very Low
Talus	Widespread	Low	Low	Very Low	Very Low
Dunes	Widespread	High	Moderate	Low	Very Low
Loess	Variable	High	High	High	Unknown
Glacial Till	Variable	Low	Low	Very Low	Very Low
Tuff	Rare	Low	Low	Very Low	Very Low
Tephra	Widespread	High	High	?	?
Residual soils	Rare	Low	Low	Very Low	Very Low
Sebka	Locally Variable	High	Moderate	Low	Very Low
(b)Coastal Zone					
Delta	Widespread	Very High	High	Low	Very Low

Esturine	Locally Variable	High	Moderate	Low	Very Low
Beach					
High Wave Energy	Widespread	Moderate	Low	Very Low	Very Low
Low Wave Energy	Widespread	High	Moderate	Low	Very Low
Lagoonal	Locally Variable	High	Moderate	Low	Very Low
Fore shore	Locally Variable	High	Moderate	Low	Very Low
(c)Artificial					
Uncompacted Fill	Variable	Very High	---	---	---
Compacted Fill	Variable	Low	---	---	---

Table B.2 Probability of Liquefaction for Each Susceptibility Category

Susceptibility Category	P [Liquefaction | PGA = a]
Very High	$0 \leq 9.09a - 0.82 \leq 1$
High	$0 \leq 7.67a - 0.92 \leq 1$
Moderate	$0 \leq 6.67a - 1.0 \leq 1$
Low	$0 \leq 5.57a - 1.18 \leq 1$
Very Low	$0 \leq 4.16a - 1.08 \leq 1$
None	0

Table B.3 Proportion of Map Unit for Liquefaction Susceptibility Class

Mapped Relative Susceptibility	Proportion of Map Unit (P_{ml})
Very High	0.25
High	0.2
Moderate	0.1
Low	0.05
Very Low	0.02
None	0

Table B.4 Liquefaction Settlement for each Susceptibility Category

Relative Susceptibility	Settlement (inches)
Very High	12
High	6
Moderate	2
Low	1
Very Low	0
None	0

B.2. Landslide

Table B.5 Landsliding Susceptibility Classification

Geologic Group		Slope Angle (Degrees)					
		0 – 10	**10 – 15**	**15 – 20**	**20 - 30**	**30 – 40**	**> 40**
DRY (groundwater below level of sliding)							
A	Strongly Cemented Rocks (Crystalline rocks and well-cemented sandstone	None	None	I	II	IV	VI
B	Weakly Cemented Rocks and Soils (sandy soils and poorly cemented sandstone)	None	III	IV	V	VI	VII
C	Argillaceous Rocks (shales, clayey soil, existing landslides, poorly compacted fill)	V	VI	VII	IX	IX	IX
WET (groundwater above level of sliding)							
A	Strongly Cemented Rocks (Crystalline rocks and well-cemented sandstone	None	III	VI	VII	VIII	VIII
B	Weakly Cemented Rocks and Soils (sandy soils and poorly cemented sandstone)	V	VIII	IX	IX	IX	IX
C	Argillaceous Rocks (shales, clayey soil, existing landslides, poorly compacted fill)	VII	IX	X	X	X	X

Table B.6 Critical accelerations and map area proportions for each landsliding susceptibility category

Susceptibility Category	None	I	II	III	IV	V	VI	VII	VIII	IX	X
Critical Acceleration (g)	None	0.60	0.50	0.40	0.35	0.30	0.25	0.20	0.15	0.10	0.05
Map Area	0	0.01	0.02	0.03	0.05	0.08	0.10	0.15	0.20	0.25	0.30

Appendix C – ADDRESSING GROUND-SHAKING-INDUCED DAMAGE OF THE GAS DISTRIBUTION NETWORK IN THE 2009 L`AQUILA EARTHQUAKE

Esposito, S., Elefante, L., Giovinazzi, S., and Iervoino, I. (2011b) Addressing ground-shaking induced damage of the gas distribution network in the 2009 L'Aquila earthquake. In *Proceeding, XIV Convegno Nazionale "L'Ingegneria Sismica in Italia".* September, Bari, Italia.

Abstract

This paper describes the assessment of the damage of the local gas network in the 2009 L'Aquila earthquake (Mw 6.3). The analysis focuses on the main components of the low and medium distribution networks, namely pipes, valves, and demand nodes. The processing of the technical reports from Enel Rete GAS (the unique gas network operator in the affected region), describing the repairs and replacements activities following L'Aquila earthquake is presented, and the resulting damage scenario is discussed. In particular, the density of repairs activities have been overlaid to the ground motion in the affected area, described in terms of peak ground velocity. Finally, the repair ratios (number of repairs per km) for the pipelines were compared with repair ratio fragility functions available in literature.

C.1. Introduction

Recent disastrous seismic events have widely documented the role of lifeline networks in supporting the emergency management and in facilitating the response and recovery phases (*resilience*) following an earthquake, thus rising the interest of both the scientific community and the stakeholders in identifying proper risk management strategies for this kind of systems (Pitilakis *et al*, 2006). Building on the results from past international research projects and existing tools for the vulnerability assessment

and seismic risk analysis of lifelines systems the SYNER-G "Systemic Seismic Vulnerability and Risk Analysis for Buildings, Lifeline Networks and Infrastructures Safety Gain", has been funded by the European Commission (2009-2012) with the aim to address criticalities.

This paper, developed as part of the SYNER-G project, analyses the impact of the 6th April 2009 L`Aquila earthquake, in Italy, on the gas network with particular focus on the damage induced by the transient ground deformation on the pipeline distribution network. In fact, in the event of an earthquake, buried pipeline can be subjected to both transient ground deformation caused by the passage of seismic waves (ground shaking) which is felt over a wide geographical area, and permanent ground deformation (PGD) caused by surface faulting, liquefaction, landslides which determine localized ground failure. Exception made for surface faulting phenomena, limited PGD were, in fact, observed following the L`Aquila earthquake. Therefore, the damage to the pipelines, has been correlated with the experienced ground shaking. The first part of the paper presents relevant information on the 6th April 2009 L`Aquila earthquake and the assessment of the peak ground velocity (PGV), virtually experienced by the gas network. The second part provides a description of the gas networks in the affected region and of the operations undertaken for securing of the system following the earthquake and for its restarting during the recovery phase. Finally, data processing and analysis for assessing the physical impact of the earthquake on the pipelines of the distribution network is presented comparing the results with existing predictive relationships of repair ratios per km.

C.2. The L'Aquila earthquake

On April 6th 2009, 03:32:40 UTC, a moment magnitude (Mw) 6.3 earthquake struck the Abruzzo region, in central Italy. The earthquake occurred at about 10 km depth along a NW-SW normal fault with SW dip, located below the city of L'Aquila (INGV 2009). Considerable damage to structures and infrastructures was detected over a broad area of approximately 600 square kilometres, including the city of L'Aquila and several villages in the Aterno River valley. After the main shock, 3 aftershocks with moment magnitude Mw > 5 were recorded (6th April, Mw 5.8; 7th April, Mw 5.3; 9th April, Mw 5.1), and 31 with a range of moment magnitude from Mw 3.5 and Mw 5. The main shock and its aftershocks were recorded by several digital stations of the Italian strong-motion network (Rete Accelerometrica Nazionale, RAN; Zambonelli *et al.*,2010), owned and maintained by the Italian Department of Civil Protection. Horizontal peak ground accelerations (PGA) recorded in the near-source region

ranged from 0.33g to 0.65g, the latter representing one of the highest values measured in Italy (Chioccarelli *et al.*,2009). Regarding geological effects induced by the earthquake, evidence of coesismic surface faulting was found in correspondence of the Paganica fault (Blumetti *et al*., 2009). A set of well aligned ground ruptures was found (traced for a length of about 2.6 km), reaching in some sites vertical offsets of 7-8 cm. Moreover, numerous rock falls occurred especially near the village of Fossa and within the Gran Sasso mountain. Evidence of liquefaction were found in a quarry near Bazzano (industrial area) and in Vittorino (near Sulmona), relatively far from the epicentre.

C.2.1. Peak ground velocity map from L`Aquila earthquake ground motion records

A continuous map of the ground motion, for all the extension of the analysed gas network, has been derived from the available records, using *ShakeMap*(TM) (Wald *et al*., 2006). The ShakeMap processing system has provided PGV values as a grid of points with associated intensity values of the shaking parameter. Fig. (C.1) shows the resulting PGV values, contoured for the maximum horizontal velocity (cm/sec) at each station, with contour intervals of 2 cm/sec. Those values have been obtained interpolating recorded values and estimated amplitudes obtained considering available information about local geology.

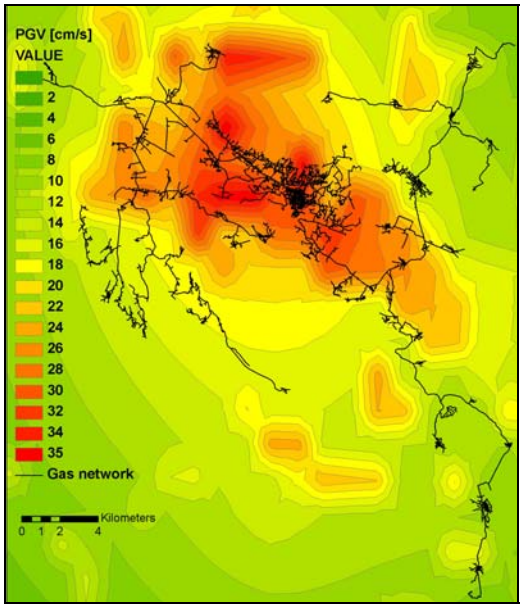

Figure C.1 Map of PGV (cm/s) contours relative to L'Aquila earthquake (from http://shakemap.rm.ingv.it) overlapped to the L'Aquila gas network

C.3. The gas network in L`Aquila and its management during the post-event phase

Principal components of a nationwide gas supply system include: (1) high-pressure transmission lines; (2) Metering/Pressure reduction stations (M/R stations); (3) medium-pressure distribution networks; (4) Reduction Groups; (5) low-pressure distribution networks; (6) demand nodes; (7) gas meters.

In Italy the high-pressure transmission lines (operated at a national level by SNAM, http://www.snamretegas.it) are made of welded–steel pipes, with an internal diameter of 103.9 mm and a thickness of 5 mm. The connection of the L'Aquila distribution medium-pressure network (MP = 64bar) to the national high-pressure transmission lines is operated via three Metering/Pressure Reduction Stations, M/R Stations (Re.Mi. "Regolazione e Misura" stations, in Italian). The three M/R stations (Re.Mi. stations) of the L`Aquila distribution system are cased in one-story reinforced concrete structures with steel roofs (Fig. C.2) hosting internal regulators and mechanical equipment (heat exchangers, boilers and bowls) where the gas undergoes the following processes: (1) gas preheating; (2) gas-pressure reduction and regulation; (3) gas odorizing; (5) gas-pressure measurement.

In L'Aquila region the gas is distributed via a 621 km pipeline network (Fig. C.2): 234 km of which operating at medium pressure (2.5 – 3 bar), and the remaining

387 km with gas flowing at low pressure (0.025 – 0.035 bar). The pipelines of the medium and low pressure distribution networks are either made of steel or HDPE (*High Density Polyethylene*). HDPE pipes have nominal diameters ranging from 32 to 400 mm, whereas diameter of steel pipes is usually between 25 and 300 mm. Different types of in-line valves are found along the pipeline network (mainly gate valves, butterfly valves, check valves, ball valves). The transformation of the medium distribution pressure into the low distribution pressure (LP) is operated via 300 Reduction Groups (RGs). Generally along the low pressure network (in some cases also along medium distribution pressure network), there are several demand nodes (IDU, "Impianto di Derivazione Utenza" in Italian) consisting of buried and not buried pipes and accessory elements to supply natural gas to utilities. Moreover, depending on the type of final client of the network and whether there is an IDU system, there are three types of RG: (a) GRM, Reduction Groups and Measure along medium distribution pressure (MP) network and direct connected to large users (e.g., industrial facilities); (b) GRU, Reduction Groups smaller than GRM for medium pressure Users connected to a medium pressure IDU system; (c) GRF, Final Reduction Group connected to low pressure network. It is worth noting that all the components contained in both the L'Aquila M/R stations and Reduction Groups are unrestrained, and therefore especially seismically vulnerable.

Figure C.2 M/R Metering/Pressure reduction station in Onna (L`Aquila, Italy)

The 300 Reduction Groups, that in the L`Aquila gas distribution allow for the transformation of the medium distribution pressure into the low distribution pressure are either buried, sheltered in a metallic kiosk or housed within/close to a building (Fig. C.3).

Figure C.3 RG housed in a masonry kiosk closed to building and damaged following the 6th April 2009 earthquake

C.3.1. Emergency management of the gas network following the L'Aquila earthquake

The first priority identified for the management of the gas network, in the first phase of the emergency immediately after the L`Aquila earthquake, was the timely securing of the network in order to avoid explosions, gas leaks and fires and to allow emergency vehicles and Search and Rescue USAR teams to act in the safest possible way. To ensure this priority, the entire network managed by ENEL Rete Gas S.p.A. (http://www.enel.it/it-IT/reti/enel_rete_gas/) in the affected area was shut off via the closure of the three operating M/R stations (Dolce *et al.*, 2010). Thanks to this decision, it was possible to timely and significantly reduce the gas pressure and to avoid the occurrence of secondary effects of the earthquake. The subsequent closure of the 300 GR Reduction Groups ensured the full securing of the network in less than two hours after the earthquake. In the days following the event, all the gas valves external to each residential building were closed as well.

The process to recovery the gas network started few days after the earthquake. To more effectively manage and prioritise the repair activities, during the recovery phase, four different areas, in the region served by the gas network, were identified, namely: Central Area (Z1); West Area (Z2), East Area (Z3), Sud-East Area (Z4). The Central Area, Z1, included the historical centre of the city and the surrounding where a large number of the collapsed and severely damaged buildings was concentrated. The

West Area, Z2, includes the west suburbs and the municipalities of Lucoli and Tornimparte, where a moderate/slight impact on the built environment was observed. The East Area, Z3, corresponds to the east suburbs, including Onna e Paganica, where a large percentage of the buildings resulted collapsed or severely damaged. The Sud-East Area, Z4, includes municipalities less affected by the earthquake (i.e. Ocre, Rocca di Cambio and Rocca di Mezzo). The areas Z2 and Z3 were the first ones to be targeted for the recovery activities. In these areas, six days after the earthquake event, the network was restored to allow for 50% of the end-users to be potentially reconnected. The reactivation of the shut-off gas network required: the check of the gas flow in the medium and low-pressure networks; the check of each external valve pertinent to each residential building previously closed; the substitution of each gas-meter. The check and reactivation of low and medium pressure networks was managed in the following four steps: (1) seal verification; (2) nitrogen check; (3) repair of damaged pipes and/or valves; (4) reopening. In the seal verification phase, the detection of broken pipes and/or the possible joint slip-off was made, acting in the first instance, from node to node, and further segmenting the network when necessary (Dolce *et al*., 2010). The material and equipment needed for the repair was immediately available from the integrated logistics system used by Enel Rete Gas. The adopted strategy ensured the remediation and testing of more than 90% of the gas network in three months time after the earthquake and the provision of the gas supply for all the end-users with a safe home. Fig. (C.4) (red line) shows the percentage of the customers that could have been potentially reconnected to the network for all the four zones. In fact, a relative minor percentage of the end-users was reactivated to the service, (Fig. C.4, blue line), since the reactivation required a safe building for the supply; i.e., green tagging by the civil protection. It is worth highlighting that data on potential reconnection and end-user activation were recorded and reported in Fig. (C.4) starting only from 6th of May. Because data were not available for the month after the earthquake, dashed lines in Fig. (C.4) represent an hypothetical trend of serviceability of the network considering that immediately after the earthquake the entire network in the affected area was shut off by the operator.

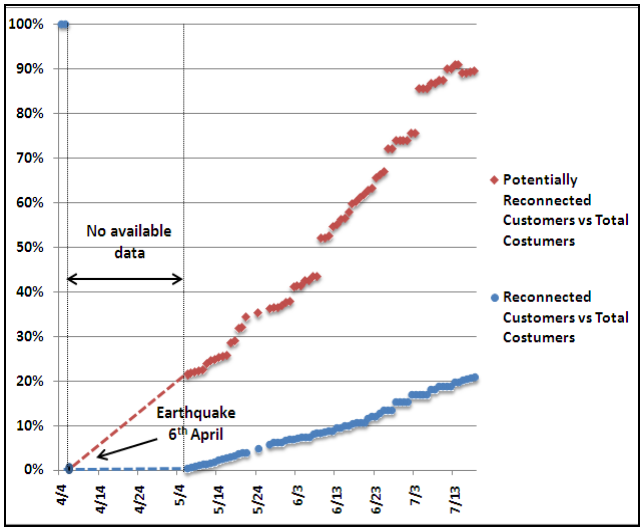

Figure C.4 Percentage of the customers potentially reconnected (red line) and reconnected (blue line) to the networks for all the four zones in the months following the earthquake referring time period when data were available

C.4. Physical damage assessment for the gas system

In order to assess the physical damage that occurred to the gas network components (described in Section C.3), the technical reports from Enel Rete GAS (the only gas network operator in the affected region), describing the repair and replacement activities following L'Aquila earthquake, have been processed. In particular, Enel Rete GAS was involved in two types of technical activities: (1) activities to recovery the system efficiency to its state before the earthquake (referred to as "Rei.activities", recover system efficiency as a result of exceptional events); (2) reconstruction activities to improve the gas network efficiency beyond its original condition (referred to as "E1E.activities", reconstruction of facilities for investments as a result of exceptional operations). More than 500 technical reports from Enel Rete GAS related to "Rei.activities" maintenance/repair activities following the earthquake were analyzed and processed, over a period of five months (from April 2009 to August 2009). Starting from those reports different maintenance operations have been identified and geocoded. (For April 2009, in a situation of full emergency, the technical reports describing the repair activities were not compiled; and only costs of the operations are available for that period. However, assistance and emergency support interventions were the main operations undertaken during the month of April, with a limited activity of repair/restoration of the gas network.) For each component,

operations where gathered in macro categories that are not exactly associated with a particular damage level, since the extent and description of the damage sustained by the network components were insufficiently reported in the technical reports, which scope was more related to price the repair activity rather than to report the damage. However, from processing of technical and economic reports, it has been possible to get an aggregate quantification of: (1) the damage to the network system' components; (2) the aggregate cost associated with different types of repair operations; (3) the time required for different types of repair operations. A more detailed description of the maintenance operations was illustrated in a previous paper of the authors (Esposito *et al.*, 2011a). Reports related to "E1E.activities" were furthermore analyzed and processed until November 2009 but more than two years after the earthquake, the "E1E.activities" activities are still on-going. Further reports will be processed, extending the observation period, to get a clearer overview on these activities and on how they have impacted in the recovery process following the earthquake.

C.4.1. Processing of technical reports and results

The processing of damage reports allowed for a classification of maintenance operations. In particular the list below illustrates the typology of maintenance operations for "Rei.activities":

- testing operations (disconnecting and reconnecting the network);
- gas leak detection and repair;
- valve replacement;
- demand node repair

As mentioned, the reports were compiled by field crews with the main objective to restore the gas system to service as rapidly as possible and price the repair; documenting damage was of secondary importance. As a results repair records have some inaccuracies, including omitted address indication, vague damage description and multiple repairs at a single site combined into one record. For these reasons, processing 513 technical reports and excluding incomplete ones, a dataset consisting of 431 records has been obtained. In order to get a clear idea of the damage undertaken by the gas network system, maintenance intervention types have been summarized identifying eight macro categories: three for pipelines (including operation for pipeline inspection or screening, P_scr, pipeline repair, P_rep, pipeline reconnection, P_rec), three for the valves (excavation for valve inspection, V_exc, valve insertion, V_ins, valve removal, V_rem); and two for the demand nodes, IDU (realization of buried,

I_rea_b, and unburied demand node, I_rea_nb). Fig. (C.5) illustrates the number of interventions included in each of the considered macro categories.

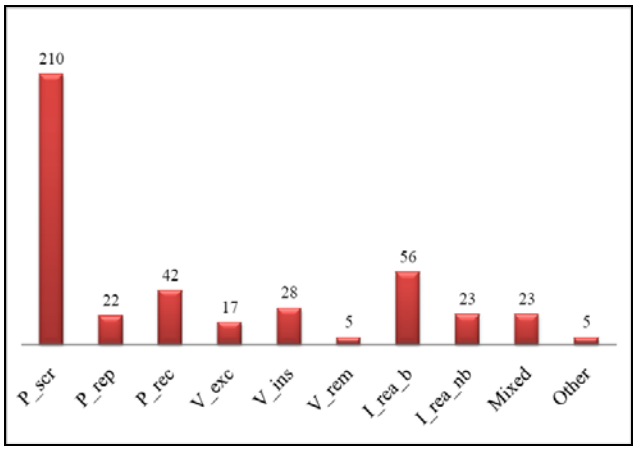

Figure C.5 Number of maintenance operations

The aim of this work is to obtain pipelines damage curves, expressed in number of repairs per km, overlaying density of repairs activities to the ground motion observed in the affected area in terms of peak ground velocity. Therefore, the database obtained was further purified of all records related to screening operations (P_scr), valve excavation (V_exc), realization of unburied nodes (I_rea_nb) and the interventions indicated as "other" that refer to transport operations or closure of excavations previously made. At the end of this process a reduced dataset consisting of 176 maintenance records was obtained. Fig. (C.6) illustrates the composition of the reduced database used for damage analysis. Damage reports of maintenance operations involved pipes operating at medium (MP) and low (LP) pressure. Moreover the pipelines of the medium and low pressure distribution networks are either made of steel or HDPE. Fig. (C.7) illustrates this operations included in the dataset distinguished in relation to pressure level and pipe material.

C.4.2. Density of repairs activities versus ShakeMap PGV values

Earthquake damage to buried pipelines can be attributed to transient ground deformation (caused by ground shaking) or to permanent ground deformation, PGD (including surface faulting, liquefaction, landslides, and differential settlement from consolidation of cohesionless soil) or both (Toprak and Taskin, 2006).

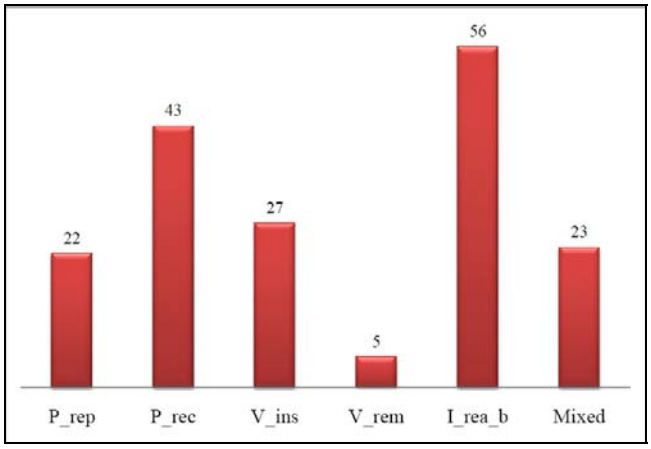

Figure C.6 Reduced database of maintenance operations

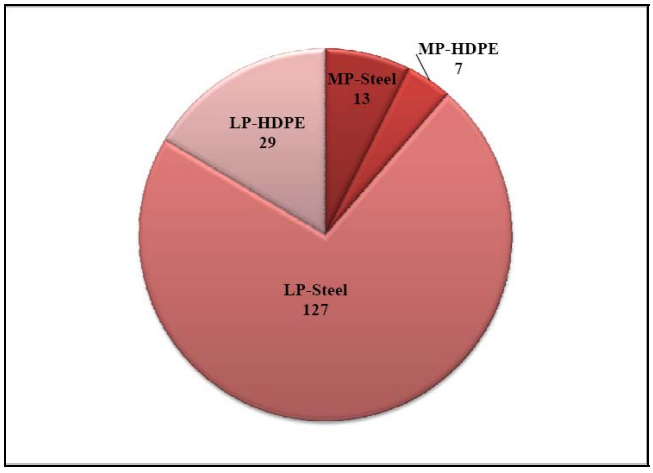

Figure C.7 Dataset distinguished in relation to pressure level and pipe material

The earthquake impact on the pipeline is commonly measured in term of the Repair Rate, R_R, which is the number of pipeline repairs in an area divided by the length of the pipelines in the same area. Empirical data on pipeline failures from past earthquakes have been processed to define Repair Rate empirical correlations, able to predict the number of repairs per unit length of pipe required as a function of a parameter representative of ground shaking (e.g., peak ground velocity or acceleration, PGV and PGA, respectively) or ground failure (i.e., PGD) (ALA 2001a). A concise summary of "Repair Rate" fragility curves for buried pipes due to ground shaking can be found in Tromans (2004) including the dataset used and the range of applicability for each relation. This study aims to derive Repair Rate values for the gas network following the L`Aquila earthquake as a function of the PGV. Exception made for

surface faulting phenomena, limited PGD were, in fact, observed following the L`Aquila earthquake (as reported in Section C.2). Therefore, the damage to the pipelines, deduced from the analyzed repair activities, has been correlated with the experienced ground shaking. Moreover, among the various seismic parameters used to correlate the ground motion effects to the damage suffered by buried pipeline, the peak ground velocity, PGV, has been identified as the one having a more direct physical interpretation (O'Rourke *et al.* 1998). Actually, PGV is correlated with the ground strain that can be transferred to the pipeline, depending on the slippage developed between the pipe and the surrounding soil. Therefore a good correlation between PGV and pipeline damage is expected.

In order to evaluate R_R data points based on L'Aquila earthquake, both the network and the damage data have been mapped using a Geographical Information Systems (GIS). For the evaluation of pipeline R_R-PGV points, the PGV values from the *ShakeMap* of Fig. (C.1) were used. It is worth noticing that, although the repairs activities dataset covers four distinct areas, as explained in Section C.3.1, only the data belonging to the Zone 1 have been considered and processed for deriving the R_R-PGV points. Actually, in the emergency management phase, following the earthquake, several repairs activities were carried out without completing the reporting documentation. Zone 1 was the only one where the repair data were completely reported, for the observation period considered in this analysis. Therefore, in order to avoid an underestimation of the repair ratio, data from the other Zones have been eliminated. Moreover since the network belonging to the historical center has been completely replaced, repairs data belonging to this zone (referred to as the "Red Zone") have been, equally eliminated, from the dataset. The resulting study area is shown in Fig. (C.8), together with the L'Aquila gas distribution system and the repairs occurring in the analysed zone. The repairs dataset used for repair ratio evaluation is composed of 85 data repairs distinguished in six macro categories, as illustrated in Fig. (C.9). This dataset includes 8 repair operations on pipes operating at medium pressure and 77 on pipes operating at low pressure. As concern to material, only 11 repair operations included in the dataset were on HDPE pipes and the remaining 74 were on steel pipes.

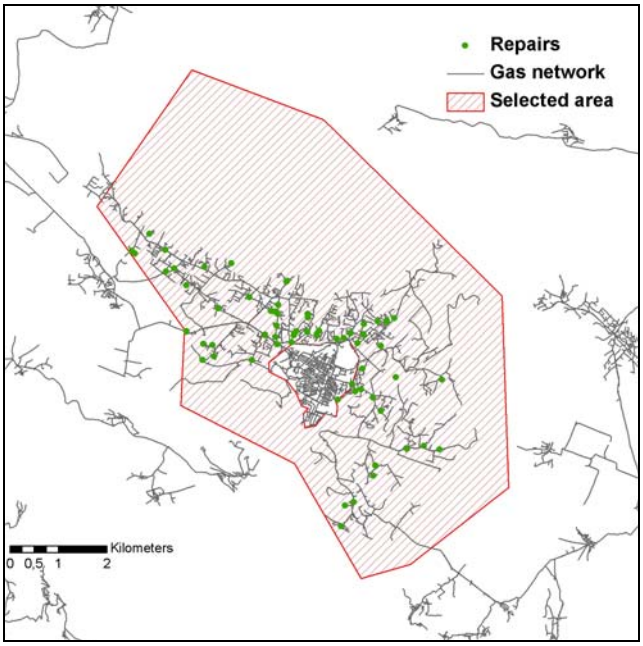

Figure C.8 Selected area for the evaluation of Repair Ratio

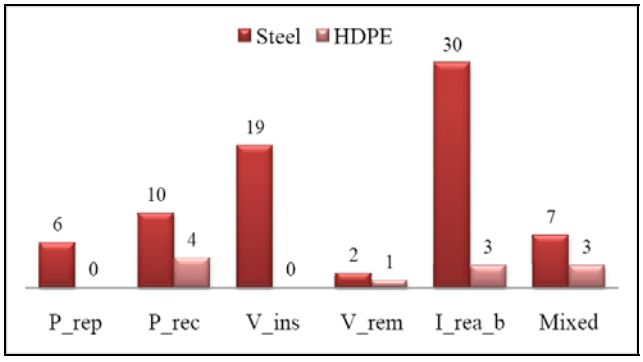

Figure C.9 Dataset for repair ratio evaluation distinguished in relation to pipe material

Using the GIS software, repair rate of the selected area have been calculated for each PGV zone combining repairs location, pipeline network and PGV contours. For each PGV zone, number of repairs and pipeline length has been calculated. The resulting points (Fig. C.10) are compared with pipeline fragility relations suitable for the L'Aquila gas network reported in Tab. (C.1)[12]. Note that data obtained from the analysis consider PGV as the maximum horizontal velocity (cm/sec); even if some fragility curves consider the geometrical mean horizontal component for PGV, no

[12] Fragility relations reported in Table 1 were converted by Tromans (2004): R_R was converted from 1/feet*10^3 to 1/km and PGV from inch/s to cm/s.

conversion has been applied ; see Beyer and Bommer (2006) for a discussion. Results shows that the trend is somehow comparable with existing pipeline-fragility curves; although the fragility curves seems to be conservative on respect to the observed damage, it must be highlighted that the scatter associated with the empirical fragility relations is quite high since those fragility curves have been obtained combining data from different kinds of pipes (e.g. ALA, 2001a).

Table C.1R$_R$ - PGV pipelines fragility relations suitable for L'Aquila gas network

Author	Fragility relation	Notes
ALA (2001a)	$R_R = K_{1ALA} \cdot 0.002416 \cdot PGV$	"backbone[13]" curve (K_1=1)
HAZUS (FEMA, 1999)	$R_R = 0.00003 \cdot PGV^{2.25}$	"ductile pipes" curve
Eidinger (1998)	$R_R = K_1 \cdot 0.0001658 \cdot PGV^{1.98}$	"best-fit" curve (K_1=1)

It is important to note that L'Aquila gas pipelines are made of steel and HDPE. HDPE is not well studied in current literature as no empirical fragility curves have been developed specifically for this material. However, the R_R resulting seems to be comparable with the fragility curve derived by Eidinger (1998).

When looking at Fig. (C.10) it is to recall that, as in some of the case studies reported in the literature, the repair rate following the L'Aquila earthquake incorporate the damage from both the ground shaking and the ground deformations, including PGD effects and surface rupture (ALA 2001b). Unfortunately data available from L'Aquila earthquake does not make possible to derive an empirical curve because of the limited PGV range [22-34 cm/s]; anyway it could be useful to include repair data obtained in this work in a pipe damage database to develop new fragility curves.

C.5. CONCLUSIONS

This paper presents the preliminary results of the data processing activities that are on-going on the L`Aquila case study to understand the impact of the earthquake on the

[13] Backbone fragility functions represent the average performance of all kinds of pipes in earthquakes. These functions can be used when there is no knowledge of the pipe materials, joint type, diameter, etc.

gas distribution system. In particular the ground shaking induced damage to the gas distribution network following the April 6th 2009 earthquake was analyzed.

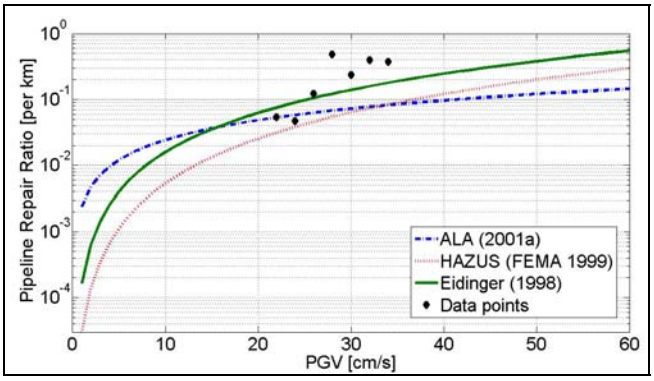

Figure C.10 R_R-PGV points compared with some fragility curves suitable for the L'Aquila gas network

To this aim the technical reports from the repair activities following the earthquakes were processed to obtain the repair rate (number of repairs per km) as a function of the level of ground shaking experienced, expressed in terms of PGV. In fact, while it is expected pipelines suffer damage (mostly) from ground displacements, insufficient PGD data were available for the region at the time of the study and therefore damage was correlated to PGV only (as in some of the literature studies at the basis of the existing fragility functions for networks' components).

The selected period refers to May 2009 - August 2009 since repair activities related to the month of April were not reported technically. However, assistance and emergency support interventions were the main operations undertaken during the month of April, with a limited activity of repair/restoration of the gas network. Many repair reports from the network operator were discarded because of incomplete or unsuitable information. Moreover, although the repair dataset covers four distinct areas, only the data belonging to the Zone 1 have been considered and processed since this area was the only one where the repair data were completely reported, for the observation period considered in this analysis.

This whole set of issues resulted in a limited data available. Nevertheless, the resulting repair rates were finally compared with those ones available from the literature to assess whether these functions can be applied in the assessment of gas distribution networks of similar types.

Appendix D – LANDSLIDE POTENTIAL CHARACTERIZATION OF L'AQUILA REGION

The methodology presented in HAZUS (FEMA, 2004) has been used to characterize landslide susceptibility of L'Aquila region, based on the geologic group, slope angle, and ground-water condition thanks to a process jointly developed by Department of Hydraulic Engineering, Geotechnical and Environmental and Department of Structural Engineering of University of Naples, "Federico II. Study by Wilson and Keefer (1985) was the foundation of this methodology, which categorizes landslide susceptibility from lowest to highest. Geology has been derived from 1:50,000 scale ISPRA geologic maps (http://www.isprambiente.gov.it). Each rock type was classified into three geologic groups using the HAZUS method (Fig. D.1). Slope angle was generated from topographic data, and was grouped into six slope classes: 3-10, 10-15, 15-20, 20-30, 30-40, >40 degrees (Fig. D.2). Ground-water conditions have been considered as wet for geologic groups B and C. A spatial overlay of these data layers (geologic group and slope angle) was performed using Arc/GIS software. The resulting polygons were then attributed with the corresponding susceptibility category (I to X). Moreover starting from the susceptibility categories, the critical acceleration map has been obtained according to the HAZUS methodology (Fig. D.3).

A map showing earthquake-induced landslide susceptibility and critical accelerations for the L'Aquila area is essential for good decision making at local and regional levels of government to accurately estimate losses from potential earthquakes. For the purpose of this thesis, these maps have been used as input for the geotechnical analysis in order to estimate the seismic demand due to landslide and to obtain the failure probability of each facility and distributing elements of the case study.

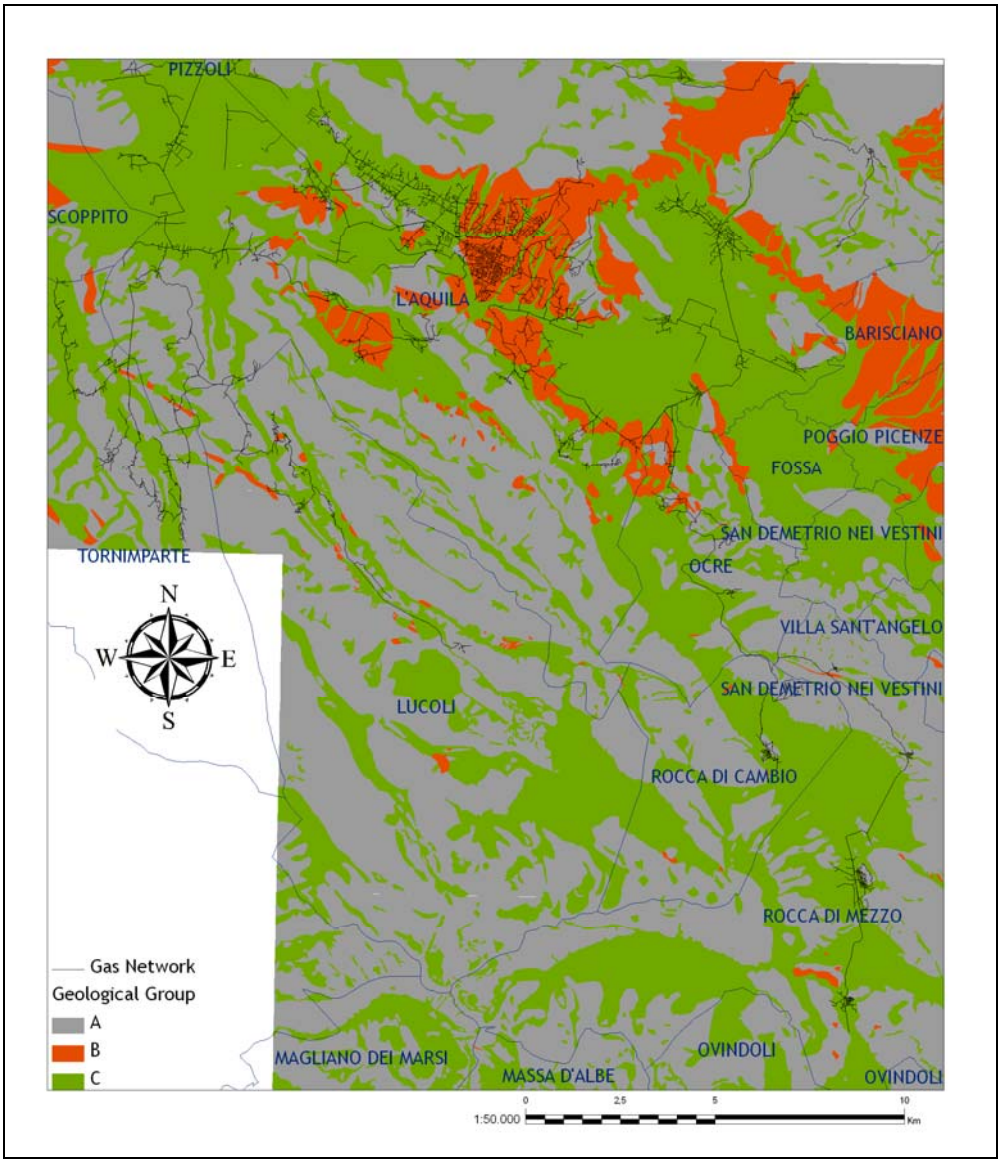

Figure D.1 Classification of geological groups for L'Aquila region according to HAZUS (FEMA, 2004) methodology

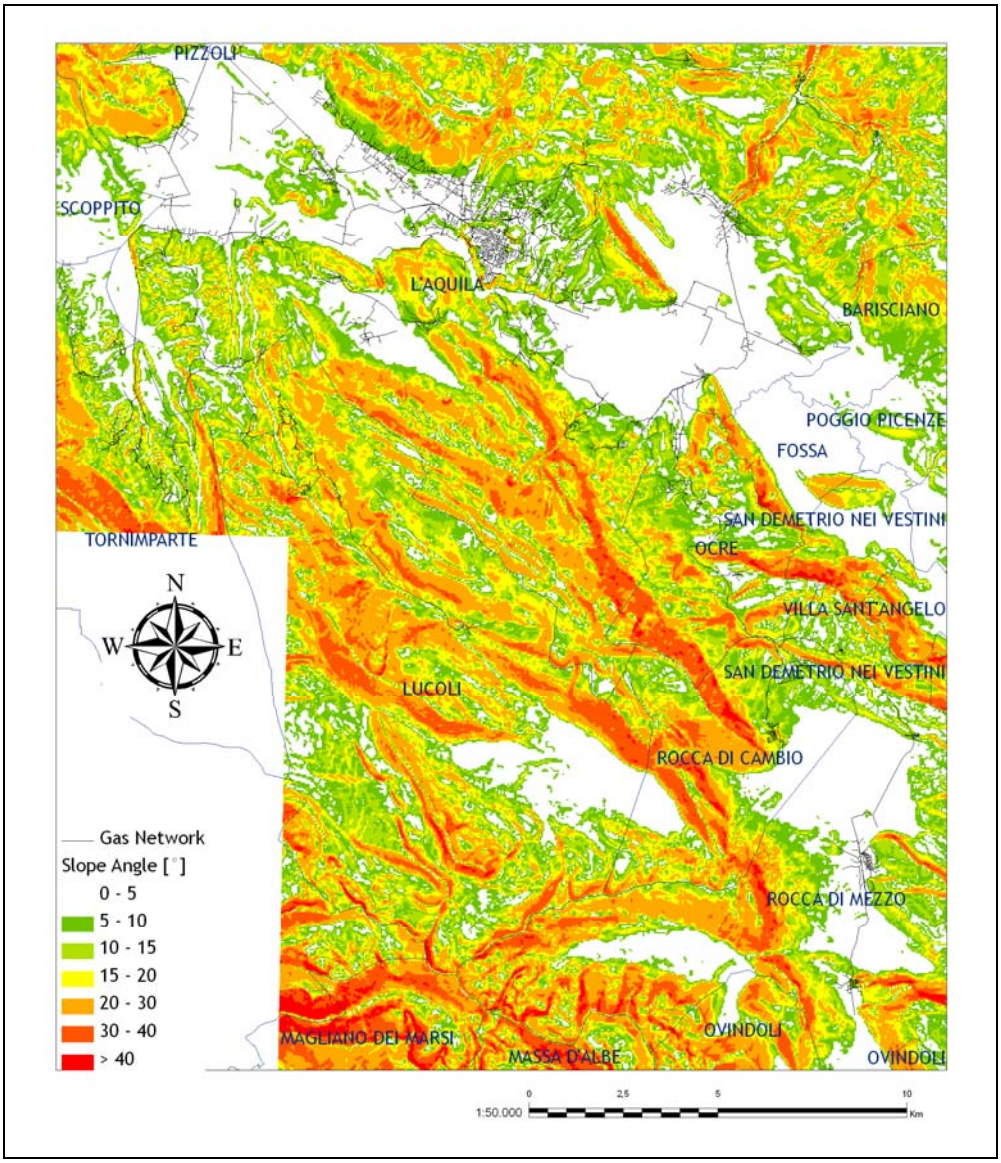

Figure D.2 Slope angles categories fro l'Aquila region

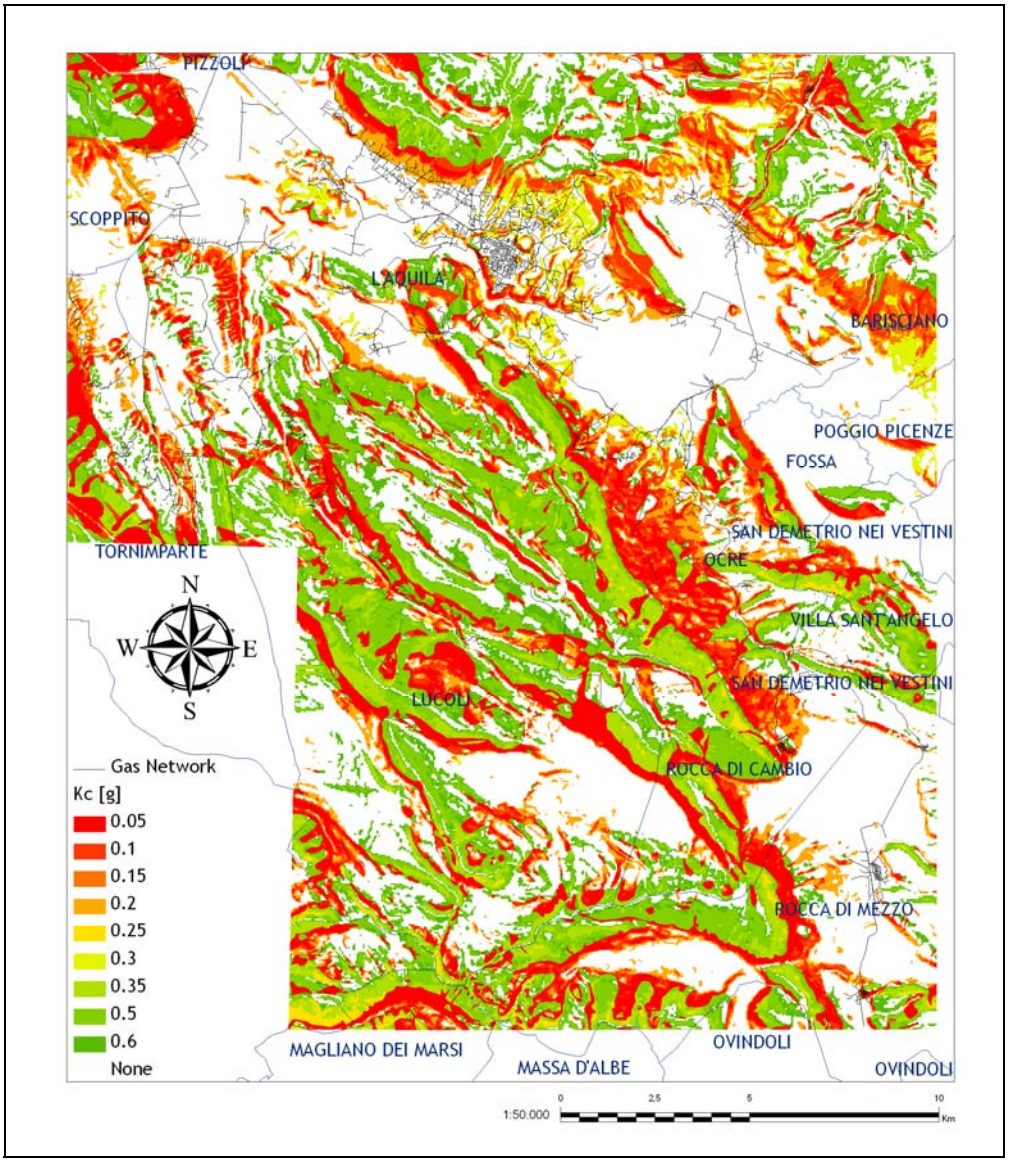

Figure D.3 Critical acceleration map for L'Aquila region according to HAZUS (FEMA, 2004) methodology

REFERENCES

Abrahamson, N.A., and Youngs, R.R. (1992), A stable algorithm for regression analyses using the random effect model. *Bulletin of the Seismological Society of America* **85 (1)**: 505-510.

Adachi, T. and Ellingwood, B.R. (2008). Serviceability of earthquake-damaged water systems: Effects of electrical power availability and power backup systems on system vulnerability. *Reliability Engineering and System Safety* **93 (1)**: 78-88.

Akkar, S., and Bommer, J.J. (2010). Empirical Equations for the Prediction of PGA, PGV and Spectral Accelerations in Europe, the Mediterranean Region and the Middle East. *Seismological Research Letters* **81 (2)**: 195 – 206.

ALA (2001a). Seismic fragility formulations for water systems Part 1 Guidelines. *American Lifeline Alliance*, ASCE.

ALA (2001b). Seismic fragility formulations for water systems Part 2 Appendices. *American Lifeline Alliance*, ASCE.

Ambraseys, N. N., Douglas, J. , Sarma, S. K., and Smit, P.M. (2005a). Equations for the Estimation of Strong Ground Motions from Shallow Crustal Earthquakes Using Data from Europe and the Middle East: Horizontal Peak Ground Acceleration and Spectral Acceleration. *Bulletin of Earthquake Engineering* **3 (1)**: 1-53.

Ambraseys, N. N., Douglas, J. , Sarma, S. K., and Smit, P.M (2005b). Equations for the Estimation of Strong Ground Motions from Shallow Crustal Earthquake Using Data from Europe and the Middle East: Vertical Peak Ground Acceleration and Spectral Acceleration. *Bulletin of Earthquake Engineering* **3 (1)**: 55-73.

ATC-25, (1991). *Seismic Vulnerability and Impact of Disruption of Lifelines in the Conterminous U.S.* Earthquake Hazard Reduction Series 58, Federal Emergency Management Agency, FEMA 224.

Baker, J., and Cornell, C.A. (2006). Correlation of Response Spectral Values for Multicomponents Ground Motions. *Bulletin of the Seismological Society of America* **96 (1)**: 215-227.

Baker, J. and Jayaram, N. (2008). Correlation of Spectral Acceleration Values from NGA Ground Motion Models. *Earthquake Spectra* **24 (1)**: 299-317.

Bardet, J.-P., Tobita, T., Mace, N., and Hu, J. (2002) Regional Modeling of Liquefaction-Induced Ground Deformation. *Earthquake Spectra* **18(1)**: 19 – 46.

Barnes, R. J. (1991). The Variogram Sill and the Sample Variance. *Mathematical Geology* **23 (4)**: 673-678.

Bazzurro, P., and Luco, N. (2005). Accounting for uncertainty and correlation in

earthquake loss estimation. In *Proceedings, 9th International Conference on Structural Safety and Reliability (ICOSSAR'05)*, G. Augusti, G. Schuëller, M. Ciampoli (eds.), Rome, Italy, pp. 2687-2694.

Bensi M., Der Kiureghian A., and Straub, D. (2009). A Bayesian network framework for post-earthquake infrastructure performance assessment. In *Proceedings, TCLEE2009 Conference: Lifeline Earthquake Engineering in a multihazard Environmental*, Oakland, California.

Beyer, K. and Bommer, J.J. (2006). Relationships between Median Values and between Aleatory Variabilities for Different Definitions of the Horizontal Component of Motion. *Bulletin of the Seismological Society of America,* **96 (4A)**: 1512–1522.

Bindi, D., Luzi, L., and Rovelli, A. (2010). Ground Motion Prediction Equations (GMPEs) derived from ITACA. Deliverable No.14. *Project S4: Italian Strong Motion Data Base*, http://esse4.mi.ingv.it.

Bindi D., Pacor, F., Luzi, L., Puglia, R., Massa, M.,Ameri, G., and Lucci, R., (2011). Ground Motion Prediction Equations Derived from the Italian Strong Motion Data Base. *Bulletin of Earthquake Engineering* (Submitted).

Blumetti, A.M., Comerci, V., Di Manna, P., Guerrieri, L, and Vittori, E. (2009). Geological effects induced by the L'Aquila earthquake (6 April 2009, Ml =5.8) on the natural enviromental. Preliminary report available on http://www.apat.gov.it/site/_files/Inqua/2009_abruzzo_earthquake_report.pdf.

Boore, D. M., Gibbs, J. F., Joyner, W.B., Tinsley, J. C., and Ponti, D. J. (2003). Estimated ground motion from the 1994 Northridge, California, earthquake at the site of the Interstate 10 and La Cienega Boulevard bridge collapse, West Los Angeles, California. *Bulletin of the Seismological Society of America* **93 (6)**: 2737-2751.

Brillinger, D.R., and Preisler, H.K. (1985). Further analysis of the Joyner-Boore attenuation data. *Bulletin of the Seismological Society of America* **75 (2)**: 611-614.

Campbell, K., and Seligson, H. (2003). Quantitative method for developing hazard-consistent earthquake scenarios. In *Proceedings, Technical Council of Lifeline Earthquake Engineering, ASCE*, J. Beavers, (editor), Long Beach, Calif., pp. 829-838.

Chang, L., and Song, J. (2007). Matrix-based system reliability analysis of urban infrastructure networks: a case study of MLGW natural gas network. In *Proceeding, 5th China-Japan-US Trilateral Symposium on Lifeline Earthquake Engineering*, November 26-28, Haikou, China.

Chioccarelli, E., De Luca, F. and Iervolino, I. (2009). Preliminary study of L'Aquila earthquake ground motion records V5.20, available at http://www.reluis.it.

Chioccarelli, E. and Iervolino, I. (2010). Near-Source Seismic Demand and Pulse-Like Records: a Discussion for L'Aquila Earthquake. *Earthquake Engineering and Structural Dynamics.* **39 (9)**:1039–1062.

Choi, Y., and Stewart, J. P., (2005). Nonlinear Site Amplification as Function of 30 m Shear Wave Velocity. *Earthquake Spectra* **21 (1)**: 1-30.

Cornell, A. C. (1968). Engineering seismic risk analysis. *Bulletin of the Seismological Society of America* **58 (5)**: 1583-1606.

Cressie, N. (1993). *Statistics for Spatial Data*. Revised edition. Wiley, New York, USA, 900 pp

Cressie, N., and Hawkins, D.M. (1980). Robust estimation of variogram. *Mathematical Geology* **12 (2)**: 115-125.

Christofides, N. (1975). *Graph Theory*. New York: Academic Press.

Crowley, H., and Bommer, J. (2006). Modelling seismic hazard in earthquake loss models with spatially distributed exposure, *Bulletin of Earthquake Engineering* **4 (3)**: 249-273.

Crowley, H., Stafford, P. J., and Bommer, J.J. (2008). Can earthquake loss models be validated using field observations? *Journal of Earthquake Engineering* **12 (7)**: 1078-1104.

Davis, M., 1987. Production of conditional simulation via the LU decomposition of the covariance matrix. *Mathematical Geology* **19 (2):** 91-98.

Min. LL PP, D.M. 24 Novembre (1984). Norme di sicurezza antincendio per il trasporto, la distribuzione, l'accumulo e l'utilizzazione del gas naturale con densita' non superiore a 0,8. *Gazzetta Ufficiale della Repubblica Italiana, 12* [in Italian].

Dolce, M., Giovinazzi, S., Iervolino I., Nigro, E. and Tang, A. (2009). Emergency management for lifelines and rapid response after L'Aquila earthquake. *Progettazione Sismica. Seismic Design Journal.* Vol 3. November 2009. IUSS PRESS Editor. ISSN 1973-7432.

Dueñas-Osorio, L., Craig, J.I. and Goodno, B.J. (2007). Seismic Response of Critical Interdependent Networks. *Earthquake Engineering and Structural Dynamics*, Special Issue on Earthquake Engineering for Electric Power Equipment and Lifeline Systems 36 (2): 285-306.

Duke, C.M., and Matthiesen, R.B. (1973). Earthquakes, lifelines and ASCE. *Civil Engineering*, ASCE, 65-67.

EERI. 1986. *Reducing earthquake hazards: lessons learned from earthquakes.* Publication n°86-02, Earthquake Engineering Research Institute, El Cerrito, CA.

Eguchi, R.T. (1983). Seismic vulnerability models for underground pipes. In *Proceeding, Earthquake behaviour and safety of oil and gas storage facilities, buried pipelines and equipment*, ASME, New-York, pp. 368-373.

Eguchi, R. T. (1987). *Seismic risk to natural gas and oil systems*. FEMA 139, Earthquake Hazard Reduction Series 30, pp. 15-33.

Eidinger, J. (1998). Water distribution system. In Anshel J. Shiff (ed.) *TheLoma Prieta, California, Earthquake of October 17, 1989 – Lifelines*. USGS Professional Paper 15552-A, US Government Printing Ofiice, Washington, A63-A78.

Eidinger, J., Tang, A., and O'Rourke, T.D. (2011). *Report of the 4 September 2010 Mw 7.1 Canterbury (Darfield), New Zealand Earthquake*. Technical Council on Lifeline Earthquake Engineering (TCLEE) Workshop on Challenges and Opportunities for Lifeline Systems Engineering. February, San Diego, CA.

Esposito, S., I. Iervolino, and G. Manfredi (2010). Pga semi-empirical correlation models based on European data. In *Proceeding, 14th European Conference on Earthquake Engineering*. 30 August – 3 September, Ohrid, Macedonia.

Esposito, S., Giovinazzi. S., Iervolino, I. and Elefante, L. (2011a). Post-Earthquake Physical Damage Assessment for Gas Networks. *9th Pacific Conference on Earthquake Engineering* April, Auckland, New Zeland.

Esposito S., and Iervolino I. (2011a) PGA and PGV spatial correlation models based on European muti-event datasets. *Bulletin of the Seismological Society of America* **101(5)**: 2532–2541.

Esposito, S., Elefante, L. Iervolino, I., and Giovinazzi. S. (2011b). Addressing ground-shaking-induced damage of the gas distribution network in the 2009 L'Aquila earthquake, In *Proceeding, XIV Convegno Nazionale "L'Ingegneria Sismica in Italia"*, September, Bari, Italy.

Esposito, S., and Iervolino, I. (2011b). Preliminary results of spatial correlation analysis for acceleration spectral ordinates from Italian data. In *Proceeding, XIV Convegno Nazionale "L'Ingegneria Sismica in Italia"*, September, Bari, Italy.

Esposito, S. and Iervolino, I. (2011c). Sytemic vulnerability and loss for gas and oil networks.Deliverable 5.3 Syner-G Project, http://www.vce.at/SYNER-G/

Eurocode 8 (2004). Design of structures for earthquake resistance, part 1: General rules, seismic actions and rules for buildings, EN 1998-1, *European Committee for Standardization (CEN)*, http://www.cen.eu/cenorm/homepage.htm.

Federal Emergency Management Agency (FEMA)-233 (1992). *Earthquake Resistant Constructionof Gas and Liquid Fuel Pipeline Systems Serving, or Regulated by, the Federal Government*. Earthquake Hazard Reduction Series 67, Washington DC.

Federal Emergency Management Agency (FEMA) (1999). *Earthquake Loss Estimation Methodology HAZUS 99 Service Release 2: Technical manual*, Washington, DC.

Federal Emergency Management Agency (FEMA) (2004). *Multi-hazard Loss Estimation Methodology-Earthquake Model: HAZUS MR4 Technical Manual,*Washington, D.C.

Franchin, P. Cavalieri, F., Pinto P.E., Lupoi, A., Vanzi, I., Gehl, P., Kazai, B., Weatherill, G., Esposito, S., and Kakderi, K. (2011). General methodology for systemic seismic vulnerability assessment. Deliverable 2.1 Syner-G Project, http://www.vce.at/SYNER-G/

Gehl, P., Reveillere, A.,Desramaut, N., Modaressi, H., Kakderi, K., Argyroudis, S., Pitilakis, K., and Alexoudi, M. (2010). Fragility functions for gas and oil systems networks. Deliverable 3.4 Syner-G Project, http://www.vce.at/SYNER-G/

Goda, K., and Atkinson, G. M. (2009). Probabilistic characterization of spatially correlated response spectra for earthquakes in Japan. *Bulletin of the Seismological Society of America* **99 (5)**: 3003-3020.

Goda, K., and Atkinson, G. M. (2010). Intraevent spatial correlation of ground-motion parameters using SK-net data. *Bulletin of the Seismological Society of America* **100 (6)**: 3055-3067.

Goda, K., and Hong, H.P. (2008a). Spatial correlation of peak ground motions and response spectra. *Bulletin of the Seismological Society of America* **98 (1)**: 354-365.

Goda, K., and Hong, H.P. (2008b). Estimation of Seismic Loss for Spatially Distributed Buildings. *Earthquake Spectra* **24 (4)**: 889 – 910.

Goovartes, P. (1997). *Geostatistics for Natural Resources Evaluation*. Oxford University Press, Oxford, New York, 496 pp.

Gutenberg, B., and Richter , C. F. (1954). Frequency of earthquakes in California. *Bulletin of the Seismological Society of America* **34**:185-188.

Hernandez-Fajardo, I., and Dueñas -Osorio, L. (2011). Sequential Propagation of Seismic Fragility across Interdependent Lifeline Systems. *Earthquake Spectra* **27 (1)**: 23-43.

Hong, H.P., Zhang, Y., and Goda, K. (2009). Effect of spatial correlation on estimated ground motion prediction equations. *Bulletin of the Seismological Society of America* **99 (2A)**: 928-934.

Iervolino, I., Fabbrocino, G., and Manfredi, G. (2004). Fragility of standard industrial

strucutres by a resposnse surface method. *Journal of Erathquake Engineering* **8 (6)**: 927-945.

Iervolino, I., Giorgio, M., Galasso, C., and Manfredi, G. (2010). Conditional Hazard Maps for Secondary Intensity Measures. *Bulletin of the Seismological Society of America* **100 (6)**: 3312-3319.

INGV, Istituto Nazionale di Geofisica e Vulcanologia (2009). Location of April 6, 2009 earthquake updated with all the available data, http://www.ingv.it.

Inoue, T., and Cornell, C.A. (1990) Seismic Hazard Analysis of Multi-Degree-of-Freedom Structures. *Reliability of Marine Structures,* RMS-8, Stanford, California.

Jayaram, N., and Baker, J.W. (2008). Statistical tests of the joint distribution of spectral acceleration values. *Bulletin of the Seismological Society of America* **98 (5)**: 2231-2243.

Jayaram, N., and J.W. Baker (2009a). Correlation model for spatially distributed ground-motion intensities. *Earthquake Engineering and Structural Dynamics* **38 (15)**: 1687–1708.

Jayaram, N., and J.W. Baker (2009b). Deaggregation of lifeline risk: Insights for choosing deterministic scenario earthquakes. In *Proceedings, TCLEE2009 Conference: Lifeline Earthquake Engineering in a multihazard Environmental*, Oakland, California.

Jayaram, N., and J.W. Baker (2010a). Considering spatial correlation in mixed-effects regression, and impact on ground-motion models. *Bulletin of the Seismological Society of America* **100 (6)**: 3295-3303.

Jayaram, N., and J.W. Baker (2010b). Characterizing spatial cross-correlation between ground motion spectral accelerations at multiple periods. In *Proceedings, 9th U.S. National and 10th Canadian Conference on Earthquake Engineering,* Toronto, Ontario, Canada.

Journel, A.G., and Huijbregts, Ch. J. (1978). *Mining Geostatistics*. Academic Press, London, 600 pp.

Kang, W.H., Song, J., and Gardoni, P. (2008). Matrix-based system reliability method and applications to bridge networks. *Reliability Engineering & System Safety* **93 (11)**: 1584-1593.

Kramer, S. L. (1996). *Geotechnical Earthquake Engineering.* New Jersey: Prentice Hall.

Kramer, S.L., and Stewart, J.P. (2004) Chapter 4: "Geotechnical Aspects of Seismic Hazards" in *Earthquake Engineering: From Engineering Seismology to Performance-Based Engineering*. CRC Press.

Lee, J., Graf, W., Somerville, P., O'Rourke, T., and Shinozuka, M. (2005). *Developing*

a Hazard-Consistent Table of Earthquake Scenarios for Risk Analysis of the LADWP Water Systems, Final Report to the Los Angeles Department of Water and Power.

Liao, S.S., Veneziano, D., and Whitman, R.V. (1988). Regression Models for Evaluating Liquefaction Probability. *Journal of Geotechnical Engineering* **114 (4)**: 389-411.

Malhotra, P. (2008). Seismic Design Loads from Site-Specific and Aggregate Hazard Analyses. *Bulletin of the Seismological Society of America* **98 (4)**: 1849-1862.

Matheron, G. (1962). *Traité de géostatistique appliquée*. Editions Technip, Paris, France, 333 pp. [in French]

Mc Guire, R.K. (2004). *Seismic Hazard and Risk Analysis*. EERI Monograph No. 10.

Meyershon, W.D. (1991). *Analitical and Design Consideration for the Seismic Response of Buried Pipelines*, Thesis, Graduate School of Cornell University, January.

Nies, S. (2008). *Oil and Gas delivery to Europe: an overview of existing and planned infrastructures.* The French Institute for International Relations (Gouvernance Europeenne et Geopolitique de l'Energie), 4 bis, ISBN 978-2-86592-363-2.

Osiadacz, A.J. (1987). *Simulation and Analysis of Gas Network.* First Edition. London: D and F.N. Spon Ltd.

O'Rourke, M. J. (1988). Mitigation of seismic effects on water systems. In *Seismic Design and Construction of Complex Civil Engineering Systems*. Symposium sponsored by TCLEE/ASCE, National Convention, St Louis, MO, pp. 65-78.

O'Rourke, M. J., and Ayala, G. (1993). Pipeline damage due to wave propagation. *Journal of Geotechnical Engineering* **119 (9)**:1490-1498.

O'Rourke, T.D., and Palmer, M.C. (1996). Earthquake Performance of Gas Transmission Pipelines. *Earthquake Spectra* **20 (3)**: 493-527.

O'Rourke, T.D., Toprak, S., and Sano, Y. (1998). Factors affecting water supply damage caused by the Northridge earthquake, In *Proceedings, 6th U.S. National Conference on Earthquake Enginnering* EERI, Seattle.

O'Rourke, M.J., and Liu, X. (1999). *Response of Buried Pipelines Subjected to Earthquake Effects*. MCEER Monograph No. 3.

O'Rourke, M.J., and So, P. (2000). Seismic fragility curves for on-grade steel tanks. *Earthquake Spectra* **16 (4)**: 801-815.

O'Rourke, M. J., and Deyoe, E. (2004). Seismic damage to segment buried pipe. *Earthquake Spectra* **20 (4)**: 1167 – 1183.

Pace B., Perruzza L., La Vecchia G., and Boncio, P. (2006). Layered Seismogenic Source Model and Probabilistic Seismic-Hazard Analyses in Central Italy. *Bulletin*

of the Seismological Society of America **96 (1)**: 107-132.

Park, J., Bazzurro, P., and Baker , J.W. (2007). Modeling spatial correlation of ground motion intensity measures for regional seismic hazard and portfolio loss estimation. *10th International Conference on Application of Statistics and Probability in Civil Engineering* (ICASP10), Tokyo, Japan.

Pitilakis, K., Alexoudi, M., Argyroudis, S., Monge, O., and Martin, C., (2006). Earthquake risk assessment of lifelines. *Bulletin of Earthquake Engineering* **4 (4)**: 365-390.

Poljanšek, K., Bono, F. and Gutiérrez, E. (2011). Seismic risk assessment of interdependent critical infrastructure systems: The case of European gas and electricity networks. *Earthquake Engineering And Structural Dynamics*. DOI: 10.1002/eqe.1118.

Pradel, D. (1998). Procedure to Evaluate Earthquake-Induced Settlements in Dry Sandy Soils. *Journal of Geotechnical and Geoenvironmental Engineering* **124 (4)**: 364 – 368.

Reiter, L. (1991). *Earthquake hazard analysis*, Columbia Press, New York.

Rhoades, D., and McVerry, G. (2001). Joint hazard of earthquake shaking at two or more locations, *Earthquake Spectra* **17 (4)**: 697–710.

Rinaldi, S., Peerenboom, J., and Kelly, T. (2001). Identifying, understanding, and analyzing critical infrastructures interdependencies, *IEE Control System Magazine*, **11**.

Saygill, G., and Rathje, E. M. (2008). Empirical Predictive Models for Earthquake-Induced Sliding Displacements of Slopes. *Journal of Geotechnical and Geoenvironmental Engineering* **134 (6)**: 790 - 803

Sokolov, V., Wenzel, F., Jean, WY., and Wen, KL. (2010). Uncertainty and spatial correlation of earthquake ground motion in Taiwan. *Terrestrial, Atmospheric and Oceanic Sciences* **21 (6)**: 905-921.

Sokolov, V., and Wenzel, F. (2011). Influence of ground-motion correlation on probabilistic assessments of seismic hazard and loss: sensitivity analysis. *Bulletin of Earthquake Engineering* (in press).

Song, J., and Ok, S.-Y. (2009). Multi scale system reliability analysis of lifeline networks under earthquake hazards. *Earthquake Engineering & structural Dynamics*, **39 (3)**: 259-279.

Strasser, F.O., Abrahamson, N. A., and Bommer, J.J. (2009). Sigma: issues, insights, and challenges. *Seismological Research Letters* **80 (1)**: 40-56.

Takada, S., and Takabe, K. (1988). Estimation of Earthquake Induced Settlements for Lifeline Engineering. In *Proceedings, 9th World Conference on Earthquake Engineering.* August 2 – 9, Tokyo, Japan.

Taylor, C.L. and Cluff, L.S. (1977). Fault displacement and ground deformation associated with surface faulting. *The Current State of Knowledge of Lifeline Earthquake Engineering*, ASCE TCLEE, 338-353.

Tokimatsu, K., and Seed, H. B. (1987). Evaluation of Settlements in Sands due to Earthquake Shaking. *Journal of Geotechnical and Geoenvironmental Engineering* **113(8)**: 861 – 878.

Tromans, I. (2004). *Behaviour of buried water supply pipelines in earthquake zones*. Thesis, Imperial College of Science, Technology and Medicine, January.

UNI EN 1555-2 (2004). Sistemi di tubazioni di materia plastica per la distribuzione di gas combustibili -Polietilene (PE) - Parte 2: Tubi. *Ente Nazionale Italiano di Unificazione (UNI)*, http://www.uni.com. [in Italian]

UNI EN 10208-1 (2009). Tubi di acciaio per condotte di fluidi combustibili - Condizioni tecniche di fornitura - Parte 1: Tubi della classe di prescrizione A. *Ente Nazionale Italiano di Unificazione (UNI)*, http://www.uni.com. [in Italian]

Wald, D.J., Worden, C.B., Quitoriano, V., and Pankow, K.L. (2006). ShakeMap Manual, technical manual, users guide, and software guide, available at http://pubs.usgs.gov/tm/2005/12A01/pdf/508TM12-A1.pdf.

Walling, M., Silva, W., and Abrahamson, N. (2008). Nonlinear Site Amplification Factors for Constraining the NGA Models. *Earthquake Spectra* **24 (1)**: 243 – 255.

Wang, M., and Takada, T. (2005). Macrospatial correlation model of seismic ground motions. *Earthquake Spectra* **21 (4)**: 1137-1156.

Wang, Y., and O'Rourke, T.D. (2008). *Seismic Performance Evaluation of Water Supply Systems*. Technical Report MCEER-08-0015.

Wang, Y., Siu-Kui, A., and Qiang, F. (2010). Seismic Risk Assessment and Mitigation of Water Supply Systems. *Earthquake Spectra* **26 (1)**: 257-274.

Weatherill, G., Crowley, H., Pinho, R., Franchin, P., Cavalieri, F., Esposito, S., and Iervolino, I. (2011). A Review and Preliminary Application of Methodologies for the Generation of Earthquake Scenarios for Spatially Distributed Systems. Deliverable 2.13 Syner-G Project, http://www.vce.at/SYNER-G/

Wells, D.L., and Coppersmith, K.J. (1994). New empirical relationships among magnitude, rupture length, rupture width, rupture area, and surface displacement. *Bulletin of the Seismological Society of America* **84 (4)**: 974-1002.

Wieczorek, G. F., Wilson, R. C. and Harp, E. L. (1985) Map of Slope Stability During Earthquakes in San Mateo County, California. *U.S. Geological Survey Miscellaneous Investigations.* Map I-1257-E, scale 1:62,500.

Wilson, R. C., and Keefer D. K. (1985). Predicting Areal Limits of Earthquake Induced Landsliding, Evaluating Earthquake Hazards in the Los Angeles Region, *U.S.Geological Survey Professional Paper*, Ziony, J. I., Editor, pp. 317-493.

Youd, T. L., and Perkins, D. M. (1978). Mapping of Liquefaction Induced Ground Failure Potential. *Journal of the Geotechnical Engineering Division*. American Society of Civil Engineers **104 (4)**: 433-446.

Youd, T. L., Hansen, C. M., and Bartlett, S. F. (2002). Revised Multilinear Regression Equations for Prediction of Lateral Spread Displacement. *Journal of Geotechnical and Geoenvironmental Engineering* **128 (12)**: 1007 – 1017.

Zambonelli, E., De Nardis, R., Filippi, L., Nicoletti, M., and Dolce, M. (2010). Performance of the Italian strong motion network during the 2009, L'Aquila seismic sequence (central Italy). *Bulletin of Earthquake Engineering* **9 (1)**: 39-65.

Zerva, A., and Zervas, V. (2002). Spatial variation of seismic ground motion, *Applied Mechanics Reviewers* **55 (3)**: 271-297.

.